KAUNAS UNIVERSITY OF TECHNOLOGY

ELECTRONICS ENGINEERING FACULTY

MEASUREMENT OF ABSORPTION OF LASER PULSES USING PHOTOACOUSTIC TECHNIQUE

Master‘s Degree Final Project

Electronics Engineering (621H61002)

Supervisor

Prof. Dr. Darius Gailius

Reviewer

Assoc. Prof. Žilvinas Nakutis

Project made by

Sotirios Gakopoulos

KAUNAS, 2017

KAUNAS UNIVERSITY OF TECHNOLOGY

Electronics Engineering Faculty

Sotirios Gakopoulos

Electronics Engineering 621H61002

‘‘Measuremet of Absorption of Laser Pulses Using Photoacoustic Technique‘‘

DECLARATION OF ACADEMIC INTEGRITY

6 June 2017
Kaunas

I confirm that the final project of mine, **Sotirios Gakopoulos**, on the subject, “Measurement of Absorption of Laser Pulses Using Photoacoustic Technique” is written completely by myself; all the provided data and research results are correct and have been obtained honestly. None of the parts of this thesis have been plagiarized from any printed, Internet-based or otherwise recorded sources; all direct and indirect quotations from external resources are indicated in the list of references. No monetary funds (unless required by law) have been paid to anyone for any contribution to this thesis.

I fully and completely understand that any discovery of any facts of dishonesty inevitably results in me incurring a penalty under procedure effective at Kaunas University of Technology.

(name and surname) (signature)

Sotirios Gakopoulos. Measurement of Absorption of Laser Pulses Using Photoacoustic Technique. Master's Final Project of Electronics Engineering degree/ supervisor Prof. Dr. Darius Gailius; Faculty of Electronics Engineering, Kaunas University of Technology.

Research field and area: Optics and photonics

Keywords: *photoacoustic technique, optoacoustic technique, laser pulses absorption, laser – material interactions, low noise amplifier*

Kaunas, 2017. 06 p.

SUMMARY

The topic of this masters' thesis project is the measurement of absorption of laser pulses using photoacoustic technique. The problem concerning the measurement of absorption is weakness of the photoacoustic signal that is generated by the absorbed light, which makes it difficult to capture. The research methods that were used, start from the literature analysis and the theoretical background of the photoacoustic effect and the laser – material interactions. Afterwards, the theory is put into simulations in order to obtain valuable information about the nature of the experiments and the problems that may be encountered. Having considered all of the above, a measurement device was proposed that will satisfy the needs of the research. Then, everything was put into practice and the final experiments were conducted. The most important conclusions that are drawn are which material provide the highest absorption and consequently the easier detection of the photoacoustic effect, what is the impact of the angle of the incident laser beam and how adequate and reliable the proposed measurement device has proved to be.

SANTRAUKA

Šio magistrinio darbo tema- lazerio impulsų sugerties matavimas optiniuose elementuose fotoakustiniu metodu. Tokio būdo problema yra ta, kad neretai generuojamas akustinis signalas yra silpnas ir dėl to kyla problemų jį registruojant. Darbo pradžioje atlikta literatūros analizė: teoriniai fotoakustinio reiškinio pagrindai, lazerio spindulio bei medžiagos sąveika. Toliau atliekamas teorinis modeliavimas siekiant gauti naudingos informacijos eksperimentų metu vykstančius procesus bei tikėtinas problemas. Po to buvo pasiūlytas matavimo įrenginys, kuris būtų tinkamas praktiniams tyrimams. Tada jis buvo praktiškai realizuotas ir atlikti eksperimentai. Nustatyta kokiose tirtose medžiagose yra didžiausia sugertis ir atitinkamai užregistruoti didžiausi akustiniai signalai; kokia yra lazerio spindulio kritimo kampo įtaka; taip pat įvertintas matavimo įrenginio tinkamumas lazerio spindulio sugerties matavimui.

ABSTRACT

In this thesis project the photoacoustic technique is utilized in order to measure the absorption of laser pulses in solid materials and especially lenses. This thesis focuses on various sides of the problem. The starting point is the theoretical background of the photoacoustic effect and the detailed mechanisms behind it. Also, critical part is the laser – material interactions induced by the lasers and they are responsible for the generation of the photoacoustic effect. For this reason, this thesis not only analyzes the previously mentioned, but also includes simulations to prove them. In second stage, a device that can be succesfully used to measure the absorption of laser pulses is proposed and implemented. Finally, having examined all the theoretical and simulation results, experiments are carried out in order to put theory in to practice. The absorption of laser pulses was measured for different sets of materials in different thicknesses using an Nd:YAG laser with a wavelength of 532 nm. The pulse duration and pulse repetion ratio were fixed during all of the experiments. The experiments were accomplished successfully and proved that the proposed device is well-suited for its purpose.

Table of Contents

ACKNOWLEDGEMENTS

Firstly, I would like to thank my thesis project supervisor Prof. Dr. Darius Gailius for trusting me during this project. He was always available was I needed his help. Whenever I ran into a trouble or I had a questions about my research project, he showed me the way in to the right direction.

Secondly, I would also like to thank Edgaras Vastakas (Ph.D) for supporting me with his experience and his willingness during this thesis. I would also like to acknowledge dr. Vygantas Augutis and I am gratefully indebted for his valuable guidance and instructions on this thesis project. I would also like to admit my gratefulness to Dr. Pranas Kuzas for his assistance.

Finally, I feel the need to express my heatfelt gratitude to my family; and especially to my father (Georgios S. Gakopoulos), to my grandfather (Sotirios I. Gakopoulos) and to my grandmother (Kiratso I. Gakopoulos) for providing me with support and encouragement throughout these two years of my studies. This accomplishment would not have been possible without them. Thank you!

INTRODUCTION

MOTIVATION OF THE THESIS

Nowadays, photoacoustic effect has reached a high level of maturity and acceptance in many scientific fields. The applications of photoacoustic methods include spectroscopy, monitoring de-excitation processes, probing physical properties of materials and generating mechanical motions. The use of photoacoustic effect is not limited only to these applications, but is it also used in imaging methods, especially in the medical field. Common to all these applications, is that the laser light is transformed into heat. This is the fundamental process of light absorption and can often be a determining factor in whether a process will be successful for a particular material under certain circumstances or not.

However, the fact that really motivated me is the unknown. Having the opportunity to conduct a research on a topic that was completely unknown to me two years ago, it was enough to light a spark inside me. It is so unique trying to "listen" to the waves that are generated by the absorption of laser pulses. It is also uniquely strange that an effect that was observed more than a hundred is still useful and is growing day by day. Moreover, it is fascinating to provide as a single person more information about the absorption of laser light.

METHODOLOGICAL APPROACH

The methodological approach of this Master thesis can be understood by reference to the structure and order of the chapters included. The work began by making an overview of the photoacoustic effect and its application fields. Then the aspects of photoacoustic effect were studied and analyzed. Hopefully, experimental results from previous experiments are available from the early stages of the discovery of the effect in the 19th century till nowadays as it is still widely used. In the following stage, various ways of measuring the waves generated by the photoacoustic effect were investigated. After that, I focused my attention on the lasers' side. The mathematical modelling of laser – material interaction was analyzed, starting from heat transfer and ended up to laser intensity and absorption inside the materials. Having grasped all the valuable theoretical information, I implemented them into simulations in order to visualize them and examine the material parameters and aspects. The next step was focus on the design implementation of the electronic device that is needed to measure the absorption of laser pulses. Attention was paid on the device in order to capture even really small signal without the affect from the noise. As long as the measurement device was ready, it was high time to try and make the first measurements. During the first attempts I decided to excite a small lens using a piezoelectric transducer and measure the vibration that the absorbed energy causes in the material. The final step, of course, was to make the measurement of absorption of laser pulses. The measurement of absorption was performermed in various optical materials.

PROJECT OBJECTIVE

The objective of this thesis project is to develop a measurement tool that will be able to provide sufficient measurements of the absorption of laser pulses utilizing the photoacoustic effect and consequently to perform experiments on various absorbing materials. Also the objective is to propose the methodoly approach that can be following in order to achieve the desired results. The objected is not limited only on the experimental part, but also on the conduction of simulations using theoretical approaches.

PROJECT STRUCTURE

Since the project involves lasers and the effects that caused by them both of these topics should be examined and narrated. Therefore, the thesis is organized in a way to proceed step by step starting with the literature analysis of photoacoustic effect from basic till deep details. Moreover, the laser-material interaction phenomena are examined using theory and simulations. Furthermore, a proposed device to measure the absorption of laser pulses using a piezoelectric transducer and a low noise amplifier is suggested. Finally, the experimental results are presented and conclusions are drawn. The thesis project is organized into following chapters.

In chapter 1, the literature analysis of the photoacoustic effect is presented based on previous implementation from the early ages till today.

In chapter 2, the essentials of laser-material interaction relevant to this thesis work are explained.

In chapter 3, the simulations of the essentials are analyzed starting from heat transfer till laser absorption and vibration models.

In chapter 4, a discussion on low amplifiers is described and leads to the design of the device alongside with results from its simulations.

In chapter 5, experimental data are presented for the measurement of absorption of laser pulses in various materials.

Finally the last chapter gives the conclusions of this project, the main achievements and also future work suggestions and improvements.

1. PHOTOACOUSTIC EFFECT ANALYSIS

The photoacoustic effect also known as optoacoustic effect is the generation of sound waves which are caused by the absorption of any source of light inside materials. More specifically, during this process the variation of the light intensity is of significant importance. This variation can be achieved by two different ways. The first way is to modulate periodically the source of light, while the second way is to use pulses of light. [1][2] The photoacoustic effect is expressed by measuring the pressure variations using the right detectors depending on the application. More common types of the detectors used are microphones or piezoelectric sensors. This variation coming from the electric signal that is generated by these detectors is actually the photoacoustic signal. The measurements of the photoacoustic signal are employed in order to determine the properties of the under investigation material. The photoacoustic signal is utilized to measure the actual light absorption either if the material is transparent or opaque. Photoacoustic effect can be also utilized when material exposes exceptional low concentrations. An increase on pulsed laser's energy is used to achieve higher sensitivity, while the use of narrower wavelengths is utilized to increase specificity. The photoacoustic effect can be created by all kind of electromagnetic radiation of any kind on frequencies ranging from gamma radiation to microwave and radio frequencies. However, most of the applications till nowadays, use the photoacoustic effect in within the visible spectrum as well as a little bit above or beyond it, specifically in the infrared and ultraviolet regions.

1.1 THEORETICAL BACKGROUND

The photoacoustic technique has its roots in the late 19th century. Alexander Graham Bell is responsible for the discovery of photoacoustic effect back in 1880, while he was conducting experiments to achieve voice transmission in long distances. His first invention was the photophone, which is working under a simple principle. As a transmitter, he used a moving mirror which was responsible for the reflection of sun light and as a receiver, he used a solar cell made of selenium [3]. Bell and Tainter devised more than fifty different configurations in the device, but the most successful form consisted of a transmitter, which was a thin silvered glass disk mounted on a frame with a flexible rubber hose. Th rubber hose's free end contained the mouthpiece [3-5, 15]. The mirror and the associated optics were arranged in such way that the sunlight was focused and then reflected light could be collected by the receiver placed on a remote place, The receiver was a parabolic mirror at whose focus a selenium cell incorporated into a conventional telephone circuit was arranged (Figure 1.1). The speech coulped into the mouthpiece caused the vibrations of the mirror, producing fluctuations in the intensity of light collected at the receiver.

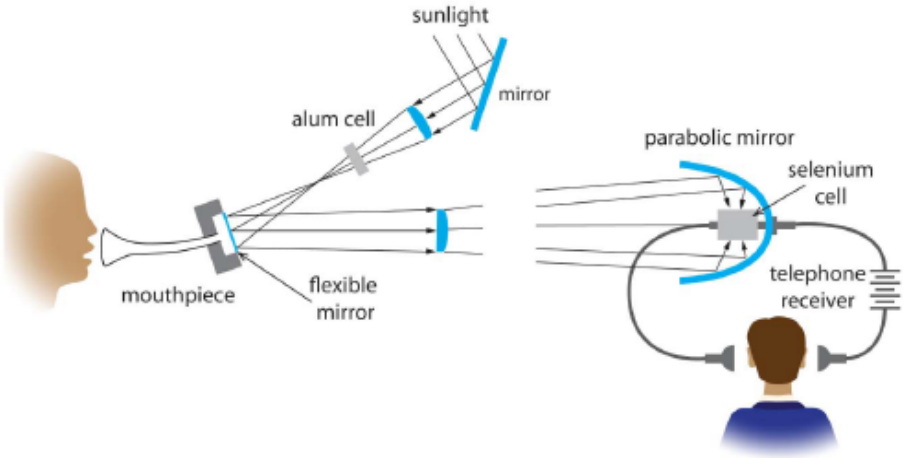

Figure 1.1: Photophone's schematic and working principle [3]

The modulated intensity of light caused by the voice is obtainable at the receiver as a modulated battery current and then using the telephone circuit was converted into sound. Photophone is considered as the first practical implementation of wireless optical communication device.

This was such an innovative concept, but besides that, Bell, observed and investigated by chance something which has was of major importance. He discovered that while illuminating different solid materials with a beam of light which was rapidly interrupted, caused the emission of acoustic waves that they interestingly were on the same frequency as the modulated light's frequency [4]. He observed that the generated acoustic wave was dependent on the type of the material and he stated that the effect was caused by the light absorption that leads to the heating of the material.

After that discovery, Bell also indicated that when the samples are exposed to ultra-violet and infra-red waves can also produce sound waves and consequently, he invented a new device, which he called "spectrophone", with the aim of applying the photoacoustic effect for spectral identification of materials. [5] Later on, Bell, Tyndall and Röntgen conducted these experiments, in liquids and gases and the same effect was demonstrated. [6][7] However, experimental results were unrefined and they were dependent only on ear detection, thus the photoacoustic technique was casted aside until the development of sensitive sensors and intensive sources of light. In 1938 Mark Leonidovitch Veingerov focused his interest in the photoacoustic effect, he utilized it and he measured miniscule carbon dioxide concentration in nitrogen gas [8].

Then the photoacoustic effect was dormant for half a century until the microphone was discovered and thus, made it possible to make the measurements more accurate. In 1973, a detailed model for the effect was developed by Allan Rosencwaig and Gersho (R-G Theory). [9] Since then research and applications grew have seen a fast incease and development, acquiring several plaits and achieved more detection sensitivity. Until this period, the produced heating caused by the absorbed light was considered to be the main reason that gives rise to the photoacoustic effect. In 1978, it was proved that gas evolution resulting from a photochemical reaction can also cause a photoacoustic effect [10].

1.2 PHYSICS BEHIND THE PHOTOACOUSTIC EFFECT

We can understand the physics of the photoacoustic effect by a simple experiment. Considering that a solid sample is completely sealed in a chamber, air is also sealed alongside with the sample and plays the role of a coupling material. A modulated light beam is then focused in the sample, with an intensity $I(t) = \frac{I_0}{2}\ (1 + e^{j\omega t})$, and ω = 2πf is the modulation frequency. The incident light is absorbed by the sample and a certain fraction (η) of the energy is converted to heat through non-radiative de-excitation processes. As a consequence, we have a periodic heat source, with the form $Ae^{-\mu_\alpha x}(1 + e^{j\omega t})$, where $A = \frac{\mu_\alpha I_0 \eta}{2\kappa}$, with μ_α the absorption coefficient, x the depth, and κ the thermal conductivity. The heat transfer occurs by thermal diffusion, the heat transfer is determined by the thermal diffusivity D = κ/ρC, where ρ is the mass density and C is the heat capacity. Equations with a periodic source term describe the thermal diffusion. These solutions are responsible why the term "thermal wave" is often used to describe this heat flow [17]. The form of a one dimension thermal wave plane thermal wave is exp (jωt – σx), where ω = 2πf is the modulation frequency, and $\sigma = (1 + j)\sqrt{\omega/2D}$ is a propagation vector.

Thus, in the material, the heat is deposited photothermally in the material as a wave which is decaying rapidly. The thermal wave interacts with the the air inside the chamber and it is quickly decayed. A thin boundary layer of the gas is involved in temperature varietions, which are periodic with the modulation frequency. As a consequence, the gas layer experiences expansions

and contractions, because of this the gas acts like a piston causing compressions and suppressions on the rest of the gas. These sound waves in the gas are captured up with a sensitive microphone that is placed in level with the inner wall of the cell.

In 1861, Ångström, conducted the first experiment in measuring the the thermal diffusivity in solids by heating a metallic rod and capturing the temperature variations away from the excitation point [18]. In 1880, Preece [19] and in 1881, Mercadier [20, 21] created the first theoretical model of photothermally induced sound waves. In the mid 1970s, Rosencwaig and Gersho [22, 23] comprehensively developed the thermal diffusivity in solids and it was used in thermal wave microscopy applications [24, 25]. Back in 1881, Rayleigh [26] and Bell [4] proposed that thermally induced expansion and contraction of the sample volume can produce an acoustic wave solids. The original method discovered by Bell may be thus described as being a gas microphone technique for detecting thermal waves produced in solids, liquids or gases. In most cases, where the modulation frequency is low, the surface vibration effect that the latter creates is small compared to the effect of the thermal wave.

Generally, photothermal spectroscopy is the field where the nature of matter is probed using optical excitation and then detecting the thermal energy, which is caused by this excitation. Sample's spectral information can be obtained when the heat detection is done in an appropriate way at different incident energies. What is more and makes it unique among other spectroscopic techniques is that thermal properties of the sample can be examined since heat flow is involved in the generation of the signal, the thermal properties of the sample can also be studied [17]. A variety of techniques can be applied to examine materials' properties using discontinuous light radiation (Figure 1.2). First of all, the gas-microphone thermal wave detection method originated by Bell [3], measurement of refractive index gradients in an adjacent coupling liquid (beam deflection spectroscopy) [29], temperature measuring using pyroelectric sensors (photopyroelectric spectroscopy) [30], measurement of thermal emission changes using infrared detectors (photothermal radiometry) [31], or photoacoustic spectroscopy that utilizes piezoelectric sensors in order to detect acoustic vibrations and waves [17]. The last mentioned, is what is utilized in this thesis and refers to vibrations of the sample due to thermoelastic expansion. This gives the opportunity to link intensity-modulated and pulsed photoacoustics.

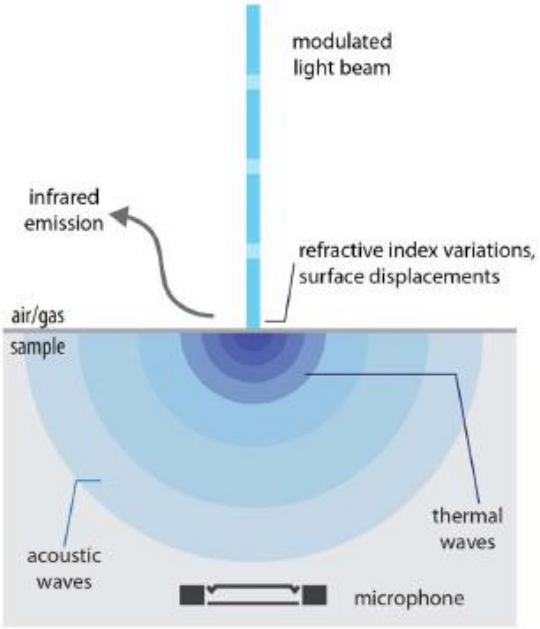

Figure 1.2: Detection techniques [17].

1.3 PULSED EFFECT

As discussed in the previous section, thermal diffussion is responsible for the deposition of local heating. The diffusion equation in which the source term has harmonic dependence on time, reduces to a Helmholtz-like equation for wave motion and has wave-like solutions. This is the origin for the use of the term "thermal waves" to describe heat flow in photoacoustic experiments [32]. However, there is also a direct coupling mechanism of the heat energy to the material's vibrational modes. There is also a stress wave that is caused by the generated pressure and responsible for this is a thermoelastic process determined by the thermal expansion coefficient. The speed of sound inside the material describes the transfer rate of this wave. Generally, this tranfer rate is non-dissipative, except in very high frequencies [33].

When the a short period of excitation is used, the absorbed energy is efficiently converted into pressure waves by the thermoelastic mechanism. As proposed in [34], when a finite duration pulse, excites a material, causes an immediate change in temperature from T_0 to T_1, the temperature-field solutions for the heat diffusion equation when introduced into Fourier's law yield, for heat flow,

$$q(x,t) = \frac{(T_1 - T_0)}{\sqrt{\pi t}} \exp\left(-\frac{x^2}{d_0^2}\right). \tag{1.1}$$

The above expression describes a Gaussian spreading of the heat with a characteristic width of $d_0 = \sqrt{4Dt_p}$, where t_p is the pulse duration and D is thermal diffusivity of the sample.

As it can been seen, a pulse of light deposits heat in the optical absorption zone following an exponential decay of light intensity. If the thermal diffusion length satisfies $d_0 < \delta_L$, where δ_L is the resolution of the sensing system, then the heating pulse is so short that thermal diffusion is not significant during the pulse. There is no leakage of energy out of the effective optical absorption zone, and we can attain maximal thermal energy densities. This is the thermal confinement regime of pulsed laser heating [35, 36]. In a similar way, a stress confinement regime can be defined in which the laser pulse duration is smaller than the time required for the stress propagation out of the heated region defined by the effective spatial resolution, for instance, $t_P < \delta_L / v_c$, where v_c is the speed of sound in the medium [35, 36]. Using pulse durations that satisfy both confinement regimes ensures that the fractional volume expansion (ΔV/V) is negligible, i.e. [38],

$$\frac{\Delta V}{V} = -K\Delta p + \beta \Delta T = 0, \tag{1.2}$$

where

K: isothermal compressibility

B: coefficient of thermal expansion

Δp: the pressure change

ΔT: the temperature change.

Thus the initial rise in pressure caused by the light absorption can be written as

$$\Delta p_0 = \frac{\beta \Delta T}{K} = \frac{\beta}{K}\left\{\frac{E_\alpha}{\rho C_v}\right\}, \tag{1.3}$$

where

ρ: mass density

C_v: the specific heat capacity at constant volume

E_α: the absorbed optical energy given by the product of μ_α absorption coefficient

I: the fluence at the local absorption point.

This can be written as:

$$\Delta p_0 = \Gamma E_\alpha, \quad where\ \Gamma = \frac{B}{K\rho C_v} = \frac{\beta v_s^2}{C_p} \tag{1.4}$$

In this equation Γ is the Grüneisen coefficient, a parameter that wedges speeed of sound, thermal expansion coefficient and compressibility. It can be observed that short excitation pulses thus satisfy both confinement regimes and ensures that the temperature rise leads to a pressure buildup.

So far, the microphones were found to be effective and were used in order to detect low-frequency sound vibrations produced caused by modulated light beams, but as technology had involelved piezoelectricity has played a crucial role in development of new ways for detecting high-frequency ultrasound vibration caused by short-pulsed radiations. In 1880, the piezoelectric effect was initially discovered by Pierre and Jacques Curie in 1880 [39] and the first of its applications was used for ultrasonic detection of submarines using thin quartz crystals [40]. This was succeeded by development of transducers for industrial inspection in the 1920s and 1930s [41, 42] and by the introduction of diagnostic ultrasound in the 1940s and 1950 [43-46].

Generally, heating can be induced by absorption of any kind of electromagnetic radiation. In fact, the first report of stress waves induced in solids due to pulsed radiant exposure is from Michaels [47] in 1961 (Figure 1.3). The main interest was in the mechanism by which stress waves are induced in a solid subjected only to a radiant heating pulse of a huge magnitude.

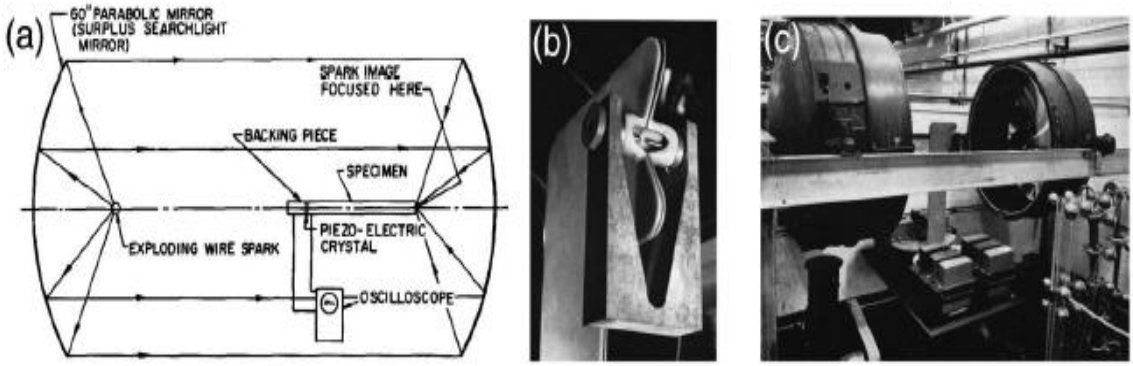

Figure 1.3: Thermal experiment of acoustic waves induced in solids due to pulsed light. (a) Schematic of the experimental setup.. (b) The exploding wire spark. (c) General view of the entire device [47].

In his experiments, Michaels used an underwater exploding wire spark was used to produce a light pulse. The light pulse was focused at one end of an aluminum rod, while on the other end a piezoelectric crystal was mounted in order to capture the acoustic waves. In 1962, White [48] studied radiation-induced stress effects using different sources, such as microwave pulse generators, pulsed ruby laser, a stroboscope lamps and pulsed electron beams. He also excitated various kind if materials such as copper andstainless steel. In 1963, White [49] developed the theory of thermoelastic wave generation in isotropic elastic bodies under several transient heating conditions.

In 1960, when the first laser was built, Prokhov investigated the effects of pulsed light in liquids and in 1963 the formation of shock waves because of the laser-water interactions [50]. The development of a new field of studies with the name of radiation acoustics was initiated [49, 51-

53]. The first studies in solids and liquids, focused on surface heating effects, where the acoustic waves were generated by the absorption of pulsed light [47-55]. This launched planar acoustic waves into solids and liquids. In 1969, Hu studied theoretically the spherical source arising when long laser pulses are focused into liquids [56] and in 1978 by Sigrist and Kneubühl studied the same but for short pulses [57]. Kasoev and Lyamshev [58], Kozyaev and Naugol'nikh [59], and Patel and Tam [60] studied and confirmed that laser beam has longer penetration in weakly absorbing liquids, so the acoustic source may be considered cylindrical. A deeply research was conducted and published by Soviet researchers and their reviews can be found in Patel and Tam [60], Tam [61], and books by Zharov and Letokhov [62], and Gusev and Karabutov [38].

Moreover, Ledbetter and Moulder [63] showed that laser-generated ultrasound in solids and particularly in metals produced longitudinal shear and surface ultrasound waves. More work in this area consolidated the theories and elucidated the mechanisms, which could be divided into the thermoelastic regime, and, at higher laser power densities, the plasma or ablation regime. The applications in this area had been investigated to varying degrees since White in 1963 (see, e.g., Refs. [64-65]), but reached a zenith in the 1980s [66-68]. The most applications were seen in nondestructive testing (NDT) of metals and other solids using near-infrared or visible lasers. Various types of ultrasound transducers were used, such as capacitance-based detectors [69, 70], electromagnetic acoustic transducers (EMATs) [71, 72], and non-contact interferometric methods [73, 74]. The latter approach of detection of laser-generated ultrasound came to be called laser-ultrasonics. Various sophisticated systems were developed in the 1980s, and these, along with applications in NDT, are described in detail in [63-65]. Other related applications in the materials industry were in material characterization by determination of elastic constants and grain sizes [75]; determination of thin film thicknesses [76], and the early beginnings of acoustic microscopy [77].

1.4 PRINCIPLES OF A PHOTOACOUSTIC EXPERIMENT

The steps involved on the photoacoustic effect are summarized in Figure 1.4. Pressure fluctuations in solid or liquid sample can be probed by piezoelectric transducers. Another way of probing the pressure fluctuations can be observed by optical methods. As previously stated, photothermal effect is caused by any light source, however, lasers are utilized as the preferred excitation source and this is beacause of two reasons: The photothermal signal that is generated, is proportional to the temperature rise in the sample. In other words, this means that is proportional to the absorbed energy of the pulsed laser. The second reason is that for many applications the selectivity of a photothermal analysis, depends on the bandwidth of the excitation wavelength [78].

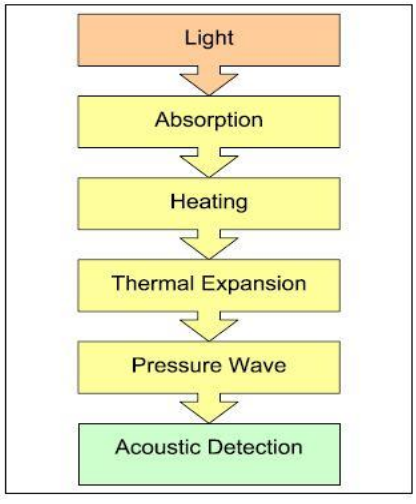

Figure 1.4: Principle of a photoacoustic experiment.

Photoacoustic effect is based on the absorption of the incident electromagnetic radiation by the material particles. The ligth absorption lead to local warming of the material under investigation. This local warming causes thermal expansion which subsequently is responsible for pressure fluctuations inside the material. To sum it up, photoacoustic spectroscopy is the transformation of an incident light into an acoustic waves. Part of the radiation that illuminates a sample is absorbed and results in excitation and this excitation is dependant on the radiation energy. This non-radiative de-excitation processes generates the generation thermal energy inside the sample. As previously mentioned the generated pressure wave has the same frequency as the modulated light.

The energy thermal wave or pressure wave is trasferred to the sample's boundaries. The generated acoustic wave is the result of the temperature variation and propagates inside the material Energy is transferred by the thermal/pressure wave towards the sample boundary, where a periodic temperature change is generated. The periodic variation in the temperature at the surface of the sample results in the generation of an acoustic wave and this wave propagates through the volume of the material. Afterwards, this wave reaches the attached detector, who is responsible for the signal production. The plotted signal as a function of wavelength gives a spectrum which is proportional to the sample's absorption. Because of that, the photoacoustic signal depends on of two types of processes occurring in the sample. The first is the absorption of radiation which is determined by the absorption coefficient and the second is the thermal propagation inside the material which is described by the thermal diffusivity. The measurement principle is shown in Figure 1.5. A focused nanosecond laser pulse illuminates the optical material and because of the absorption, some of its energy is deposited inside the material. This leads to local heating after the thermalization process of the deposited energy. As a consequence, thermal expansion causes the emission of a pressure wave. A piezoelectric transducer attached to the edge of the sample detects the photoacoustic wave.

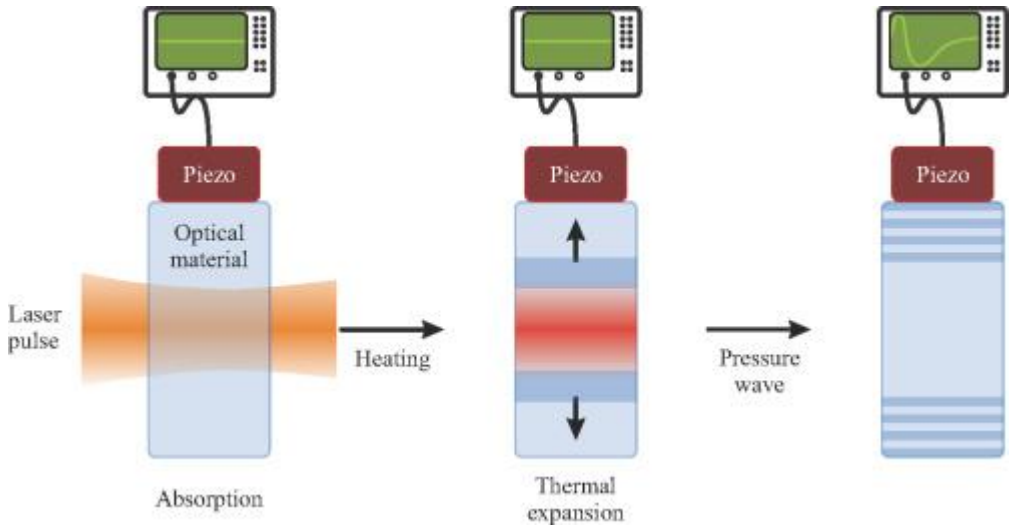

Figure 1.5: Measurement principle of the photoacoustic effect [114].

During some photoacoustic measurements the material under investigation is hermetically closed in photoacoustic cell. In such a case, the photoacoustic effect is based upon the detection of acoustic waves generated by the absorption of laser radiation by the local transfer heating and expansion. When the laser hits the target, some of its energy is absorbed in the samples resulting in a region of higher temperature. This temperature rise generates an expansion and a pressure wave propagates away from the heat source. This periodic pressure wave is detected by a transducer which is in contact with sample or in contact with the photoacoustic cell. (Figure 1.6) for details. The transducer's signal is proportional to the pressure wave's the amplitude.

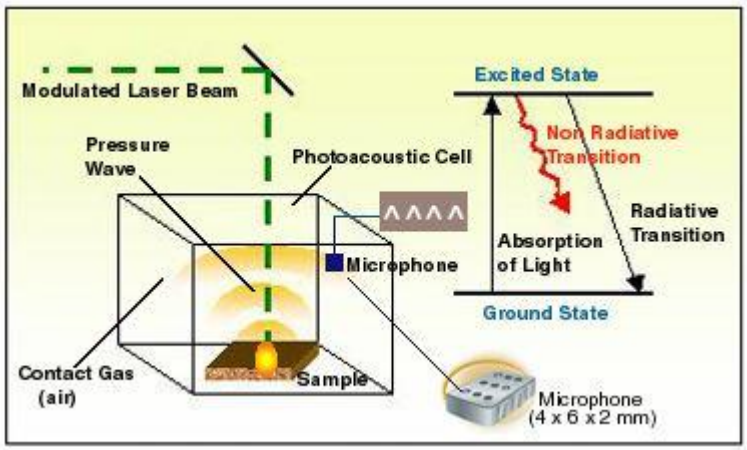

Figure 1.6: Photoacoustic effect from a sample [115].

The sample's photoacoustic spectrum can be obtained by adjusting the incident's light wavelength and obtaining the photoacoustic signal at each wavelength. When the wavelength couples theenergy transition in the material, a variation occurs there in the photoacoustic signal.

1.5 PHOTOACOUSTIC SPECTROSCOPY TECHNIQUES

In this section, the techniques that are involed in photoacoustic spectroscope will be presented.

1.5.1 Excitation

As stated above, mentioned earlier, the photoacoustic effect is generated by the heating that is caused by optical absorption. Periodic heating and cooling of the sample is compulsory for the generation of acoustic waves, otherwise the pressure waves cannot be detected by the transducer. In essence, two different ways can be utilized to implement pressure fluctuations. We can either use modulated or pulsed excitation (Figure 1.7).

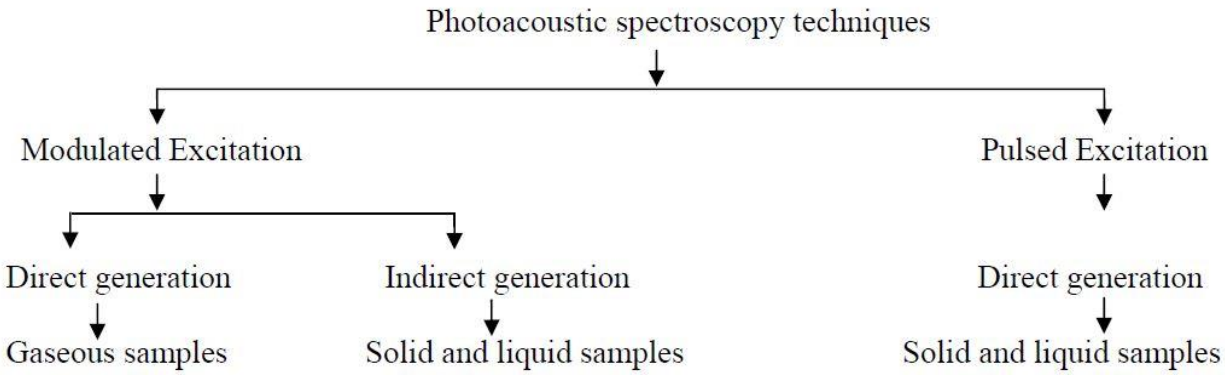

Figure 1.7: Photoacoustic techniques.

1.5.2 Modulated excitation and pulsed excitation

In cases where modulated excitation is used, the source's intensity changes periodically in a form of a square or a sine wave. In this case the duty cycle is 50%. In order to achieve this fluctuation, a mechanical chopper is utilized to modulate the source of light. If we want to achieve a duty cycle higher than 50%, we can perform phase modulation on the light. In opaque materials, modulated sources are used for the determination of absorption. Modulation

frequencies oftenly range from a few Hz up to several kHz. This frequencies are used, because they result in fluctuations within human's audible range and they can be captured by microphones. In modulated excitation, data analysis is performed in the frequency domain. For this reason, lock-in amplifiers are utilized for capturing the signal, and we can analyze the amplitude and the phase of the sound wave.

In cases where pulsed excitation is used, the laser pulses have nanosecond a pulse width. The repetition rate is within a few Hz and thus, the sample is illuminated for a short period of time and a longer dark period is following. This results in a low duty cycle. Short illumination period leads to a rapid thermal expansion of the sample. In pulsed excitation, data analysis is performed in time domain. When the signal is transformed into frequency domain, the spectrum of acoustic waves is wide and goes to the ultrasound range.

1.5.3 Direct and indirect Photoacoustic generation

In the direct photoacoustic generation, short condensed matter, short laser pulses are employed. Short pulses have high peak power and cause rapid expansion in the material. The generated pressure waves, progate in the speed of sound inside the material. These ultrasonic waves are detected directly in the material boundaries. Signal's amplitude is linearly dependent on the energy of the excitation light as well as on the sample's absorption coefficient. The waves can be described by the following equation, $P = \beta c2\ E0\mu a/Cp$. In this equation, β is the thermal expansion coefficient, Cp is the material's heat capacitance and c is the speed of sound. Moreover, the propagation time can be obtained and in fact is the delay between laser pulse and the pressure detected. Consequently, the depth absorption of the material is calculated using the nect formula $z = c \cdot t$. The optical penetration length is the factor that limits the investigation of maximum depth, $\delta = 1/\mu a$.

In the indirect photoacoustic generation, the haeting of the sample is induced by modulate excitation. As a result, the local heating is actually the interferance between the sample and the adjacent gas. For the detection of the photoacoustic signals, photacoustic cells are coupled to spectrometers.

1.5.4 Signal detection

Either in direct or indirect photoacoustic generation, in most of the cases, pressure waves are detected by microphones. However, microphones are not well-suited in highly concentrated materials. This is because of the mismatch of the acoustic impedance and because microphones have a limited bandwidth, so the use of piezoelectric transducers is necessary. Therefore, in quite a lot of cases, piezoelectric transducers are utilized in order to detect of ultrasound pulses in samples. Quartz crystals, piezoelectric ceramics such as lead zirconate titanate (PZT), lead metaniobate, and lithium niobate as well as piezoelectric polymer films can be applied to the detection of laser-induced shock pulses.

A commonly used piezoelectric polymer is polyvinylidene fluoride (PVDF). The limitation of PVDF is the small sensitivity because of its small thickness. For this reason, piezoelectric ceramics are used. When the thickness of the piezoelectric material increases, its sensitivity is also increased. In piezoceramics, the acoustic waves decay exponentially and the pressure waves are overlapped by the very first signal. However, this is not true in case of nanosecond pulses. This is not observed when nanosecond pressure pulses are detected by thin piezoelectric polymer films.

As previously mentioned, laser pulses are cylindrical acoustic sources and they generate cylindrical waves and they are detected vertically to the laser beam. In non-transparent materials, because of the lower optical penetration depth, spherical waves are generated. In such a case, the detection can be done also parallel and perpendicular to the laser beam. In pulsed PA analysis of

solid samples, the generated pressure pulses are often detected in backward mode, where excitation and detection are performed at the same side of the sample. Generally, piezoelectric transducers are opaque, so it is imposible to illuminate through the piezoelectric transducer and detect at the same point. In photoacoustic sensors a transparent prism is used as coupling material for both illumination of the sample and transfer of the acoustic energy to the detector. Another possibility is to illuminate the sample by means of an optical fiber and to detect the pressure pulses by a piezoelectric ring around the fiber. Besides the acoustic detection, optical detection, but these cases are beyond of the scope of this project. of pressure waves is also used.

1.6 CONCLUSIONS

To sum up, the photoacoustic effect is the generation of pressure waves caused by light absorption inside a sample. In order to create this effect, light intensity must be varied, either as modulated light or aspulsed light. The photoacoustic effect can be expressed by measuring the changes in pressure waves by using the appropriate detectors. The variation coming from the electric signal that is generated by the detectors is actually the photoacoustic signal. The measurements of the photoacoustic signal are employed in order to determine the properties of the under investigation material. The photoacoustic effect can be created by all kind of electromagnetic radiation of any kind on frequencies ranging from gamma radiation to microwave and radio frequencies.

In the photoacoustics, the transfer of heat deposited locally takes place via thermal diffusion. A second transport mechanism in which there is direct coupling of the heat energy to the vibrational modes of the material. This is a thermoelastic process governed by the thermal expansion coefficient where a pressure build-up is generated, releasing a stress wave. The rate of transfer of this wave is described by the speed of sound in the material.

A focused nanosecond laser pulse illuminates the sample and, due to absorption, deposits some part of its energy inside the material. This leads to local heating after thermalization of the deposited energy. As a consequence, thermal expansion causes the emission of a pressure wave. A piezoelectric transducer, which is attached to the edge of the sample, is responsible for the detection the photoacoustic wave.

In order to generate acoustic waves, which can be detected by pressure sensitive transducers, periodic heating and cooling of the sample is necessary to generate pressure fluctuations. When modulated excitation is used, light intensity fluctuates periodically with a duty cycle of 50%. For modulated excitation, data analysis is performed in the frequency domain. When pulsed light is used, the laser pulses have a duration in the nanosecond range and the repetition rates are in the range of a few Hz, which results to a low duty cycle. In pulsed excitation, data analysis is performed in the time domain.

2. FUNDAMENTALS OF LASER – MATERIAL INTERACTIONS

2.1 LASER ABSORPTION IN MATERIALS

As mentioned in the first chapter, the first laser was introduced in 1960. This gave a huge rise in the studies of the effects that lasers have on the materials. The first lasers had a lot of limitations, as they were not powerful enough and they were not provide stability during their usage. Since then, lasers and photonics have developed so much and modern lasers are able to be used in a huge variety of applications. Nowadays, lasers provide higher energy, exceptionally good beam qualities, high precision and lasers with different wavelengths are available. The true pioneer of laser metal processing is the Nd:YAG laser and also the CO2 laser, operating in the near infrared region (Figure 2.1). The Nd:YAG and the Nd:YLF lasers are used widely for a lot of processing applications that require the use of lasers.

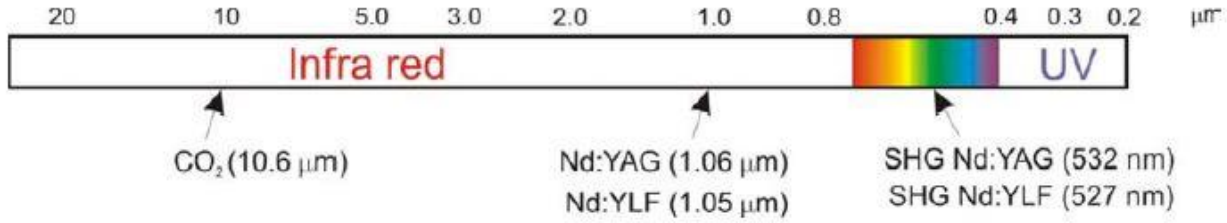

Figure 2.1: The spectrum positions of the CO2, the Nd:YAG and the Nd:YLF laser wavelengths. SHG denotes the second harmonic generated [79).

For the viability of laser applications, laser's electromagnetic energy must be transformed into thermal energy inside the material. The material's light absorption is responsible for determining quantity of the transformed energy. The absorbed energy is the fact that generates the heating and produces the desire effect. Laser absorption is depended on numerous parameters, implicating the laser as well as the material. The most important laser parameters are the wavelength, of the light, the incident angle and the beam polarization. Rarely, the intensity can also affect the absorption. On the material's side, the main parameter that determines the quantity of the absorbed light is the composition [79]. When energy is deposited to the material, it causes local heating and as the temperature is rised, the amount of absorbed light may change, because both electrons and atoms in the material acquire kinetic energy.

One characteristic of lasers is the accurate delivery of huge amount of energy into a limited area of the material with the aim of achieving the desired response. In non-trasparent materials, energy is absorbed near the surface [80-82]. Since the first days of the lasers, researchers noticed that the interaction of high energy lasers with a material is possible to drive into permanent changes in the properties of the material. Numerous books and references could be found about this topic [83-86].

2.2 LIGHT PROPAGATION IN MATERIALS

In some applications it is necessary to control laser intensity and focus the laser on the desired region of a material. The leading ways of controlling the beam methods for control include beam steering, converging optics, and beam shaping with homogenizers [87], refractive elements [88], and diffractive optical elements [89]. However, more advanced optical devices can be utilized such as spatial light modulators [90], deformable mirrors [91], and tunable acoustic gradient index lenses [92]. More information about beam shaping can be found in [93, 94]. When a source of light hits the material's surface, a part of it, is reflected and the rest is propagated inside

the material. The fraction of the incident power that is reflected from the surface R depends on the polarization and angle of incidence θi of the light as well as the index of refraction of the atmosphere n1 and the material n2. The reflection coefficients for the s-polarized and p-polarized components of the light can be calculated from the Fresnel equations [95] (Equations 2.1 and 2.2):

$$R_s = \left[\frac{E_r}{E_i}\right]^2 = \left[\frac{n_1 \cos(\theta_i) - n_2 \cos(\theta_t)}{n_1 \cos(\theta_i) + n_2 \cos(\theta_t)}\right]^2 \quad (2.1)$$

$$R_p = \left[\frac{E_r}{E_i}\right]^2 = \left[\frac{n_1 \cos(\theta_t) - n_2 \cos(\theta_i)}{n_1 \cos(\theta_t) + n_2 \cos(\theta_i)}\right]^2 \quad (2.2)$$

and are related to the transmission coefficients through Ts = 1-Rs and Tp = 1- Rp. When the surface is flat, the above equations can be reduced as shown in equation 2.3:

$$R = R_s = R_P = \left(\frac{n_1 - n_2}{n_1 + n_2}\right)^2 \quad (2.3)$$

A material's reflectivity depends on the frequency of the incident light of a given material will depend on the frequency of the light source. For example, when the light is a normal incidence, the reflectivity of metals are typically between 0.4 and 0.95 in the near UV and visible spectral range, and between 0.9 and 0.99 for the IR [84]. The reflectivity also dependends on the temperature [96]. When small materials are considered, extra optical resonances may occur, which can have an effect on absorption or reflection due [97].

When the light is in the material, light intensity decays with the depth. This is caused because of the absorption and it is determined by the material's absorption coefficient α. In general, α is a function of wavelength and temperature. For constant α, the intensity decays exponentially with depth z as stated by the Beer–Lambert law.

$$I(z) = I_0 e^{-\alpha z} \quad (2.4)$$

where I0 is the intensity just inside the surface having considered the reflection loss.

The absorption depth, δ = 1/α, can be defined as the depth in which the intensity of the transmitted light drops to 1/e of its initial value at the interface. The optical absorption depths of various semiconductors and metals as a function of wavelength can be seen in Figure 2.2. It is worth noted that the absorption depths are short relative to bulk material dimensions.

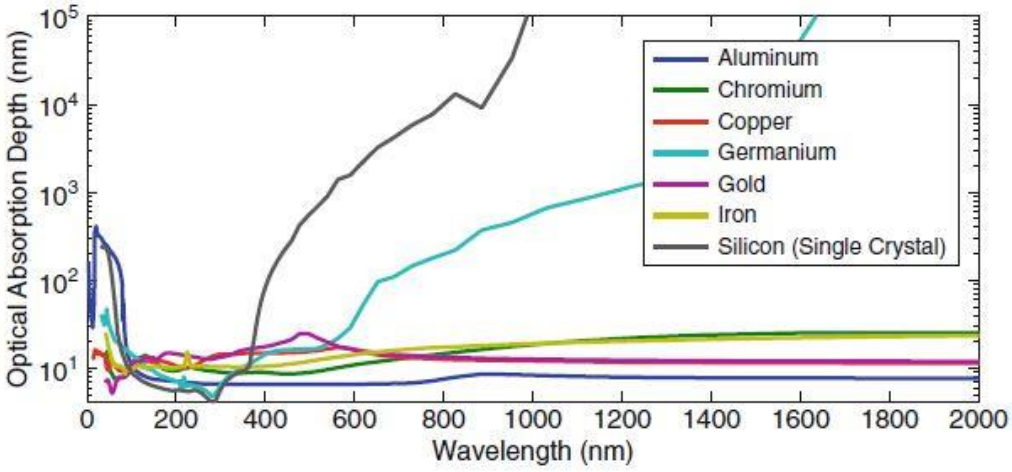

Figure 2.2: Optical absorption depths different materials as a function of wavelength [107].

Everything that was stated so far in this chapter is applicable only in linear optical phenomena. On the other side, some materials, such as glasses, expose non-linearities in their refractive index [98], which can lead to effects such as self-focusing or defocusing [99]. Lasers also exhibit some limitations. In case of laser pulses with a nanosecond duration, we are dealing with the assumption that the absorption is caused only because of single photon interactions. In case of picosecond and femtosecond laser pulses, the exceptionally high momemtary intensity triggers phenomena such as optical breakdown and multiphoton absorption that can lead to a considerably reduction in the absorption depth [100].

2.3 ENERGY ABSORPTION MECHANISMS

The absorption coefficient, is responsible for defining the light absorption in a material as a function of depth. Nevertheless, the material type plays the major role on the mechanisms related to the absorption occurence. Photon energy is responsible for the coupling of photons with the material's free electronic or vibrational states. The laser light absorption in insulators is mainly happen via resonant excitations. After these excited states the energy is transferred to photons. If the energy of the photons is lower that the material's band gap, the energy is not absorbed. For insulators, these energies are close and below to UV frequencies. For seminductors, is beneath the visible and close to infrared frequencies. spectrum for semiconductors [101].

In conductors, free electrons influence the optical absorption [102] and as a consequence, the energy is transferred to lattice phonons due to collisions. In conductors, the plasma frequency is of major importance as it correlates the electron density with the optical properties. When the light frequency is beneath plasma frequency, absorptance and reflectivity are high. On the other hand, when light freaquency is greater than the plasma frequency, reflectivity and absorptance decrease dramatically [103].

In most of the conductors, the thermalization time is ranged between $10^{-12} - 10^{-10}$ seconds, whereas in insulators, the maximum thermalization time is 10^{-6} [84]. In cases where the thermalization rate is higher than the laser excitation rate, we can consider that the absorbed laser energy is directly transformed into heat. This process is called photothermal and the response from the material is handled in a totally thermal way. In case where the thermalization rate is lower than the laser excitation rate, huge excitations are created in the intermediary states and sometimes they are able to break the bonds. This process is called of photochemical and the system's temperature remains stable. When femtosecond laser pulses are utilized, the photochemical processing may be activated [102, 104]. Photophysical mechanisms exhibit both thermal and non-thermal mechanisms [84].

2.4 THE HEAT EQUATION

In photothermal processing, the increased temperature lead to the material response. For this purpose, heat flow in the material is very significant. The heat equation governs both temporal and spatial temperature field development in a material. The heat equation is derived from the conservation of energy and Fourier's law of heat conduction, which states that the local heat flux is proportional to the negative of the gradient of the temperature. In a fixed system with a laser beam the heat equation can be seen in Equation 2.5:

$$\rho(x,T)c_\rho(x,T)\frac{\partial T(x,T)}{\partial t} - \nabla[\kappa(x,T)\,\nabla\,T(x,T)] + \rho(x,T)c_\rho(x,T)\,v_s\,\nabla T(x,T) = \\ = Q(x,T) \tag{2.5}$$

where

ρ: the mass density

c_p : the specific heat at constant pressure

k: the thermal conductivity

and v_s : the velocity of the substrate relative to the heat source.

The left part of the heat equation, describes the evolution of temperature due to heat conduction as well as the convective term v_s to account for the shift in reference frame. The right part embodies how the heat sources and sinks contribute through the volumetric heating rate Q (x, t).

The volumetric heating term Q (x, t) as well as the boundary conditions drive the evolution of the temperature inside the material. In the boundary conditions, convection and radiation cause heat exchange. In most cases, laser irradiation is the main source of volumetric heating. Generally, when the beam profile is of high complexity, the wave equation for the whole spatial intensity distribution inside the material has to be solved, then as input into the heat equation the volumetric heating rate the magnitude of the gradient of intensity has to be used beacause of laser absorption. However, for the case of shallow surface absorption, this contribution can approximately be separated into a spatial shape g (x, y) determined by the beam's profile, an attenuation term f (z) determined from (3.4), as well as a temporal shape q (t), which could be a constant for a continuous wave, a pulse, or even a sequence of pulses. Phase changes or chemical reactions can be accounted for by U (x, t) and the volumetric heating term becomes as shown in Equation 2.6.

$$Q(x,T) = g(x,y)\,f(z)\,q(t) + U(x,t) \tag{2.6}$$

Generally, heat equation is a non-linear partial differential equation, which is difficult to solve and in real systems can be even more complicated because of the changes in optical properties in interaction the light intensity and the temperature. In such cases, the finite element method can be used. Thus, quantitative information generally requires methods such as finite difference or finite element numerical analysis. It must also be considered that the material is heated very quick, the heat equation is not usable and molecular dynamic simulations are required [105]. Nevertheless, afterwrds the first interaction, the heat equation regains validity.

A very significant parameter is the thermal diffusion length $l_T \approx \zeta \sqrt{D_\tau}$, where D = $\frac{\kappa}{\rho c_p}$ is the thermal diffusivity of the material. The thermal diffusion length shows the distance over which temperature changes propagate in time. The factor ζ is a geometric constant. Typically, τ is the laser beam's temporal pulse width. After the first interaction, the thermal propagation results in higher temperatures across the thermal diffusion length. Moreover, changes in the material properties can be monitored, when laser pulse's energy spread during and after the interaction are combined. Utilizing all of the above

2.5 CONCLUSIONS

Light absorption mechanisms determine the amount of transformed energy in the material. The laser parameters of importance are the wavelength, the incident angle and the beam polarization In some cases, the intensity may also be significant. When the light is in the material, light intensity decays with the depth. This is caused because of the absorption and it is determined by the material's absorption coefficient α. In general, α is a function of wavelength and temperature. For constant α, the intensity decays exponentially with depth z as stated by the Beer–Lambert law.

In cases where the thermalization rate is higher than the laser excitation rate, we can consider that the absorbed laser energy is directly transformed into heat. This process is called photothermal and the response from the material is handled in a totally thermal way. In case where the thermalization rate is lower than the laser excitation rate, huge excitations are created in the intermediary states and sometimes they are able to break the bonds. This process is called of photochemical and the system's temperature remains stable. When femtosecond laser pulses are utilized, the photochemical processing may be activated. Photophysical mechanisms exhibit both thermal and non-thermal mechanisms. In photothermal processing, the increased temperature lead to the material response. For this purpose, heat flow in the material is very significant. The heat equation governs both temporal and spatial temperature field development in a material. The heat equation is derived from the conservation of energy and Fourier's law of heat conduction, which states that the local heat flux is proportional to the negative of the gradient of the temperature.

Having utilized all of the above mentioned, we can grasp the significance a laser interacting with a material and the complexity behind this interaction. To sum up, The optical absorption depth is tiny for non-trasnsparent samples. Shorter laser pulse width causes evenly small thermal diffusion length and as a consequence we can deem all of the absorbed energy without thermal diffusion.

3. SIMULATIONS

3.1 HEAT TRANSFER IN SOLIDS 2D

For understanding the mechanism of heat transfer in solids, I simulated 2D models in Comsol Multiphysics software. I chose to run time dependent simulations on two different elements, copper and silicon.

To begin with in 2D simulations, I draw a rectangle geometry with dimensions 5 cm width and 10 cm height. For the first material I used copper which has high thermal conductive of 400 W/(m*k) as shown in Table 3.1 and for the second material I used silicon which has lower thermal conductivity which is 130 W/(m*k) as shown in Table 3.2. The heat is dispersed equally on the whole surface of the material. The external temperature is 298.15 K and the material temperature is 293.15 K. The heat flux is applied on each side of the rectangle and the heat transfer coefficient in free convention air is h = 0.5 W/(m^2*k) as can be seen in Table 3.3.

Table 3.1: Copper properties

Property	Name	Value	Unit
Heat capacity at constant pressure	Cp	385[J/(kg*K)]	J/(kg*K)
Density	ρ	8700[kg/m^3]	kg/m^3
Thermal conductivity	K	400[W/(m*K)]	W/(m*k)
Relative permeability	mur	1	1
Electrical conductivity	S	5.998e7[S/m]	S/m
Coefficient of thermal expansion	αv	17e-6[1/K]	1/K
Relative permittivity	ε_r	1	1
Young's modulus	E	110e9[Pa]	Pa
Poisson's ratio	ν	0.35	1
Reference resistivity	r_0	1.72e-8[ohm*m]	Ω*m
Resistivity temperature coefficient	a_T	0.0039[1/K]	1/K
Reference temperature	Tref	298[K]	K

Table 3.2: Silicon properties

Property	Name	Value	Unit
Heat capacity at constant pressure	Cp	700[J/(kg*K)]	J/(kg*K)
Density	ρ	2329[kg/m^3]	kg/m^3
Thermal conductivity	K	130[W/(m*K)]	W/(m*k)
Relative permeability	mur	1	1
Electrical conductivity	S	1e-12[S/m]	S/m
Coefficient of thermal expansion	αv	2.6e-6[1/K]	1/K
Relative permittivity	ε_r	11.7	1
Young's modulus	E	170e9[Pa]	Pa
Poisson's ratio	ν	0.28	1
Refractive index	n	3.48	1
Refractive index	ki	0	1

Table 3.3: Heat fluxes for various cooling or heating transfer modes (Based on 85° C surface temperature and 20°C ambient temperature.)

Cooling / Heating mode	Heat flux (kW/m^2)
Free convection air	0.5
Forced convention air	5
Free convection immersion	10
Forced convection immersion	500

Then I meshed the rectangle using finite element method. Each element is a free triangular. The maximum element size is 0.001 m and the minimum element size 1.5E-5 m. The maximum element growth is 1.3 and the curvature factor 0.3. The object can be seen in Figure 3.1.

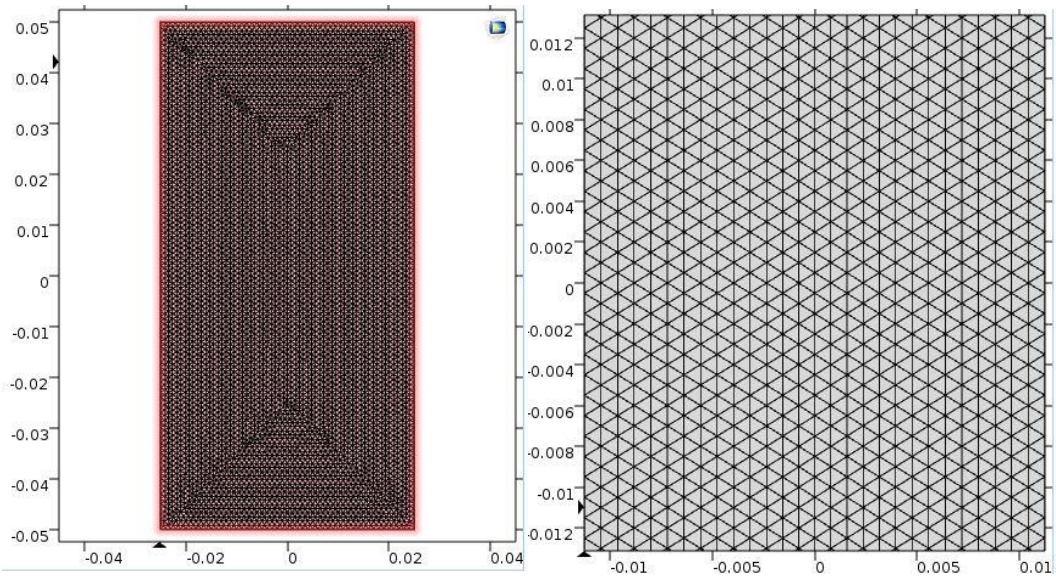

Figure 3.1: Left hand side image - Free triangular finite elements on the object. Right hand side image - Zoomed area of the object.

The time dependent simulation was performed in the interval 0-10 sec with a time step of 1 sec. The summary results can be seen in the following figures. (Figures 3.2, 3.3, 3.4 & 3.5)

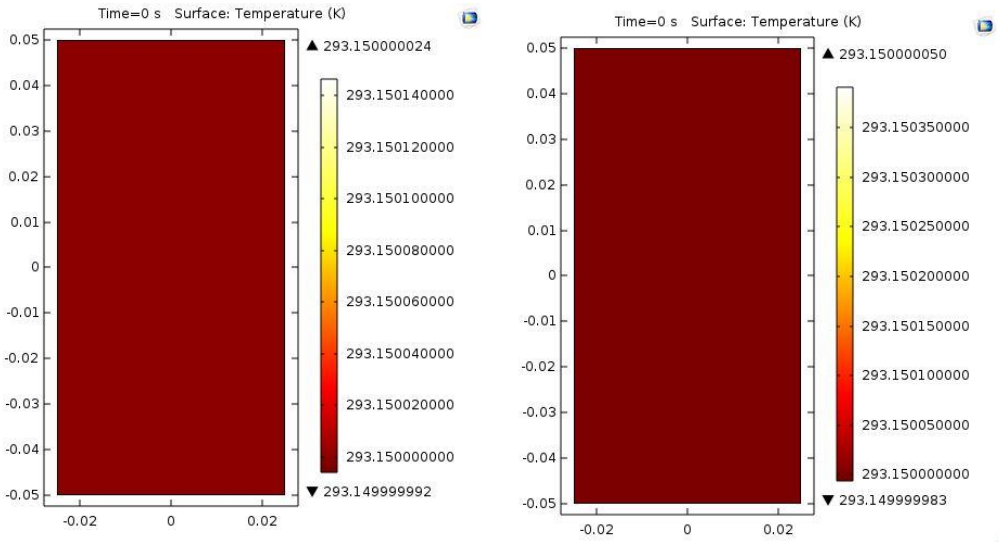

Figure 3.2: 2D model initial temperatures for copper (left) and silicon (right).

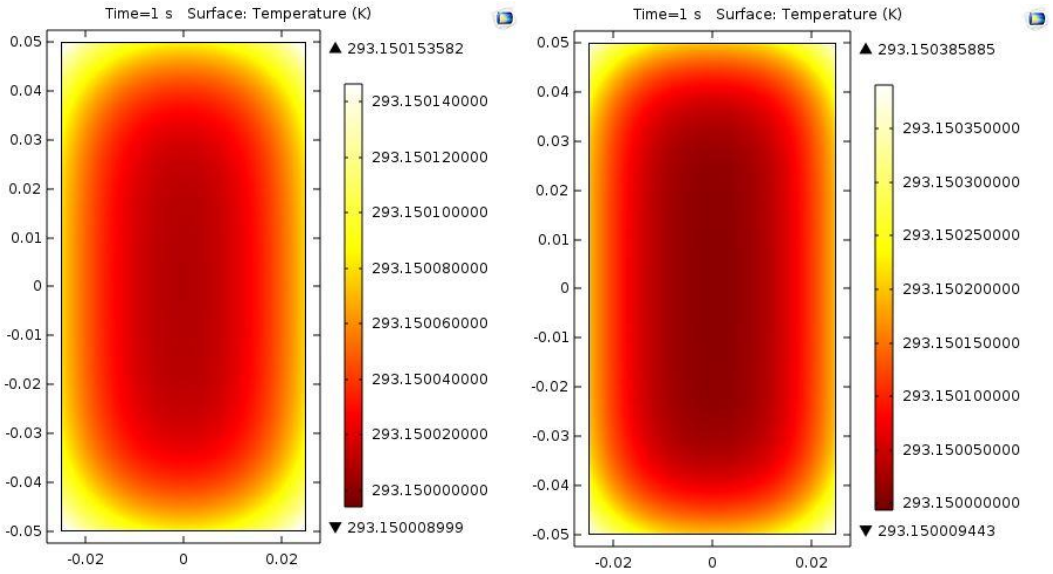

Figure 3.3: Heat Absorption 2D model - Temperatures after 1 sec for copper (left) and silicon (right).

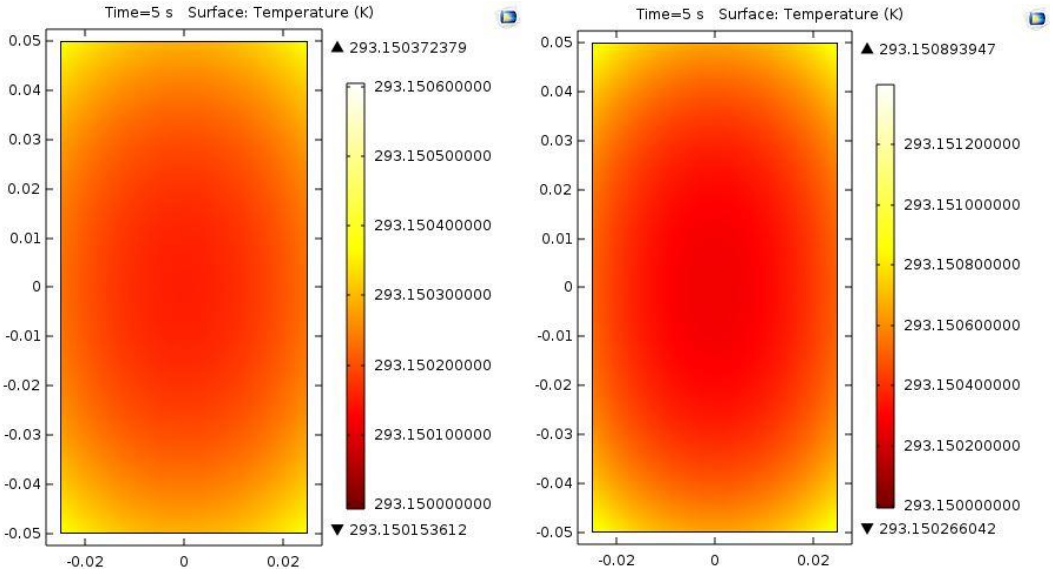

Figure 3.4: Heat Absorption 2D model - Temperatures after 5 secs for copper (left) and silicon (right).

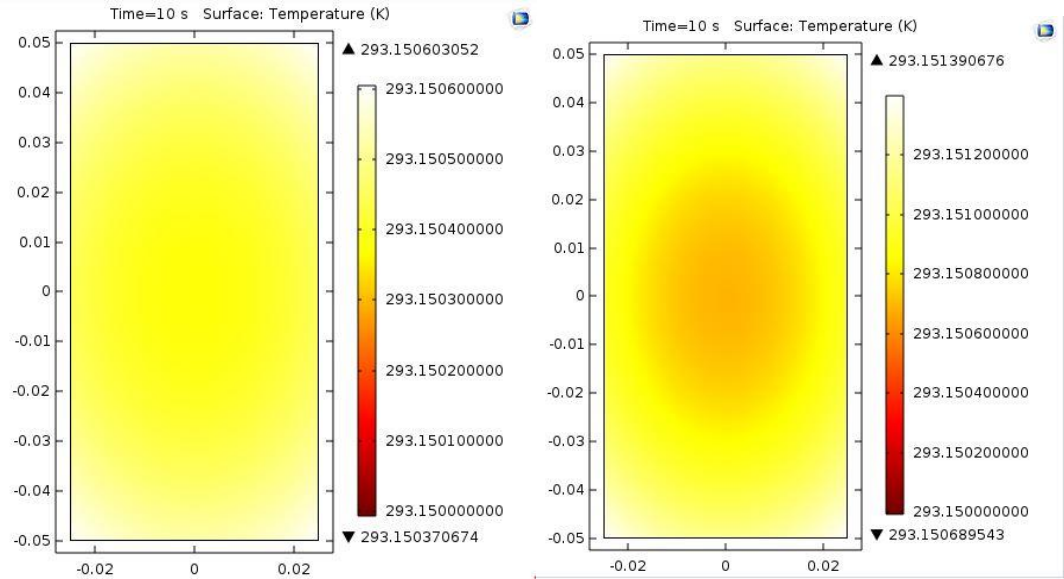

Figure 3.5: Heat Absorption 2D model - Temperatures after 10 secs for copper (left) and silicon (right).

3.2 LASER MATERIAL INTERACTIONS USING THE BEER – LAMBERT LAW

As previously mentioned, when an incident laser beam impringes a transparent material, some of the beam energy is deposited inside the material. In such a case, Beer-Lambert law can be used in order to describe this absorption. In the below simulation model, I have simulated the heating process that is caused by the laser absorption. The following model demonstrates the absorption of the laser light and the resultant heating for a material with temperature-dependent absorptivity [106]. In this simulation it is assumed that the laser light is a single wavelength and the material is set to be transparent. So, there is When light is incident upon a transparent material, some of the energy will be absorbed by the material itself. The Beer-Lambert law was previously examined and can take the next differential form for the light intensity:

$$\frac{\partial I}{\partial z} = a(T)I$$

Because the temperature is varied both in space and time, I have also chosen to solve the partial differential equation for temperature distribution inside the material:

$$\rho C_P \frac{\partial T}{\partial t} - \nabla \cdot (k \nabla T) = Q = a(T)I$$

In this equation Q is the source term and is equal to the incident light absorption.

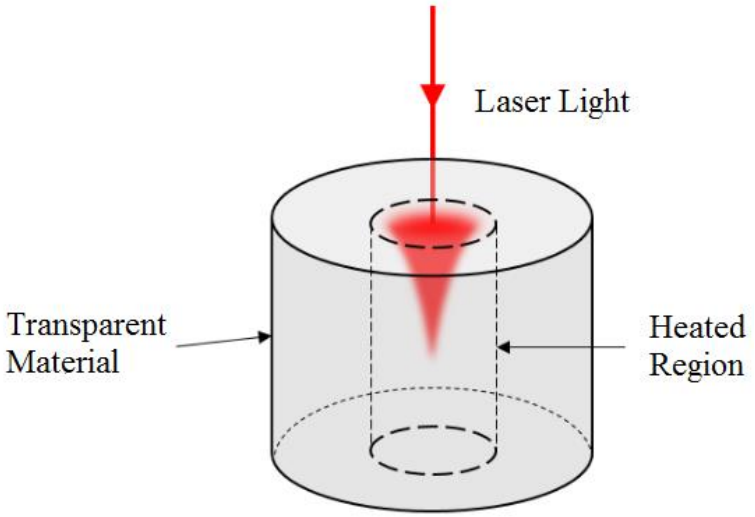

Figure 3.6: The region that will be aimed by the laser light.

For this problem a solid cylinder of material with dimension of 20 mm in diameter and 25 mm in length (figures 3.6 & 3.7) with a laser incident on the top is designed. For this simulation I have splitted the object in two partitions. Both volumes represent the same material, the Beer-Lambert law will be solved for both the inside and outside domains - both regions are heating up by the beam.

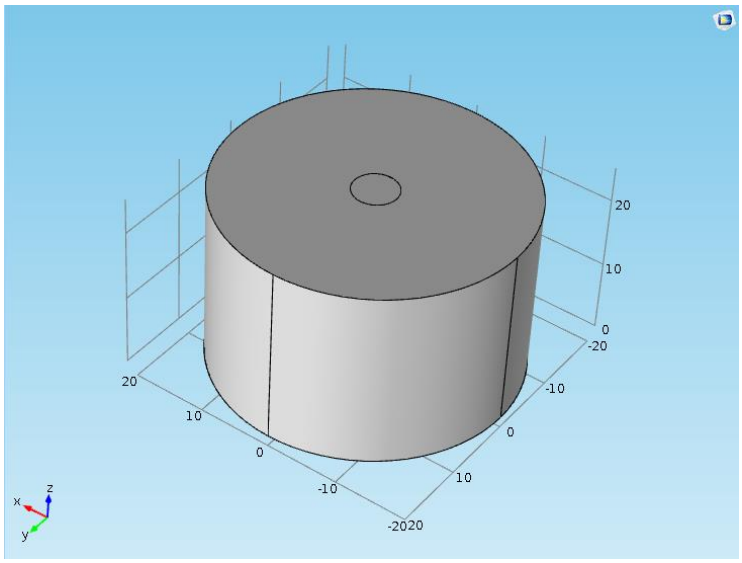

Figure 3.7: The cylindrical geometry.

The general form PDE is used for the Beer-Lambert law implementation. The dependent variable is light intensity I. The units for this model are intensity and heat source. All of the previously mentioned are shown in the figure below (Figure 3.8).

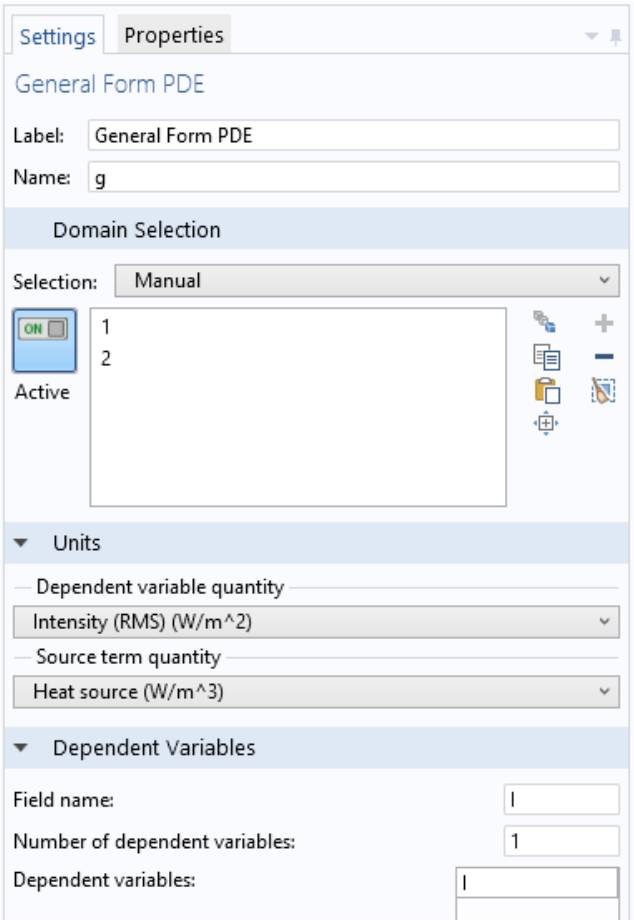

Figure 3.8: The Dependent Variables and Units settings.

The implementation of Beer-Lamber law is illustrated in Figure 3.9 and uses a temperature-dependent absorption coefficient.

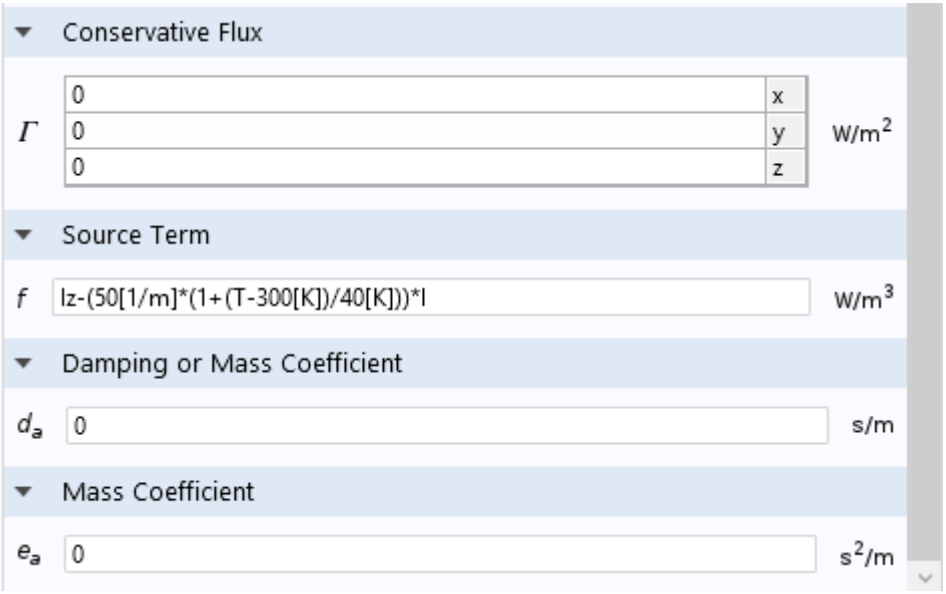

Figure 3.9: Implementing the Beer-Lambert law.

The initial values have no effect in the solution of the equation as it is stationary and linear. Next, I set zero flux boundaty condition in all surfaces except the top surface which is the surface where the incident light enters the material. Zero Flux boundary condition is appropriate on most faces, with the exception of the illuminated face. The laser beam follows a Gaussian. After that, I set the intencity of the incident light at 1 W/mm2. Because part of the laser beam is reflrcted, the intensity of the light is reduced to the 95% of the initial intensity.. I have done the implementation using Dirichlet Boundary Condition (Figure 3.10). At the bottom surface I also applied a Zero Flux boundary condition, because the laser light goes out of this domain.

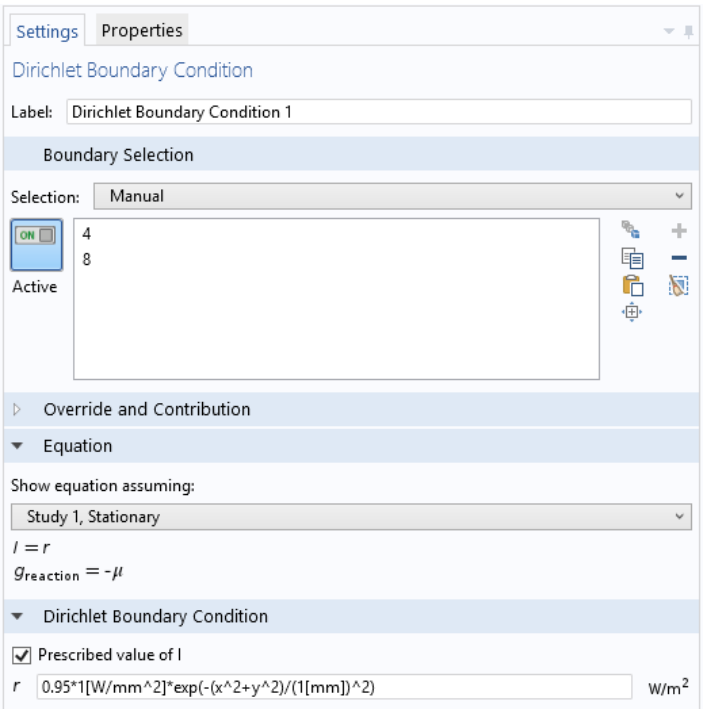

Figure 3.10: The Dirichlet Boundary Condition and the incident intensity inside the sample.

Finally, for the material I used a glass (quartz) material. Glass (quartz) properties can be seen in Figure 3.11.

	Property	Name	Value	Unit	Property group
☑	Density	rho	2210[kg/m^3]	kg/m³	Basic
☑	Thermal conductivity	k	1.4[W/(m*K)]	W/(m·K)	Basic
☑	Heat capacity at constant pressure	Cp	730[J/(kg*K)]	J/(kg·K)	Basic
	Relative permeability	mur	1	1	Basic
	Electrical conductivity	sigma	1e-14[S/m]	S/m	Basic
	Relative permittivity	epsilonr	4.2	1	Basic
	Refractive index	n	1.5	1	Refractive index
	Refractive index, imaginary part	ki	0	1	Refractive index

Figure 3.11: Glass (Quartz) properties.

The heat source itself is simply the absorption coefficient times the intensity, or equivalently, the derivative of the intensity with respect to the propagation direction, which can be entered as shown below (Figure 3.12).

Figure 3.12: The absorbed light is used as the heat source.

For the top surface boundary, because of the temperature rise that is caused by laser light, an important heat loss may be experienced. For this reason, the top surface is set as a diffuse boundary condition. (Figure 3.13).

Figure 3.13: Top surface thermal radiation using surface emissivity.

So, everything is ready to run the simulations. The figures below shows the surface temperature (Figures 3.14, 3.15 & 3.16), temperature inside the material (Figures 3.17, 3.18 & 3.19), and light intensity in the material (Figure 3.20).

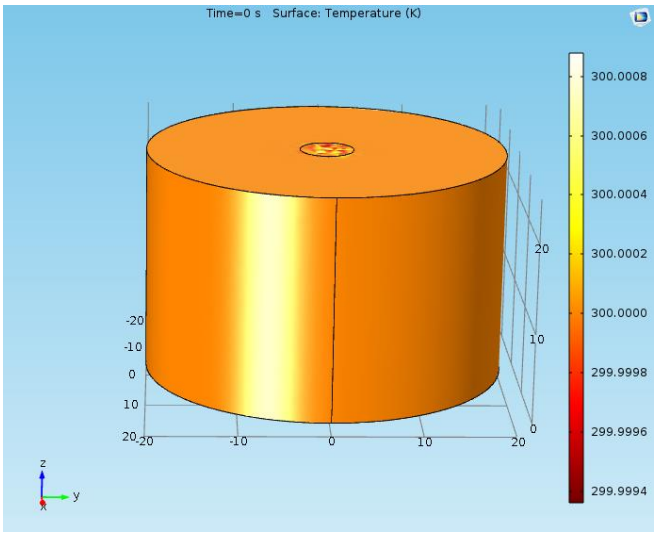

Figure 3.14: Surface temperature for t = 0 sec.

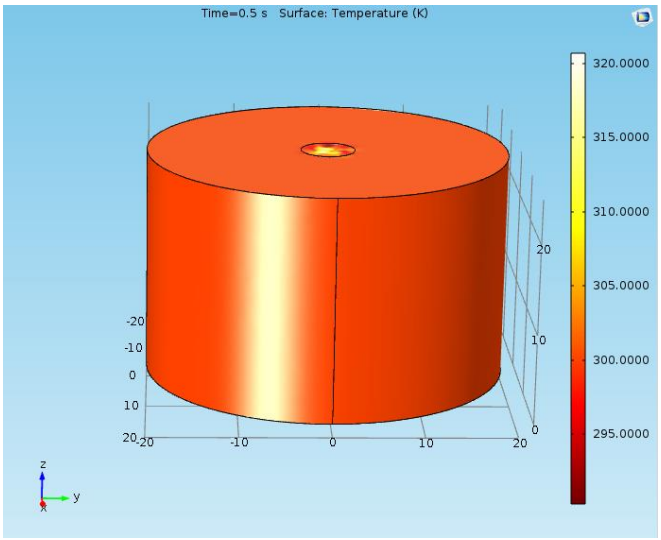

Figure 3.15: Surface temperature for t = 0.5 sec.

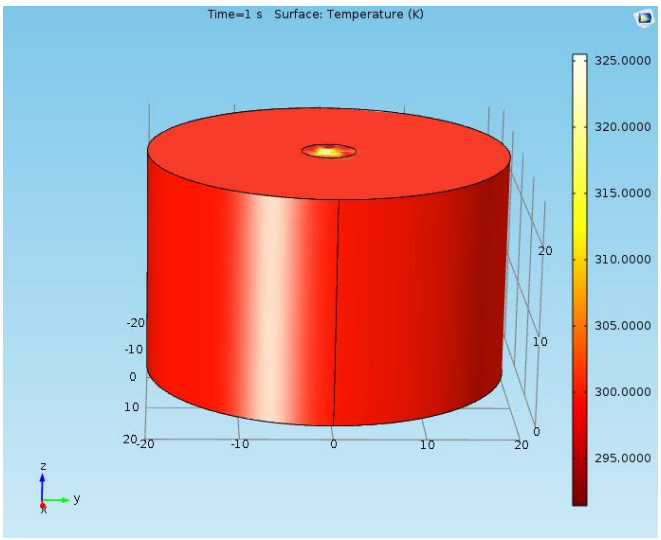

Figure 3.16: Surface temperature for t = 1 sec.

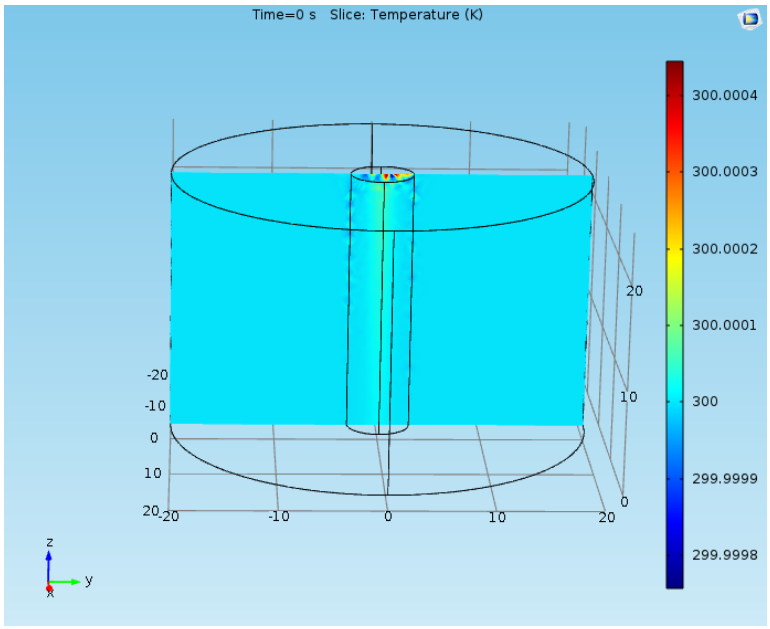

Figure 3.17: Central slice temperature t = 0 sec.

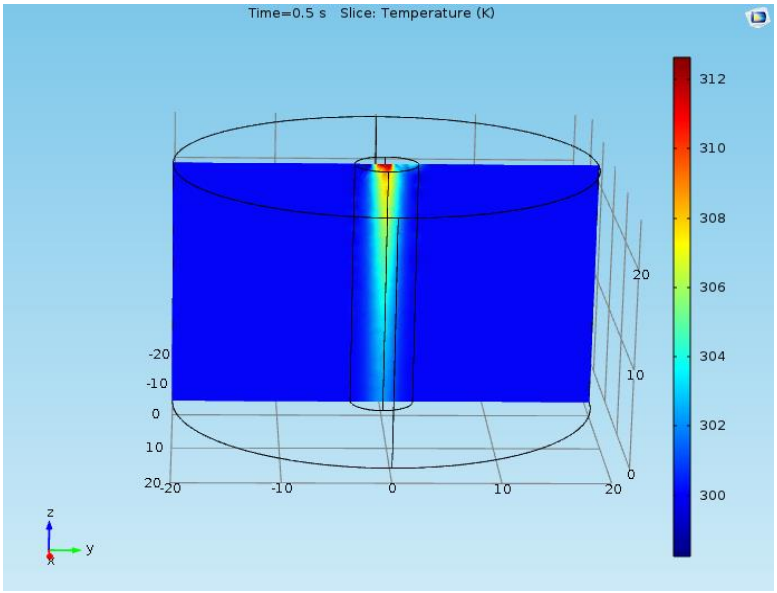

Figure 3.18: Central slice temperature t = 0.5 sec.

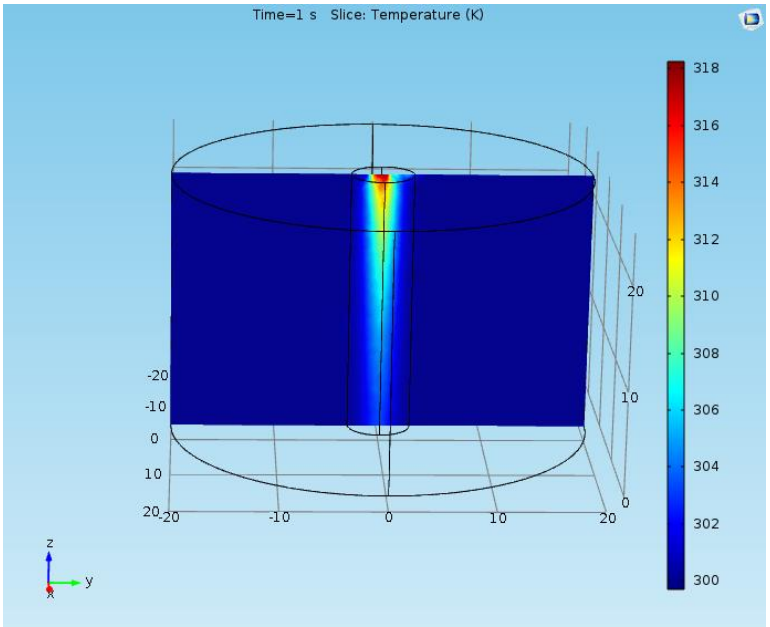

Figure 3.19: Central slice temperature t = 1 sec.

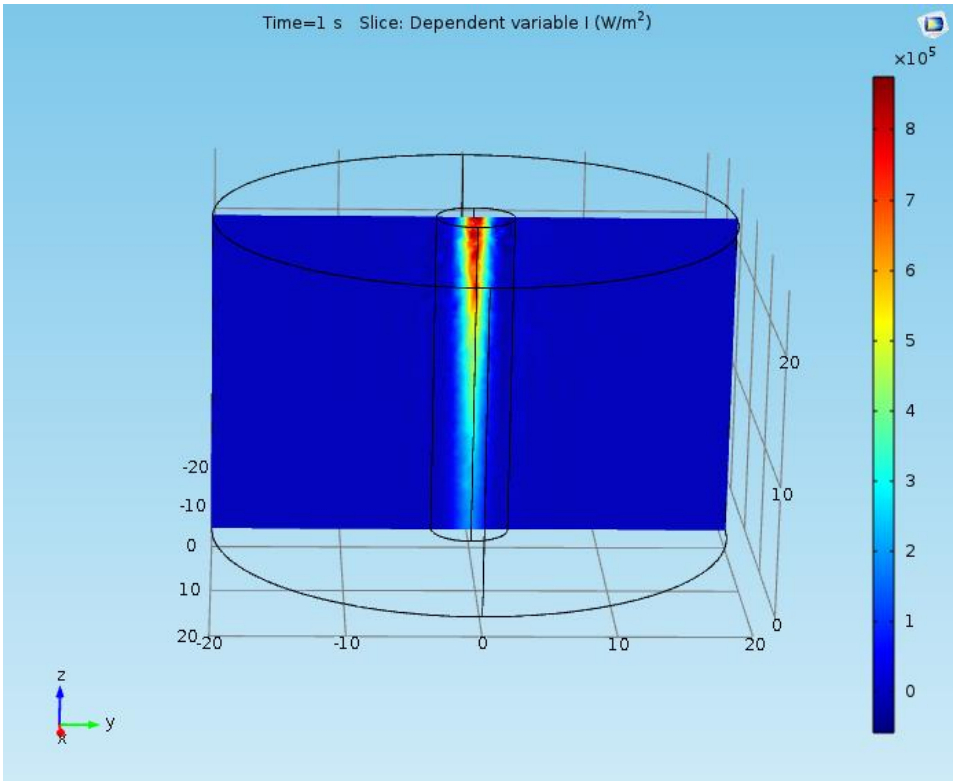

Figure 3.20: Light intensity inside the material.

The next model is based on the calculation of heating a rectangular thin metallic film with a laser beam of nanosecond and picosecond pulse duration and analyzing the accompanying temperature change in the material. The parameters considered in the modeling include donor film thickness, laser fluence, pulse duration, thermo-physical and optical properties of material [106, 107].

In case of nanosecond pulses it is a good approximation to use a one-step heating process as the electron-phonon thermal relaxation is much shorter compared to the laser pulse length and it gets sufficient time to establish local thermal equilibrium with the lattice. It is assumed that the incident energy is converted into heat instantaneously. The heat transfer using a nanosecond to tens of picosecond pulse duration laser source can be modeled by Eq.3.1.

$$\rho C \frac{\partial T}{\partial t} = \nabla \cdot (k.\nabla T) + Q(x, y, t) \tag{3.1}$$

where Q(x, y, t) [W/m^3] is the laser energy density applied to the material, it is a function of laser intensity and Lambert-Beer law and mathematically expressed by Eq. 3.2 below.

$$Q(x, y, t) = I(x, t) * (1 - R) * a * \exp(-a * y) \tag{3.2}$$

Here I(x, t) ([W/m^2] is the laser intensity term in temporal and spatial domain. A Gaussian laser pulse in temporal and spatial domain is used and hence it can written in mathematical form as given by Eq. 3.3 below.

$$I(x,t) = I_0 * \exp\left(-\frac{x^2}{r^2}\right) * \exp(-\frac{3.5(t-\tau)^2}{\tau^2}) \quad (3.3)$$

The incident laser intensity I_0 [W/m^2] can be expressed by Eq. 3.4

$$I_0 = \frac{E}{\tau * A} \quad (3.4)$$

The optical properties of the material (α and R) are function of wavelength, and are calculated for the wavelengths of the laser pulse used in the model. These parameters can also be a function of temperature and wavelength. The values of reflectivity, absorption coefficient and optical penetration depth at different wavelengths are summarized in table 3.4. Also the thermo-physical properties like thermal conductivity, heat capacity and material density can behave differently at elevated temperatures and it is discussed in table 3.3.

Table 3.4: Optical properties of the material at different wavelengths.

Wavelength (nm)	Absorption coefficient (1/m)	Optical penetration depth (nm)	Reflectivity
355	6.8E+07	14.6	0.42
535	6.1E+07	16.4	0.61
1064	8.1E+07	12.3	0.97

The material properties used in this modeling work include absorption coefficient, reflectivity, heat capacity, thermal conductivity and density. It can be categorized into optical and thermo-physical properties.

Absorption Coefficient (α): The absorption coefficient α, is a function of wavelength, λ, and mathematically it is given by Eq. 3.5.

$$a = \frac{4\pi\kappa}{\lambda} \quad (3.5)$$

where is k the extinction coefficient. At λ=355 nm, k = 1.93. On substituting the values in Eq. 3.5, the absorption coefficient of copper at =355 nm can be obtained as 6.8*10^7 m^{-1}. The absorption coefficient, reflectivity and optical penetration depth of copper at 355 nm, 532 nm and 1064 nm wavelength at room temperature is summarized in table 3.4. The absorption coefficient can also vary with respect to target. The formula for absorption coefficient as a function of temperature at a fixed wavelength and temperature coefficient of resistance. It is expressed in mathematical form by Eq. 3.6.

$$\alpha(T) = \sqrt{\frac{4\pi\sigma_0}{\varepsilon_0\lambda c[1+\beta(T-T_0)]}} \quad (3.6)$$

where T[K] represents temperature at a given position and time, σ_0 [Ω^{-1} m^{-1}], target conductance, ε_0 [Fm^{-1}], permittivity of free space, λ[m], laser wavelength, c[ms^{-1}], laser propagation velocity in vacuum, β[K^{-1}], target temperature coefficient of resistance, T0[K], initial temperature. The plot of absorption coefficient vs. temperature is made for copper. It can be observed from figure 3.21, the absorption coefficient decreases at elevated temperature.

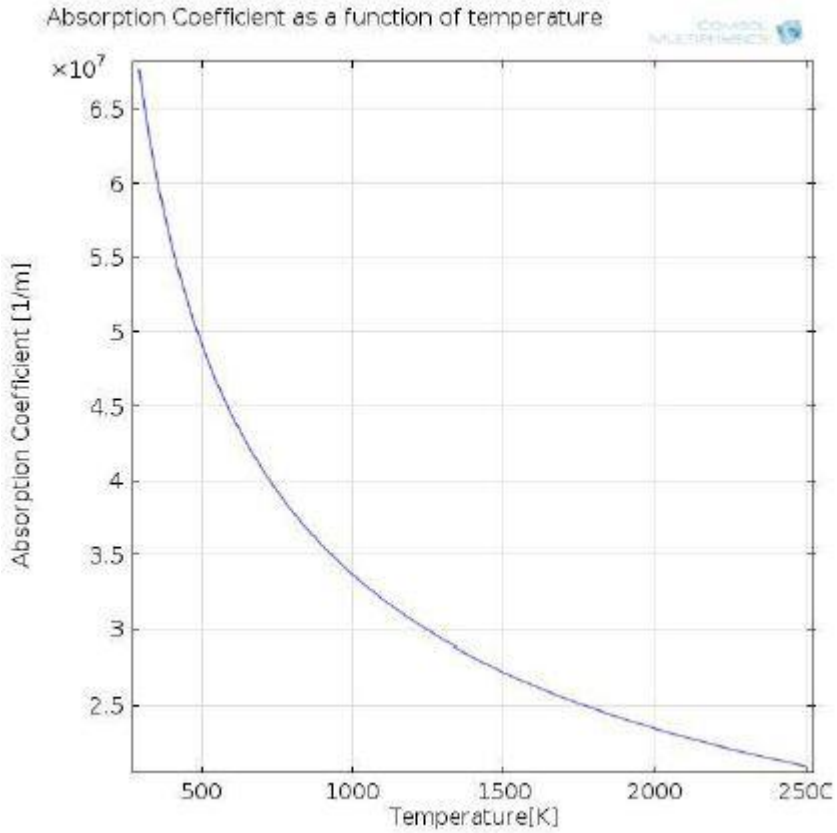

Figure 3.21: Absorption coefficient as a function of temperature.

Reflectivity of a material is a function of wavelength and temperature. For a fixed wavelength, R can be calculated by Eq. 3.7.

$$R = \frac{(1-n)^2+\kappa^2}{(1+n)^2+\kappa^2} \tag{3.7}$$

where n and k are refractive index and extinction coefficient of a material. At λ=355 nm, n=1.34 and κ=1.93, therefore R=0.42036. Reflectivity is also dependent on temperature, it decreases with increasing temperature and the difference is visible for longer wavelength, but for 355 nm wavelength, the change is reflectivity is almost negligible and hence a constant value is used in the simulations.

The heat capacity of copper at constant temperature is taken from Table 3.1 as 385 [J/(kg*K)] An expression for temperature dependent heat capacity for bulk copper is taken from the references, the constant values denote the polynomial curve fit data and it can be given by Eq. 3.8.

$$C_P(T) = 313.7 + 0.324 * T - 2.687 * 10^{-4} * T^2 + 1.257 * 10^{-7} * T^3 \tag{3.8}$$

A plot of C_p (T) vs. T is shown in Figure 3.22, it can be observed that C_p increases linearly until it reaches melting point but once the material melts, the increase is exponential.

The thermal conductivity of copper at fixed temperature is 388 [W/m*K].The thermal conductivity of a material changes with change in target temperature and for copper; the

temperature dependent k for bulk copper is taken from references, the constant values denote data for polynomial curve fit, and given by Eq. 3.9.

$$k[T] = 407.9 - 0.0272 * T - 2.658 * 10^{-5} * T^2 - 3 * 10^{-9} * T^3 \quad (3.9)$$

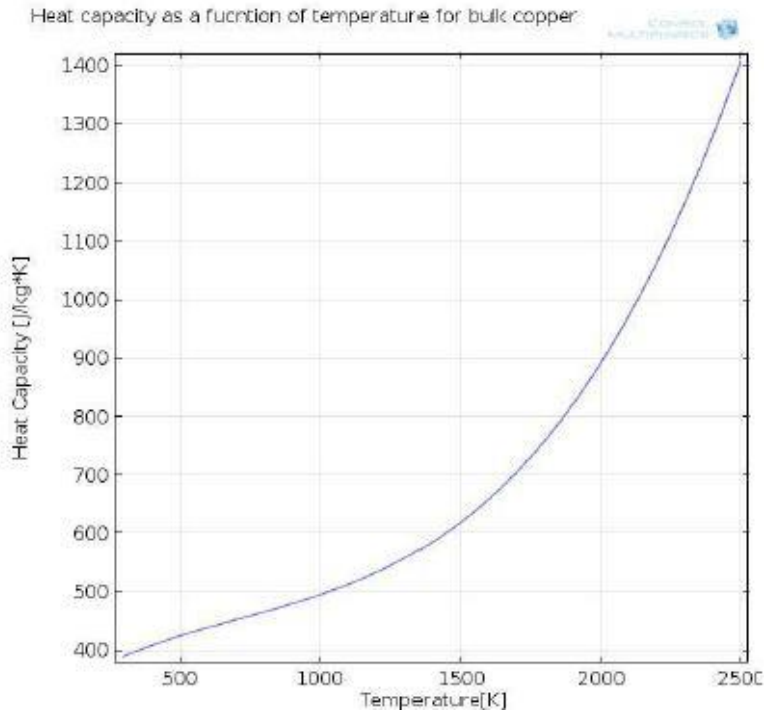

Figure 3.22: Heat capacity as a function of temperature for bulk copper.

A plot of temperature vs. thermal conductivity is shown in Figure 3.23, it can be observed from the graph that, with increase in temperature thermal conductivity decreases which can be ascribed to the scattering effects with increasing temperature. The thermal conductivity can also be defined as a function of film thickness, The thermal conductivity of thin copper films has been measured for a temperature range of 100-500 K, it was observed that the thermal conductivity decreases with decreasing thickness which can be due to scattering of electrons from thin film surface or and due to impurity scattering.

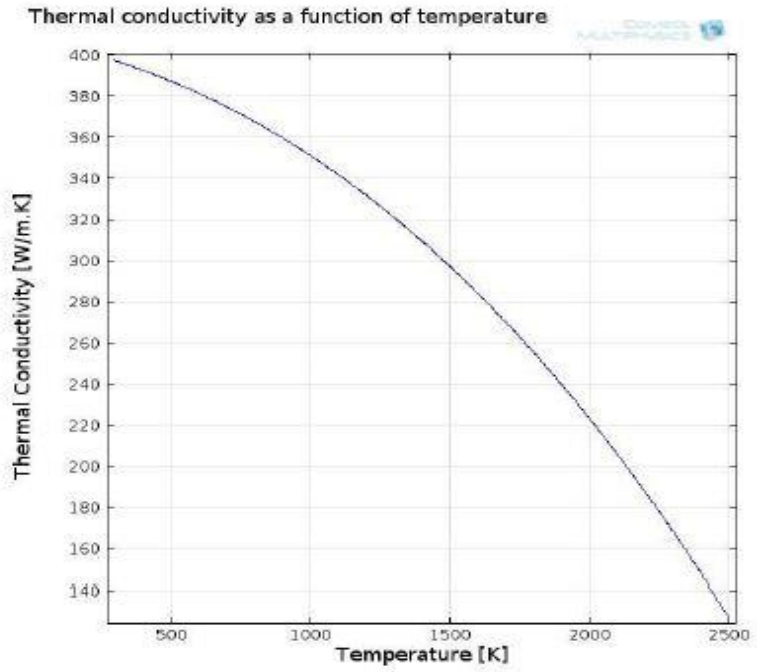

Figure 3.23: Thermal conductivity as a function of temperature for bulk copper.

Table 3.5 : Material properties of copper 2.

Properties	Symbols	Units	Constants
Density	P	kgm^{-3}	8940
Heat Capacity	C_P	J/kg*K	385
Thermal Conductivity	K	W/m*K	388
Reflectivity (at λ=355nm)	R	--	0.42036
Absorption Coefficient (at λ=355nm)	A	1/m	6.7681*10^7
Melting Temperature	T_m	K	1357
Boiling Temperature	T_b	K	2835

In order to understand the transfer process using a nanosecond and a picosecond laser pulse, surface temperature as well as thermal contours plot is analyzed to study the heat diffusion mechanism. Figure 3.24 display the temperature distribution in a 200 nm thick copper donor layer irradiated with a fluence of 583 mJ/m^2 at 15 ns pulse length and 293 mJ/m^2 at 10ps pulse length respectively. The wavelength considered is 355 nm.

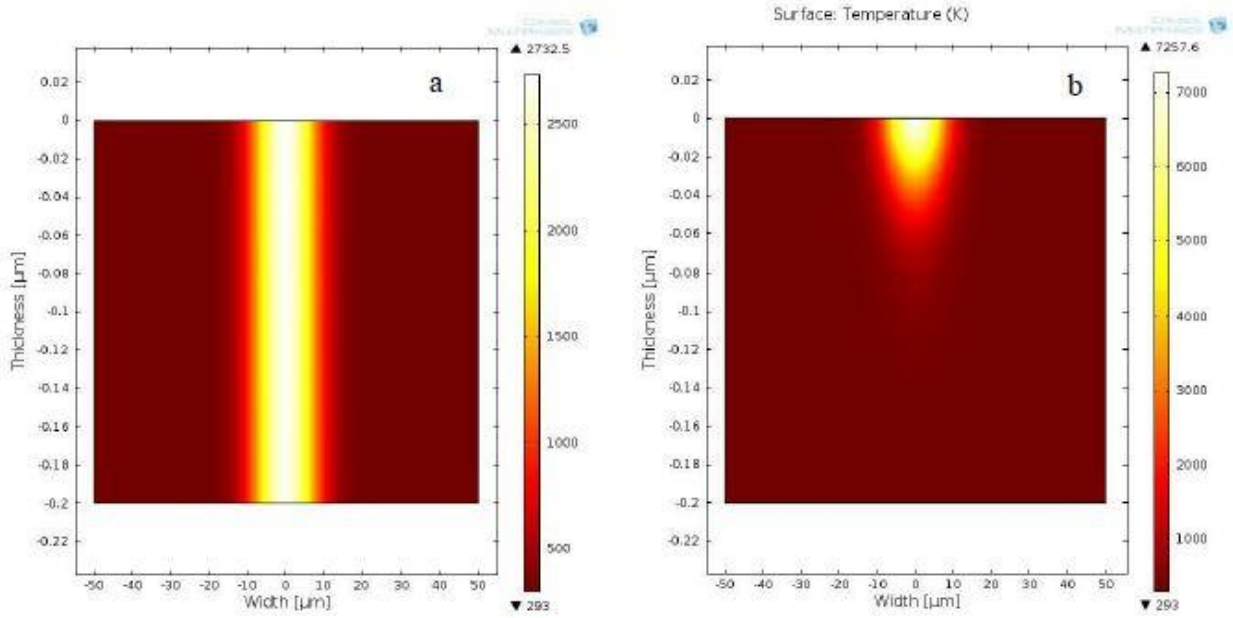

Figures 3.24: Left hand side - Heat distribution along a 200 nm thick copper layer at a wavelength of 355 nm, 583 mJ/cm2 at 15 ns pulse duration and the diffusion time is 15 ns. Right hand side 293 mJ/cm2 at 10 ps pulse duration and the diffusion time is 10 ps. The color legend represents temperature. The Gaussian beam used has a beam diameter of 17.5 µm.[107].

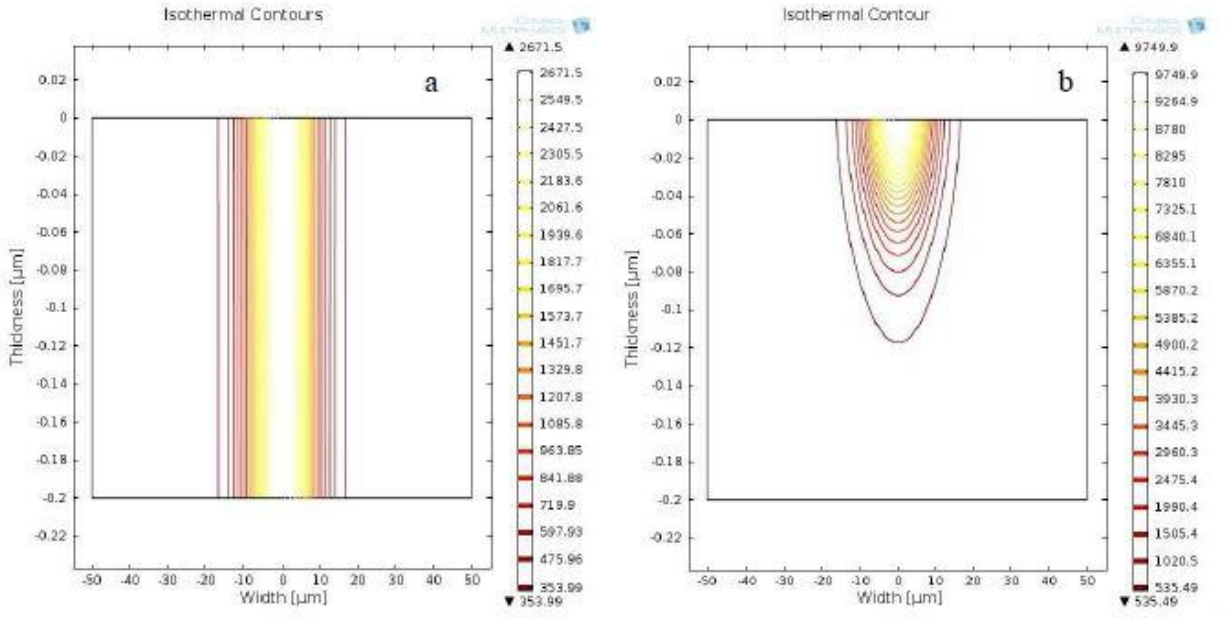

Figures 3.25: Left hand side - Thermal contour plots of a 200 nm thick copper layer with a laser irradiance of 583 mJ/cm2 at 15 ns pulse duration. Right hand side 293 mJ/cm2 at 10 ps pulse duration. The color legend represents temperature and the Gaussian laser beam has a diameter of 17.5 µm.[107]

From Figures 3.24 and 3.25, it is observed that heat diffuses to a longer extent for a nanosecond pulse compared to a picosecond pulse and again the reason could be due to the longer thermal penetration depth of a nanosecond pulse compared to a picosecond pulse.

3.3 BEAM SPLITTER

A beam splitter is an optical devicethat is used for splitting a beam of light in two parts. One possible way of creating a beam splitter is to deposit a thin layer of metal between two glass prisms. The incident beam is slightly attenuated within the layer and then split into two different paths. In this simulation model the thin metal layer using a transition boundary condition. The losses in the thin metal layer are also computed. The beam splitter model in the 2D plane, is shown in Figure 3.26, with the assumption that the electric field is polarized perpendicular to the plane. A Gaussian beam of wavelength 700 nm propagates in the x axis through the glass (quartz) prism of refractive index n = 1.5. A 13 nm thin layer of silver deposited between the two prisms splits the beams. [108]

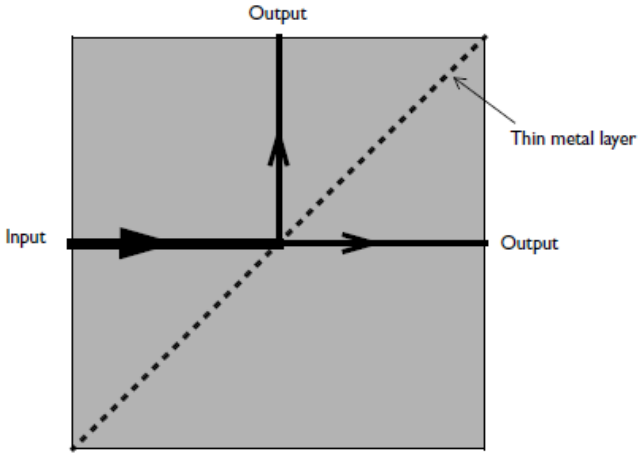

Figure 3.26: A beam splitter composed of two prisms with a thin layer of metal between them.

The model geometry is a square region and the Gaussian beam crosses the silver layer. The focus of the beam is at the left boundary, so the expression for the beam intensity at the focal plane can be used as the excitation. The expression for the relative electric field intensity at the focal plane of a Gaussian is

$$E(y) = \exp(-(\frac{y}{w})^2)$$

where w = 3500 nm is the beam waist, and the y = 0 is the position where the beam is cenetered and hits the target. This expression is used as a port boundary condition on the left side to model the incident beam. All the other domain boundaries models were specified using Scattering Boundary Conditions. These conditions are appropriate when they are placed several wavelengths away from any scattering objects and the wave is known to be traveling at normal incidence.

The thin silver layer is modeled using a Transition Boundary Condition. At a free-space wavelength of 700 nm, the dielectric of silver is about $\varepsilon_r = -16.5 - 1.06i$, where the imaginary part is responsible for the losses. According to Comsol Multiphysics guidelines it is imperative to mesh the two domains with triangular elements, with the maximum size set such that there are six elements per wavelength in the glass.

For understanding the mechanism of optical scattering and the use of beam splitter, I simulated 2D model in Comsol Multiphysics software. I chose to run simulations in frequency domain. To begin with, we should define some global parameters as shown on the following table (Table 3.6).

Table 3.6: Global Parameters for the model.

Name	Expression	Value	Description
Ida0	700[nm]	7E-7 m	Vacuum wavelength
Ida	Ida0/1.5	4.667E-7 m	Material wavelength
f0	C_const/Ida0	4.283E14 1/s	Frequency
h_max	0.2*Ida	9.333E-8 m	Maximum mesh element size
eps_AG	-16.5-1.06*i	-16.5-1.06i	Relative dielectric constant for silver

In these parameters, c_const is a predefined Comsol constant for the speed of light in vacuum and lda is the wavelength i n the material, defined as the vacuum wavelength divided by the refractive index. In this case, 1.5 is the refractive index of the glass material that is used in the model.

For the geometry of the prism, I draw two polygons (triangles). Next the boundary conditions must be defined. First of all, starting from the scattering boundary conditions. In these boundaries the incident beam light will be scattered. For this purpose, I chose boundaries 2, 4 and 5 (Figure 3.27).

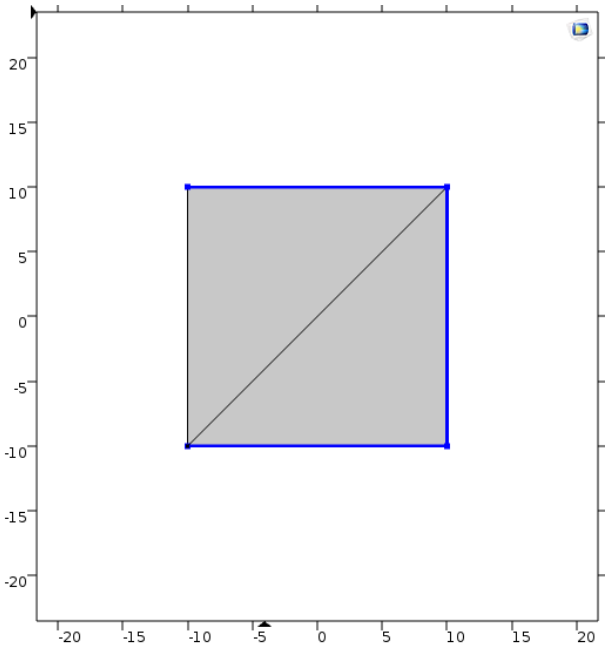

Figure 3.27: The scattering boundaries.

Secondly, the port boundary must be defined. The port boundary is the place where the incident beam light enters the prism. The wave excitation will be on this port. Port boundary has chosen to be boundary 1 (Figure 3.28).

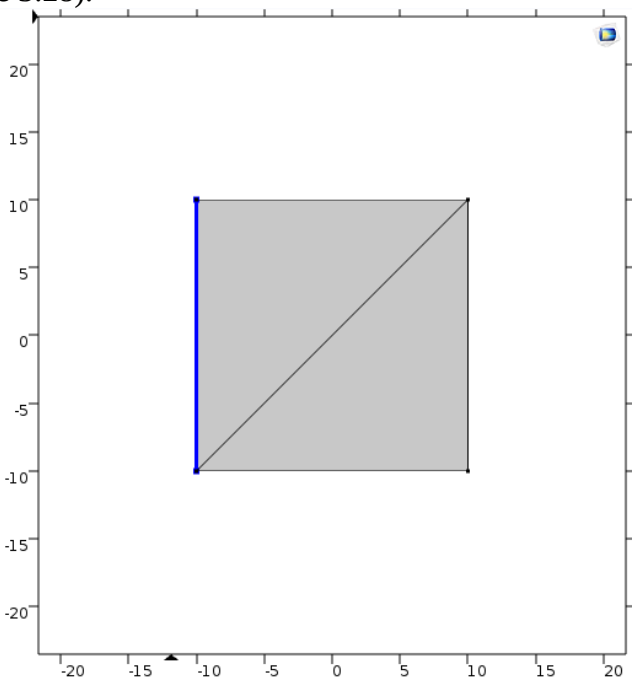

Figure 3.28: The port boundary.

Finally, the transition boundary must be defined. Transition boundary is where the light beam is splitted. As transition boundary the boundary 3 is selected (Figure 3.29).

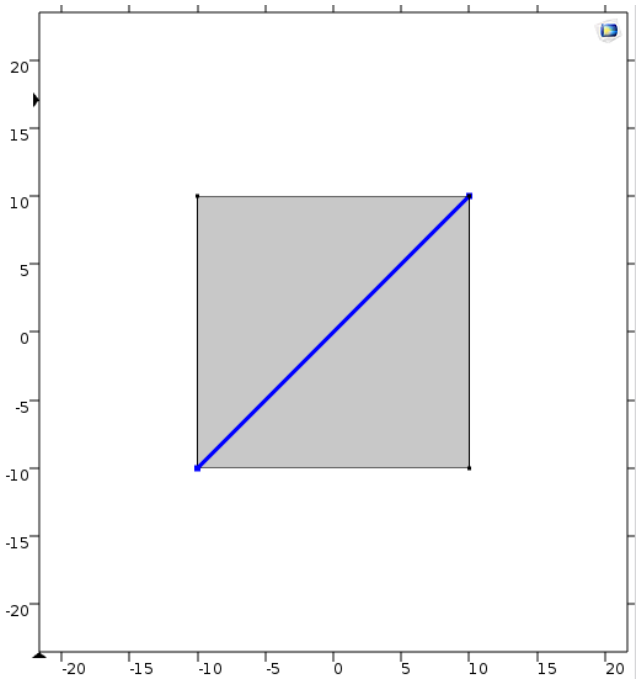

Figure 3.29: The transition boundary.

For the transition boundary, the relative permittivity ε_r must be chosen to be -16.5-1.06i (silver material), the relative permeability μ_r should be 1 and the electrical conductivity σ is 0. The thickness of the boundary is set to be 13 nm. The material that is used for the prism in this model is glass (quartz). The properties of glass were presented previously in Figure 3.11.

Then I meshed the prism. Each element is a free triangular. I Coose the maximum mesh element size in the glass domain smaller than 0.2 material wavelengths using the parameter h_max that I defined earlier. The object can be seen is Figure 3.30.

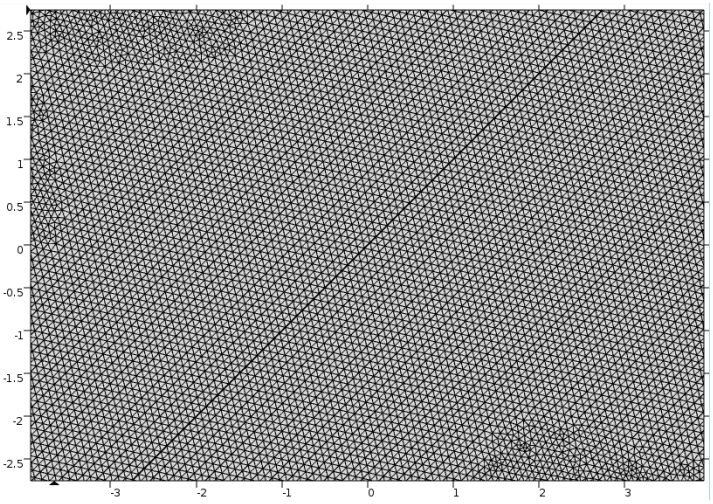

Figure 3.30: Free triangular mesh on the object.

Figure 3.31 shows the electric field intensity in the modeling domain. The beam is split into two beams, one propagating in the x direction and the other one in the y direction. The splitting can be evaluated by computing the flux crossing the incoming boundary and the two outgoing boundaries. Figure 3.32 plots the power crossing these boundaries as well as the losses at the mirror.

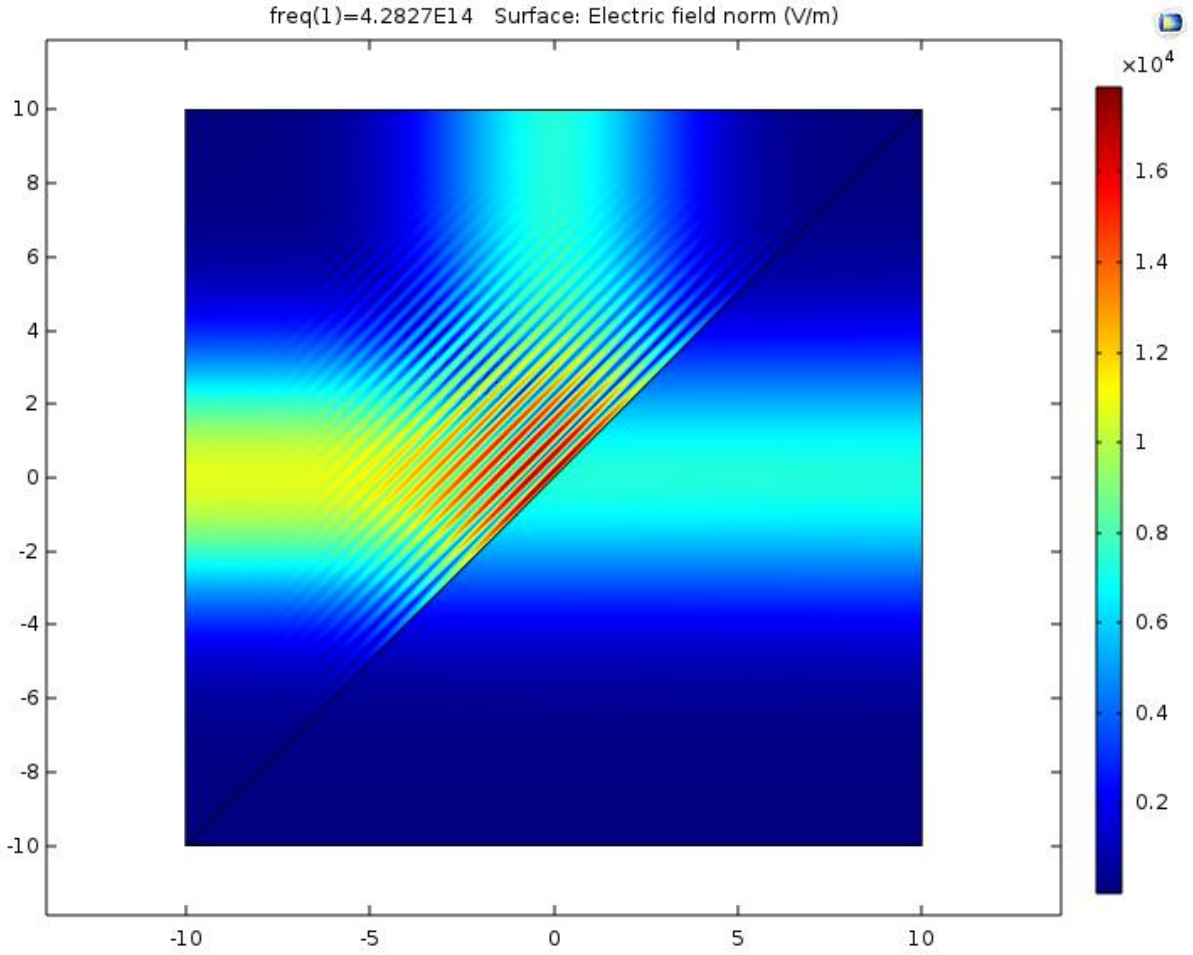

Figure 3.31: The electric field intensity shows that the incoming beam is split into two beams of approximately equal intensity.

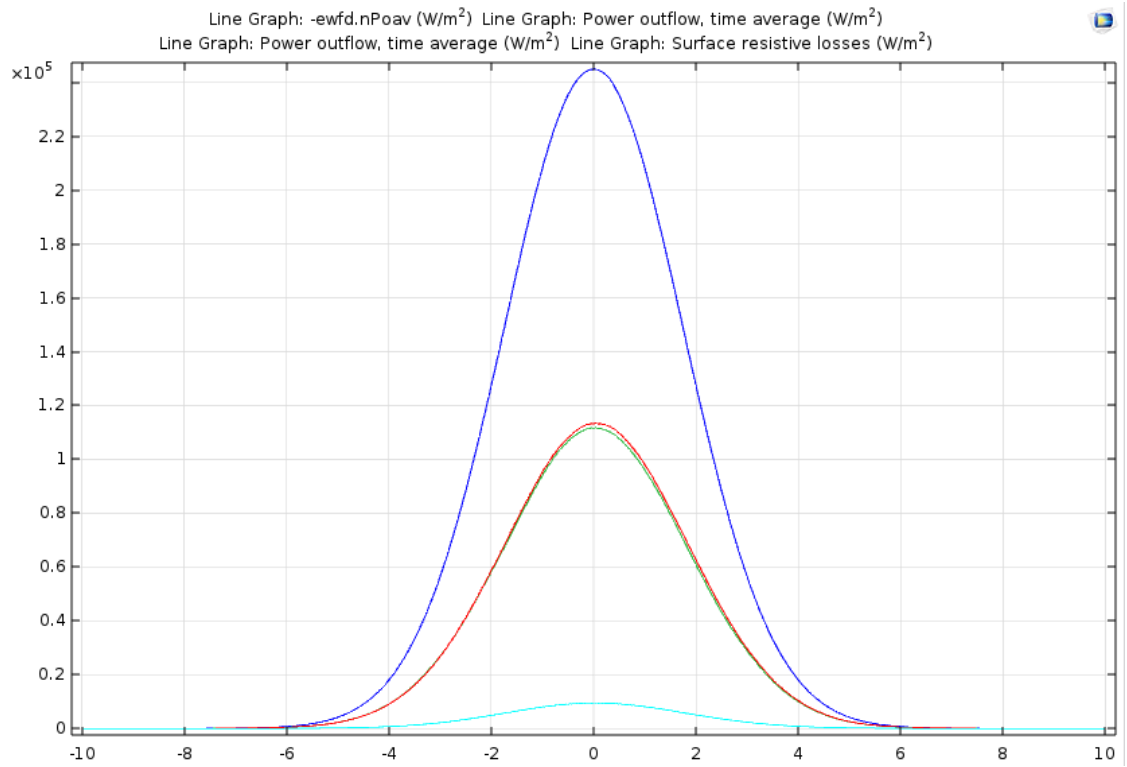

Figure 3.32: The power flux crossing the input boundary (dark blue line) and the two output boundaries (red and green lines) as well as the losses at the silver surface (light blue line).

As it can be seen from the simulations, the divided beam is splitted into two beams, each of them having approximately equal intensity. For the loses occured in the two beams, responsible is the silver surface inside the prism.

3.4 VIBRATION MODEL

This is a simple examle to show the vibrations of a meterial in response to different frequencies. The material used is bulk copper. The outline (boundary conditions) of the object are considered and defined as fixed point. That means that they are susceptible to vibrations and they do not experience any kind of displacement. Moreover, it should be noted that the boundaty conditions are ideal and they do not reflect the wafes. To visualize the vibrations the thermoacoustic model in Comsol Multiphysics was utilized. In order to minimize computational time, the copper material was considered as a membrane. The thickness of the membrane is not playing a role in this simulation, beacuse its width is not affecting the wave dispersion. In order to excitate the material, an electrostatic forces is applied, thus one of the material‘s layer is considered as terminal and the other as ground. The simulation results are shown as a displacement depending on different frequencies in the following figures.

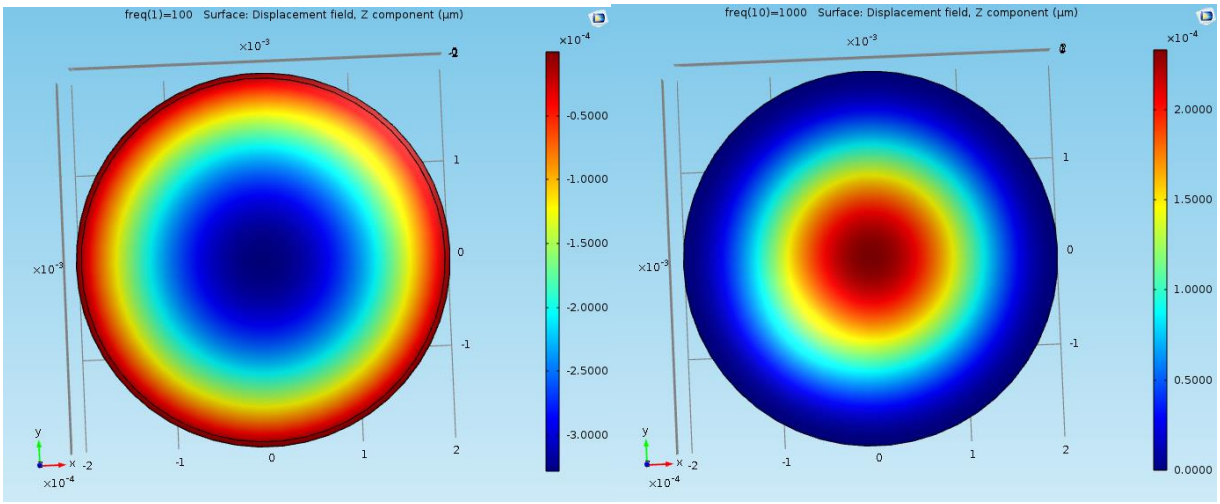

Figure 3.33: Left-hand side picture shows the displacement in the frequency of 100 Hz. Right-hand side picture shows the displacement in the frequency of 1 KHz.

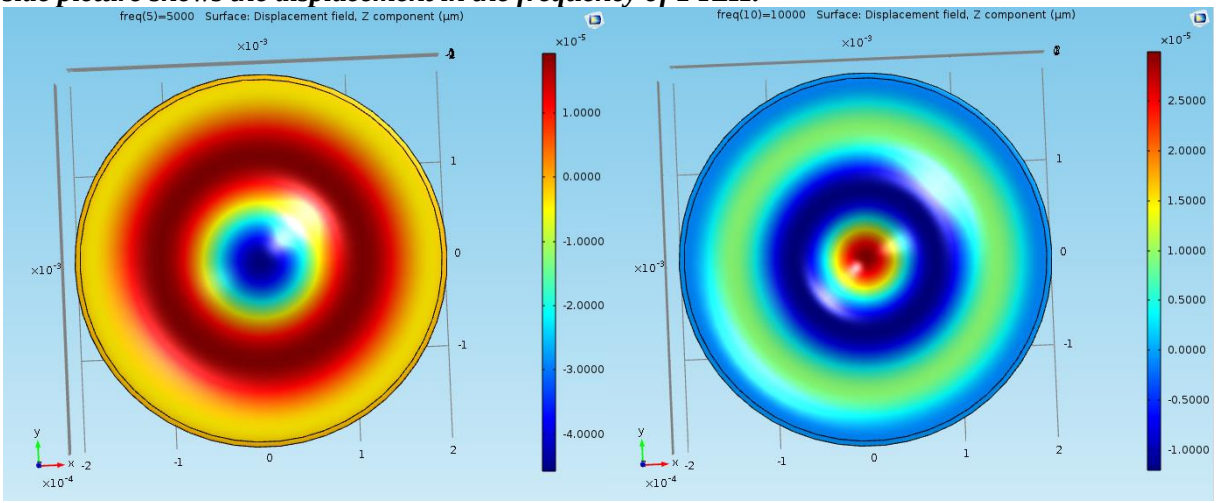

. Figure 3.34: Left-hand side picture shows the displacement in the frequency of 5 KHz. Right-hand side picture shows the displacement in the frequency of 10 KHz.

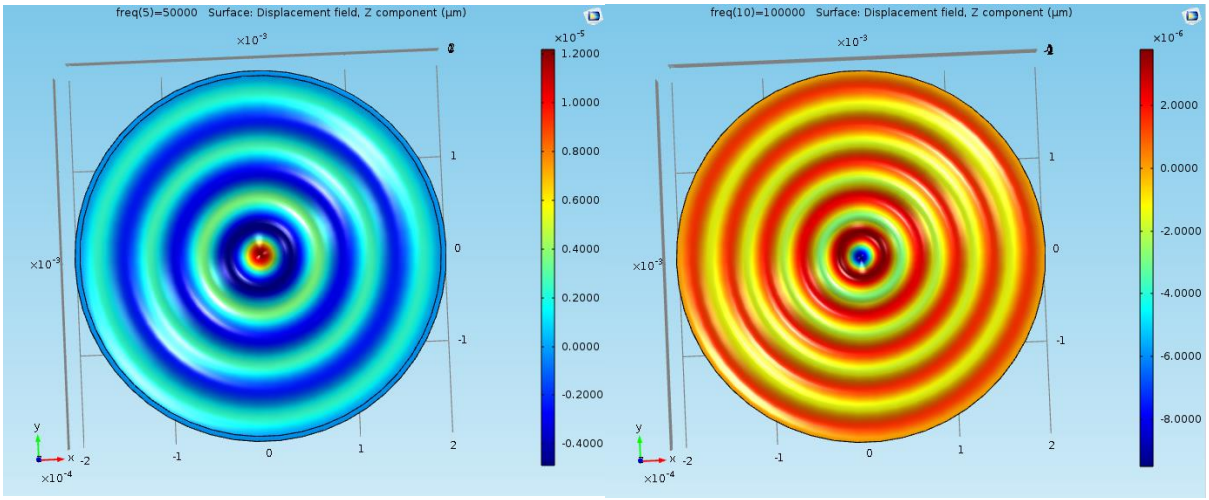

Figure 3.35: Left-hand side picture shows the displacement in the frequency of 50 KHz. Right-hand side picture shows the displacement in the frequency of 100 KHz.

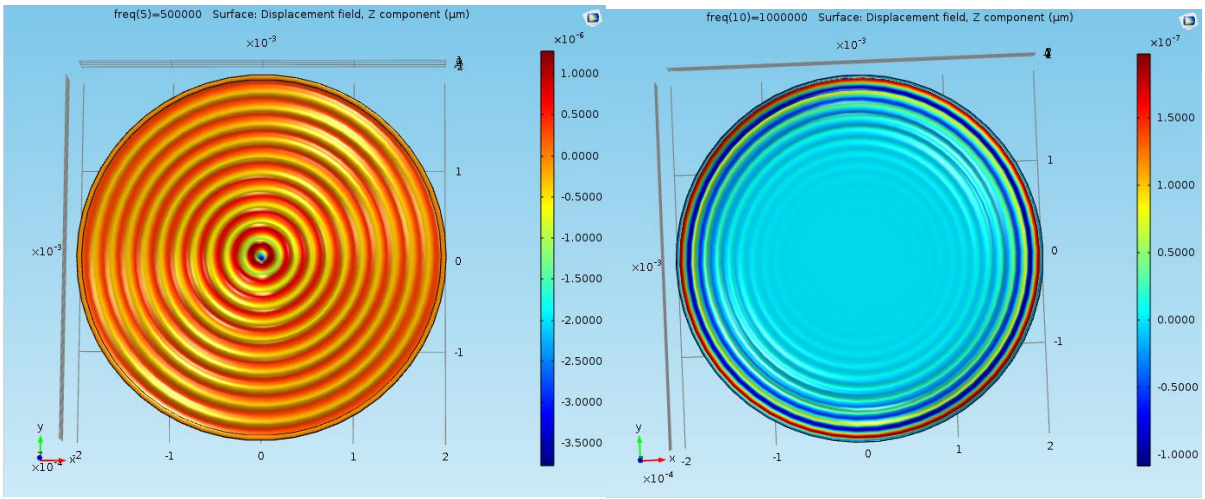

Figure 3.36: Left-hand side picture shows the displacement in the frequency of 500 KHz. Right-hand side picture shows the displacement in the frequency of 1 MHz.

As it can be seen from the previous simulations, the lower is the excitation frequency, the higher the vibrations that causes to the material.

3.5 CONCLUSIONS

From the above simulation about heat transfer in solids, it can be concluded that the factors that affect heat transfer in solids are the thermal conductivity, heat capacity and material density. It can be shown than in the materials examined (copper and silicon) even if copper has more than three times higher thermal conductivity [400 W/(m*K)] than silicon [130 W/(m*K)], temperature rises slower. This can be justified because silicon has higher heat capacity [700 J/(kg*K)] and lower density (2329 kg/m^3).

In the next simulation about laser-material interactions it is highlighted how the General Form PDE can be utilized in order to implement the Beer-Lambert law on a transparent material (quartz glass in this case) which is heated by a laser light and also has temperature-dependent absorptivity. In the approach examined in this simulation, the material is assumed to be completely opaque to ambient thermal radiation. Also, the Beer-Lambert law assumes that the incident light is perfectly aligned and propagates in one direction. It can also be observed that bigger pulse width (15 ns) leads to bigger penetration width and causes lower temperature rise.

On the other side, smaller pulse width (10 ps) leads to smaller penetration depth and causes higher temperature rise.

For the simulation about the beam splitter, we can conclude that the silver surface which is sandwiched between the two prisms, is responsible for the losses that we have on the two splitted beams. However, what concern us, is that the two beams have almost the same intensity.

4. LOW NOISE AMPLIFIER

The proposed device that is responsible to get as an input the signal from the piezoelectric transducer is a low noise amplifier. For the development different topologies of JFETs are utilized in order to obtain the best result. The choise of implementing a low noise amplifier using JFETs is based on the permormance of such devices. JFETs are unipolar devices. The current conduction through the device is only through majority carriers either holes in P channel or electrons in N channel. Thus, FETs are less noisy compared to BJTs as no recombination currents are required for their operation.

Moreover, JFETs exhibit high input resistance typically of the order of mega ohms. In JFET this is due to reverse biasing both the junctions of JFET thereby reducing drastically the conductance of channel. The inputs of JFETs are always reverse biased (gate to source) so they provide higher input impedance. Due to its high input Impedence the input and output circuit is physically isolated. However, as frequency increases this is not true due to feedback provided by the internal capacitance. Finally, JFETs, ensure much less noise than BJTs and they are excellent signal choppers as they exhibit no offset voltage at zero drain current. JFETs are relatively immune to radiation.

4.1 NOISE CONCEPT

Noise is the typical limitation of all electronic circuits. The dynamic range the test results during the measurements is limited by the noise and the distortion. Noise is a random electrical waveform fluctuation that can conceal the desired signals and is a common characteristic that is manifested in all electronic devices [110]. Noise generated by electronic devices varies greatly as it is produced by several different effects [111]. The random nature of a noise voltage waveform means it contains no predictable periodic frequency components and its amplitude at any future time is unpredictable. Unlike periodic signals that consist of one or more discrete spectral lines corresponding to their frequency components, random noise has a spectrum that is a continuous function of frequency and contains no discrete line components (Figure 4.1).

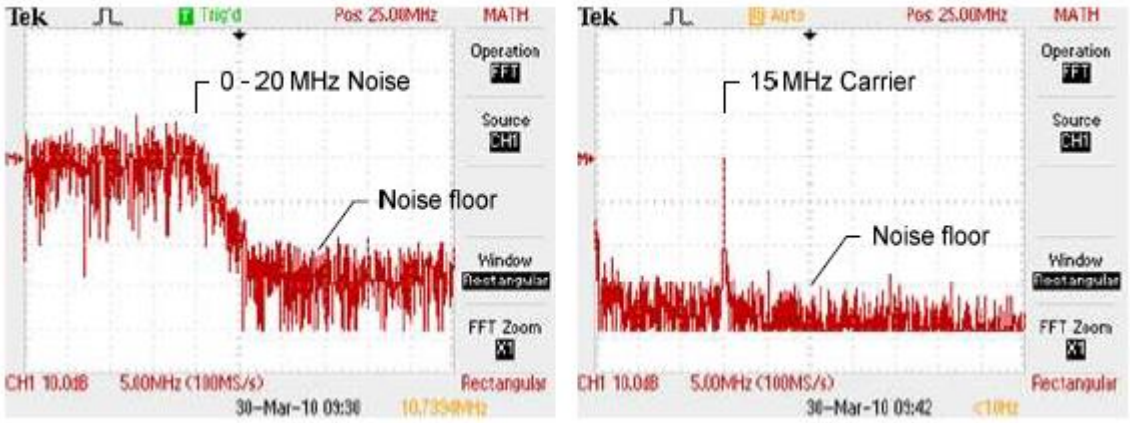

Figure 4.1: Noise and periodic signal spectrums. Left: The noise spectrum is produced by a 20 MHz random noise generator and displayed on an oscilloscope. The noise extends continuously four divisions (5 MHz/div) from the left scale and drops off due to the lowpass filter in the generator. Right: The periodic signal is an unmodulated 15 MHz carrier wave (CW) indicated as a single spectral line located three divisions from the left scale [111].

4.1.1 Background Theory – Frequency and Time Domain

According to Fourier series theory any physical signal, is a combination of sine waves, which waves, when they are poperly combined, produce the time-domain signal under examination. Fourier transform is responsible for transforming a signal from time into frequency domain. In this way, we have two different representations, of the same signal [116].

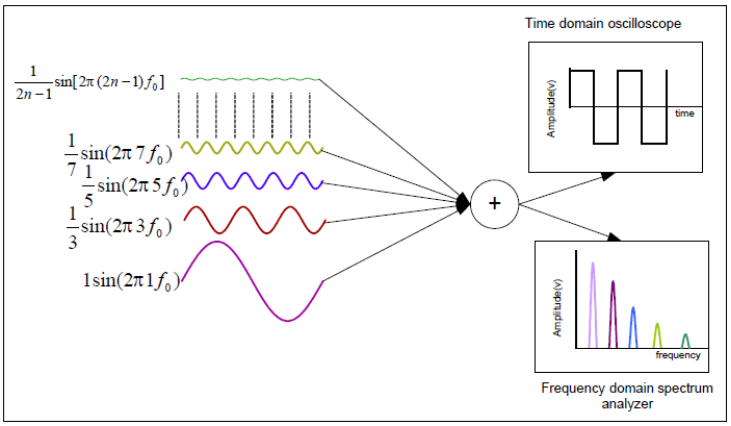

Figure 4.2: Time and frequency domain [116].

Figure 4.2 shows a square wave signal both in time and frequency domains. The time domain depicts the amplitude versus time, while the frequency domain shows the amplitude versus the frequency of each sine wave in the spectrum. However, there is no need to perform measurements in both domains. we have no need to perform both domain measurements. Some measurements can be made only in the time domain such as rise and fall times of a waveform, while other measurements like harmonics content, can be made only in frequency domain.

4.1.3 Noise Amplitude

Because noise is a random process, it is analyzed on a statistical basis. The noise amplitude prediction probability is given by a function called the amplitude probability density distribution p(v). When multiplied by a small voltage increment dv, the amplitude probability density distribution function gives the probability that, at any given instant, the voltage lies in the interval v to v + dv. The amplitude density distribution can take on many forms but, as will be seen, only one form is of most interest to us. Since the noise voltage, v, must exist at some value, the total probability over an infinite range is 1 (100%). In other words, the sum of all the individual products of p(v) and dv throughout the range of p(v) will be

$$P(v) = \int_{-\infty}^{+\infty} p(v)dv = 1 \tag{4.1}$$

We also are interested in determining the probability that the noise voltage amplitude will fall below some given value. The sum of the amplitude density distribution over part of the voltage amplitude range is called the cumulative amplitude probability distribution P(v) and is defined as

$$P(v) = \int_{-\infty}^{v} p(v)dv \tag{4.2}$$

P(v) also is called the cumulative probability and is the probability that a noise voltage lies below the voltage v at any given time. It is the area under the p(v) curve between the extreme negative value (-∞) and v. P(v) varies from 0 to 1. When P(v) is 0, there is 0% chance the voltage is below v, and when P(v) is 0.5 there is a 50% chance the voltage is below v, and so on. We cannot say what the values will be at any instant, only that there is a calculated probability it will be below that value.

Similarly, we are interested in the probability that the noise voltage amplitude will fall within a given range, say v1 and v2. In this case,

$$P(v) = \int_{-\infty}^{v1} p(v)dv - \int_{-\infty}^{v2} p(v)dv \tag{4.3}$$

When we analyze noise and its effects, we must make some assumptions. One is that the statistical averages of the noise, such as its amplitude distribution and spectrum, do not change over time (the noise is said to be stationary, a property analogous to oscillator stability). Also, we assume the probability density of the noise is Gaussian; that is the noise conforms to a particular mathematical function called the Gaussian, or normal, distribution. The normal distribution describes the probability that a particular amplitude will be exceeded (or not exceeded) in any given measurement period. When plotted the normal distribution yields the familiar bell-shaped curve (Figure 4.3). Other distribution functions exist, but it has been determined both theoretically and experimentally that thermal and shot noises and many other conditions we encounter in radio astronomy are Gaussian, so we will concentrate on the Gaussian distribution. It should be noted that many types of interfering noise are not Gaussian. They have strong periodic components and thus do not meet the definition of noise for our purposes. Manmade radio frequency interference is an example of non-Gaussian noise.

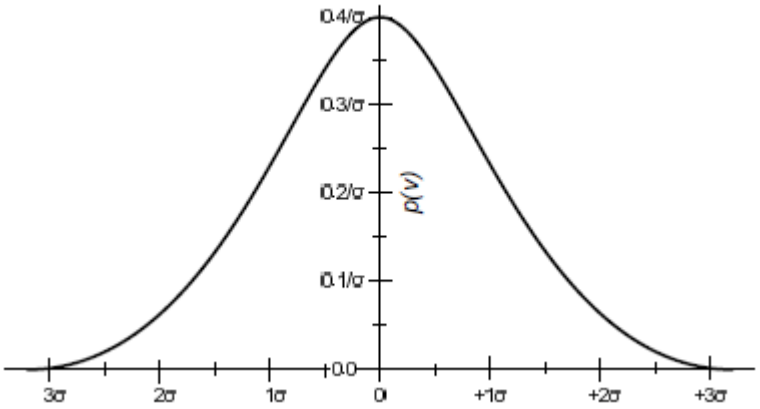

Figure 4.3: Gaussian distribution (bell-shaped or normal distribution) curve. Almost 99% of the area under this curve lies between -3σ and +3σ [113].

For the Gaussian amplitude density distribution

$$p(v) = \left[\frac{1}{\sigma \cdot \sqrt{2\pi}}\right] \cdot e^{-\frac{v^2}{2\sigma^2}} \tag{4.4}$$

and for the Gaussian amplitude distribution

$$P(v) = \frac{1}{2}\left[1 + \text{erf}\left(\frac{1}{\sigma \cdot \sqrt{2}}\right)\right] \tag{4.11}$$

where
σ root-mean-square (rms) noise voltage, also called standard deviation
erf error function

There is no theoretical upper amplitude limit that noise could reach, but very high amplitudes have very low probability, and real electronic systems have practical amplitude limits. If a large number of instantaneous amplitude measurements are made on a noise source, it will be found

that most of measurements fall within a range around a certain value, the average value, and only a few have higher or lower values.

4.2 NOISE MEASUREMENTS

To optimize measurement accuracy, it's important to understand the signal analyzer's inherent accuracy and identify the sources of error in the connection of the device under test (DUT). A combination of good measurement practices and useful analyzer features will mitigate errors and may shorten test time. Digital IF technologies yield a high level of basic accuracy, especially when enhanced with internal calibrations and alignments. For example, self-generated corrections and highly repeatable digital filters give you the freedom to change settings during a measurement with little impact on repeatability. Typical examples include resolution bandwidth, range, reference level, center frequency, and span. [112]

Once the device under testing is connected to the spectrum analyzer, the signal-delivery network (Figure 4.4) may relegate or induce variations the signal we are interested in. Correcting or compensating for these effects will ensure the best accuracy. This is can be done - conveniently and effectively - using the analyzer's built-in amplitude correction function alongside with a signal source and a power meter.

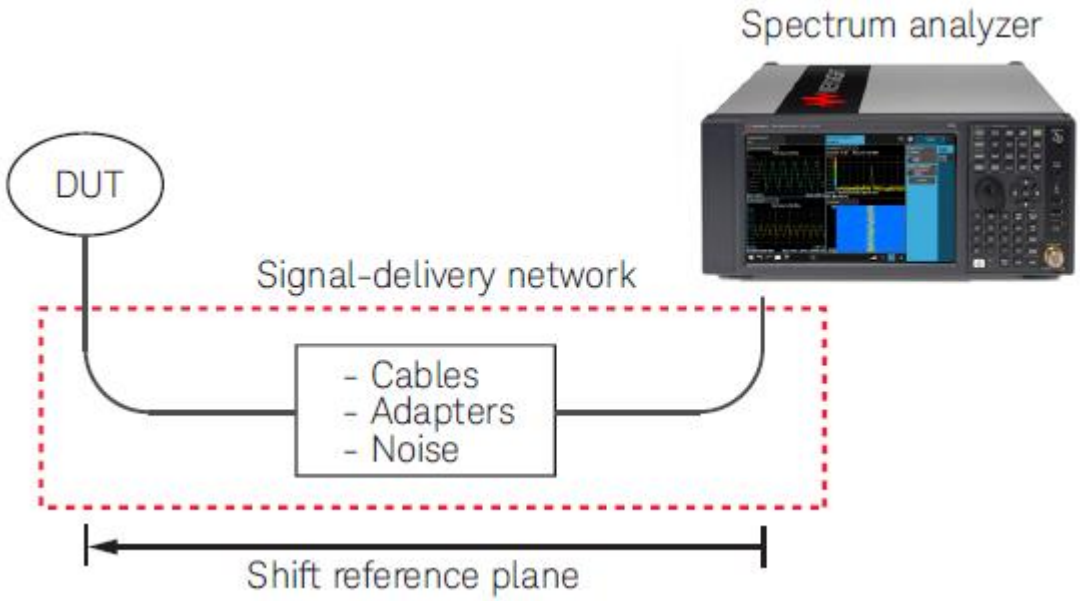

Figure 4.4: The quality of the DUT/analyzer connection can have a significant effect on measurement accuracy and repeatability. This effect grows as frequencies increase [112].

In electronic circuits, the noise is caused by randomly moving electrons. The electon motions are independent from each other and a huge number of electrons are involved. Consequently, the variation in the rate of current flow takes the form a bell-shaped curve. This curve is the Gaussian Probability Density Function in accordance with the central limit theorem from statistics. The Gaussian PDF is shown in Figure 4.5. The Gaussian PDF describes some of the characteristics of a noise signal that can seen in an oscilloscope. This signal has no imaginary components, thus is a real signal [113].

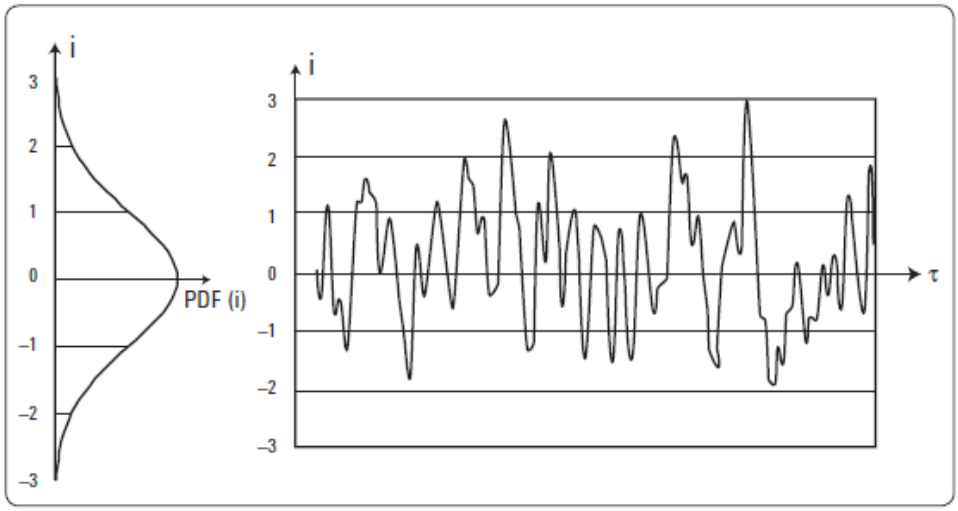

Figure 4.5: Left hand-side shows the Gaussian PDF. It can be observed that PDF is maximum at zero current and dropsas is moving away from zero. Rigth hand-side depicts a random noise waveform.

4.3 CIRCUIT DESIGN AND SIMULATIONS

The schematic of the proposed low noise amplifier can be seen in Figure 4.6. The first two stages are common source topologies. Though, the device's output resistance is not large enough for a rational transconductance amplifier and at the same time is not nor low enough for a proper voltage amplifier. Moreover, the amplifier has a limitation in high frequency response. For this reason, the output of the second stage is routed into a common drain stage (voltage follower) and into a common gate (current follower stage), this is done so as to obtain more approving and appropriate output and frequency characteristics. This implementation is called cascode amplifier.

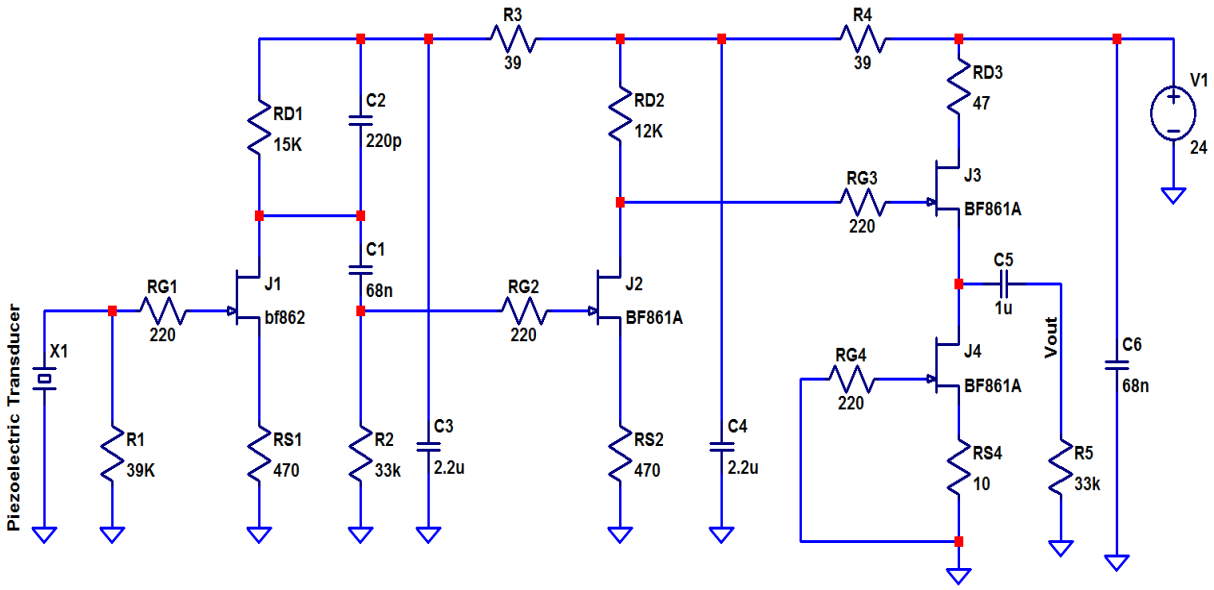

Figure 4.6: Schematic diagram of the proposed low noise amplifier.

The next step is to conduct all the required simulations that prove that the circuit is adequate for the measurement of laser absorption. Figure 4.7 shows the amplifier's noise performance. It must be noted that the simulation is with 24 Vdc power supply. In order to lower the noise of the amplifier, lower voltage supply can be used, but as a consequence the amplifier's gain will be reduced.

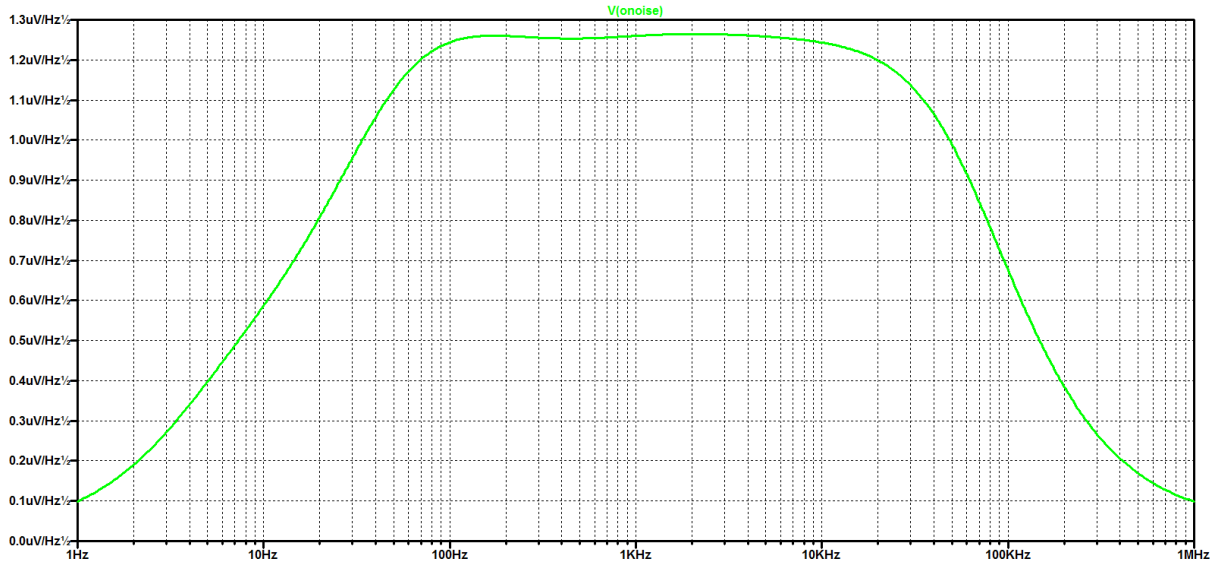

Figure 4.7: Amplifier's noise voltage density.

The next figures show the AC small signal analysis of the low noise amplifier in the form of Bode plots. The input signal is 1 uV p-p, 10 uV p-p and 100 mV p-p respectively.

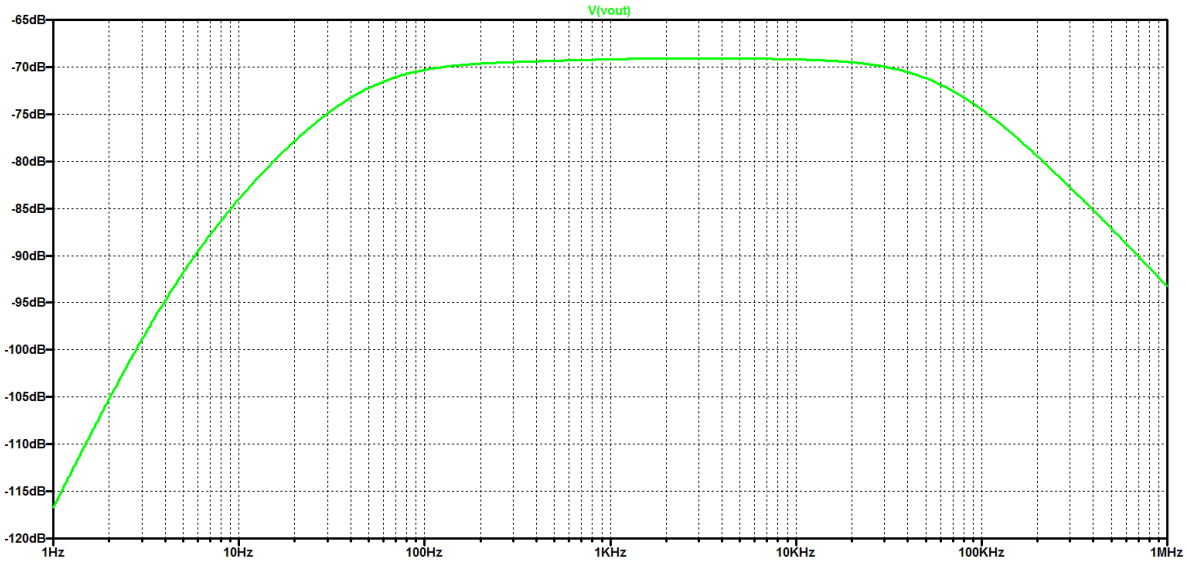

Figure 4.8: Amplifier's Bode magnitude plot. AC small signal analysis, input voltage = 1uV p-p

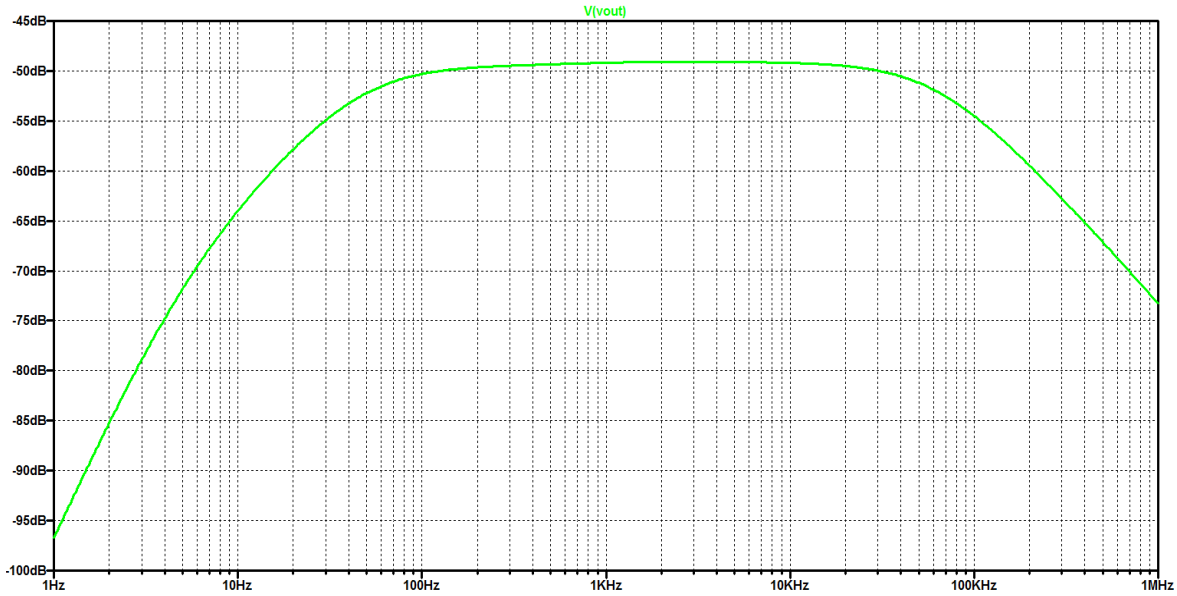

Figure 4.9: Amplifier's Bode magnitude plot. AC small signal analysis, input voltage = 10uV p-p

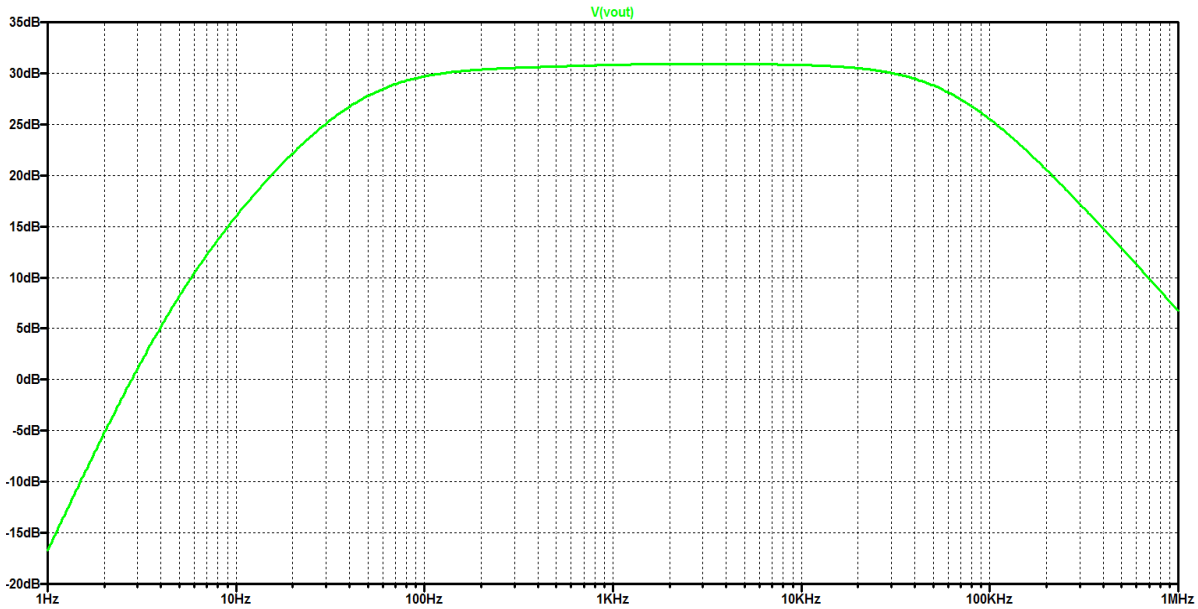

Figure 4.10: Amplifier's Bode magnitude plot. AC small signal analysis, input voltage = 100 mV p-p

In the next simulation a pulse is set as amplifier's input. The initial voltage is 0 Volts and the Von voltage is 100 mV. The pulse has the following characteristics: rise time Trise = 0.1 us, fall time Tfall = 0.1us and the enable time is 8 ms. Pulse repetition frequency is 1 kHz and it is repetitive for 6 cycles. The input pulses and output response are depicted in Figure 4.11. Figure 4.12 shows a zoomed version of the previously mentioned waveforms.

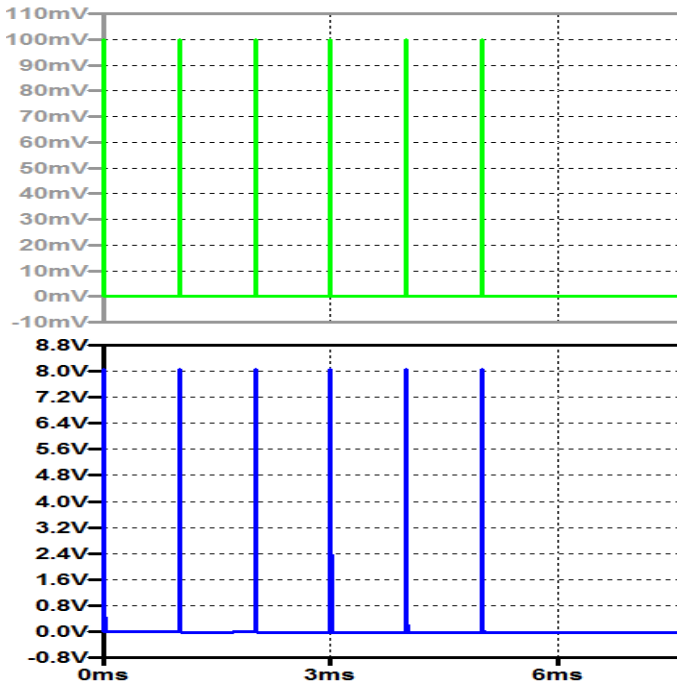

Figure 4.12: Top plot - The input pulse signal. Bottom plot - The output response signal.

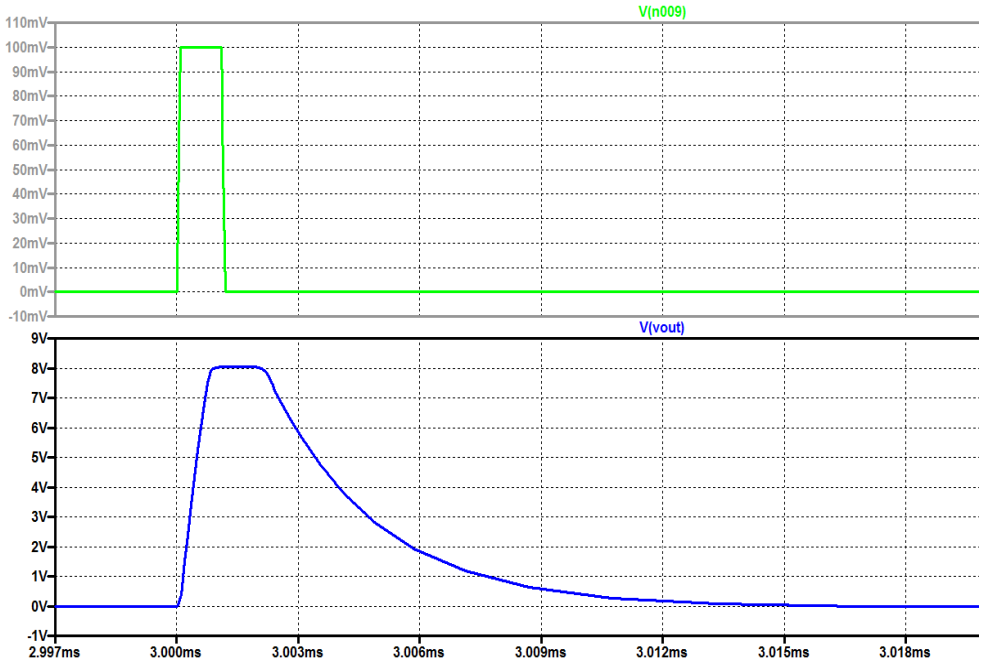

Figure 4.12: A zoomed representation of input and output signals. Top plot - The input pulse signal. Bottom plot - The output response signal.

Then, a Fast Fourier Transform is implemented on the output response as seen in the following Figure 4.13.

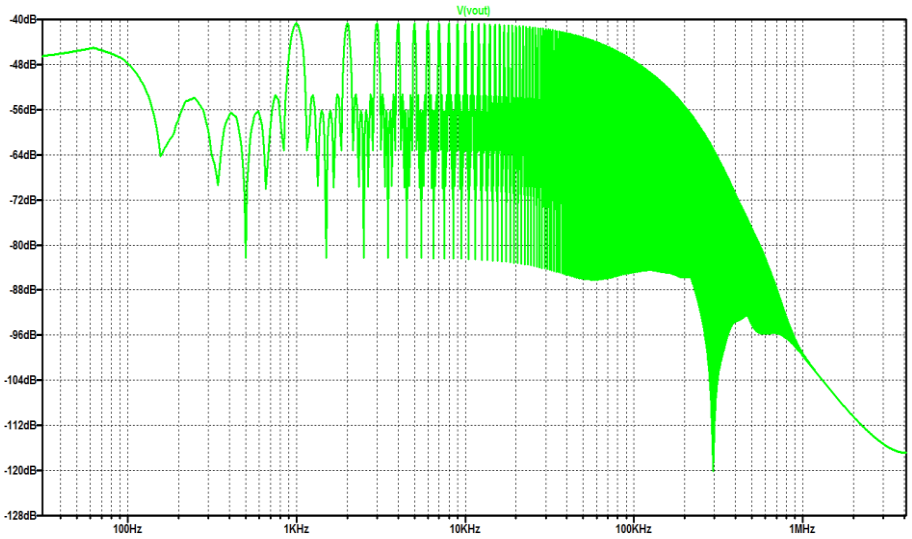

Figure 4.13: Frequency response of the output signal.

Having seen that the low noise amplifier is considered as adequate from the laser absorption measurements. I desinged the PCB using Altim Designer software. The PCB can be seen in Figure 4.14. The components are placed closely to each JFET minimizing the trace width and length in order to reduce the trace impedance. Attention was also paid to reduce stray capacitance, so power traces are kept away from sensitive nodes.

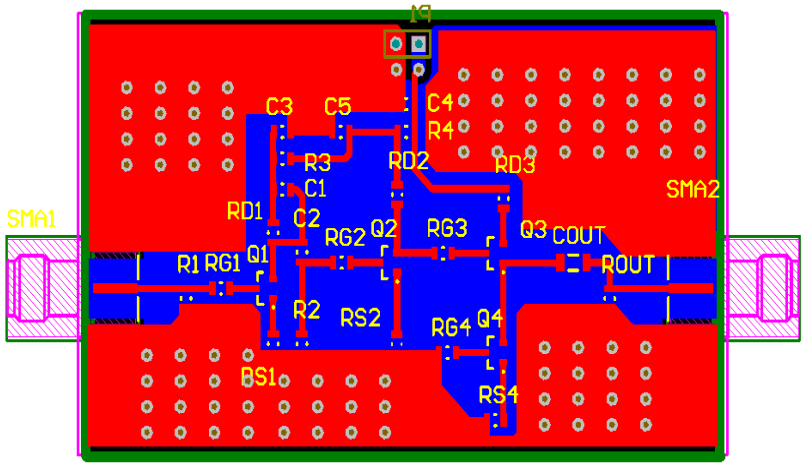

Figure 4.14: PCB Design of the proposed circuit.

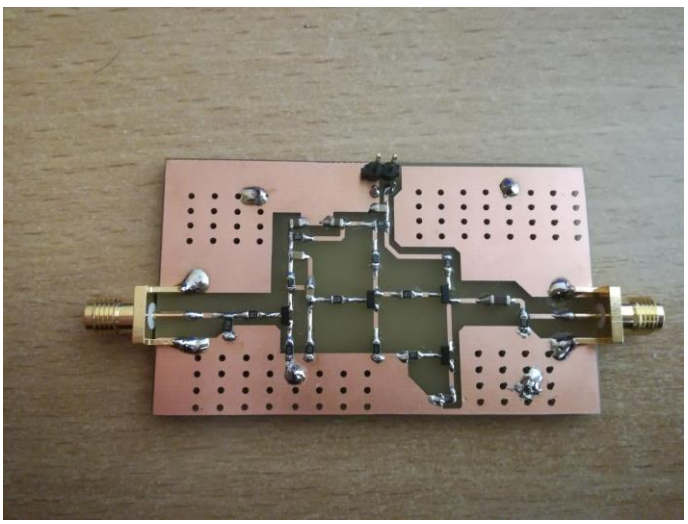

Figure 4.18: The implemented low noise amplifier.

4.4 CONCLUSIONS

From the above simulations we can conclude the following. First of all the amplifier's bandwidth is ranging from 40 Hz till 79 KHz. From the AC analysis it can be seen that when the ac input signal is 1 uV p-p, the gain is -69.1 dBV. For input signal 10 uV p-p, the gain is -49 dBV and for input signal 100 mV p-p, the gain is 30.9 dBV. Also, the amplifier's noise was found to be 1.26 uV/√Hz.

5. EXPERIMENTAL RESULTS

5.1 EXCITATION USING PIEZOELECTRIC TRANSDUCER

This is the early stage experiment. Itis performed in order to test the functionality of the equipment which will be used in the final experiment. In this experiment a piezoelectric transducer is driven by a pulse created from the signal generator and through the experimental process its pulse width and repetition frequency are changed. The piezoelectric transducer which is responsible for excitation is attached using sticky tape as coupling material on a red-colored, cylindrical lens with dimensions 2.54 cm diameter and 0.2 cm width. The other piezoelectric transducer is placed on the edge of the lens and captures the vibration waves that created inside the material and convers them to voltage. These waves are pretty similar to the waves created by the laser pulses. The voltage generated by the piezoelectric transducer is then amplified using an ultra-low noise amplifier. Following that, the amplified signal is captured by the oscilloscope. Finally, data from oscilloscope are obtained by the computer in order to be processed. Matlab software is utilized for this purpose. The experimental schematic diagram is shown in Figure 5.1.

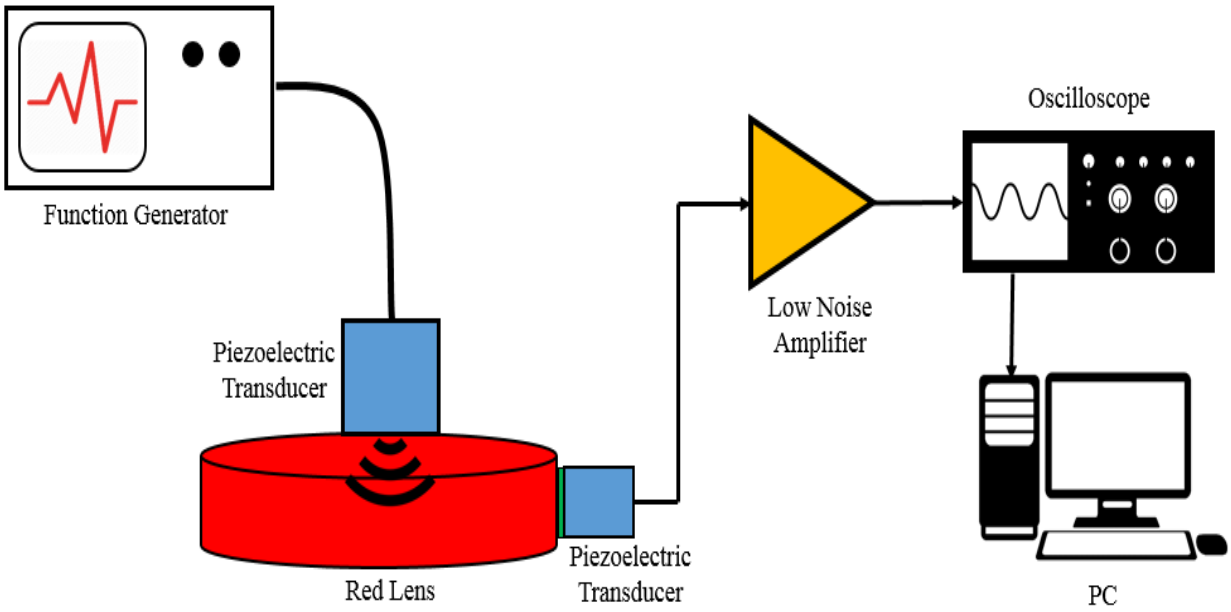

Figure 5.1: Experiment schematic.

Matlab depicts the both the excitation and response signals in time domain. Furthermore, Matlab is also used for implementing Fast Fourier Transform to the signal in time domain to transfer it in frequency domain.

A set of three different experiments are performed so as to evaluate the effect of different excitation pulse widths and also the effect of pulses' repetition frequency. The lens is fixed on a holder and its top and bottom surfaces are not in touch with other objects that may affect the wave propagation inside the lens.

For the first experiment the piezoelectric transducer is fed with a pulse generated from the function generator. The pulse has the following characteristics. The pulse voltage is 5 Volts peak to peak with a DC offset of 2.5 Volts. The pulse width is 1 us and the pulse repetition frequency is 100 Hz (Figure 5.2). The impluse response in time and frequency domain can be seen in Figures 5.3 & 5.4.

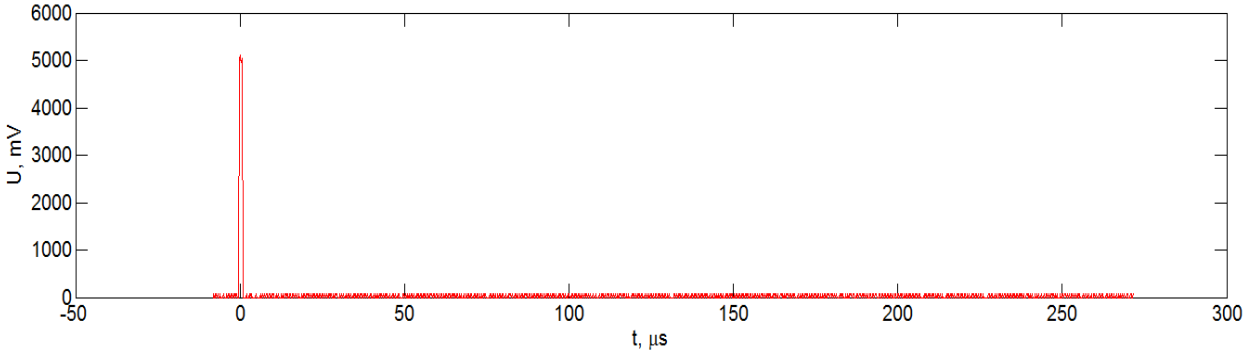

Figure 5.2: The excitation pulse in time domain. Pulse amplitude is 5 Vpp and pulse duration is 1 us.

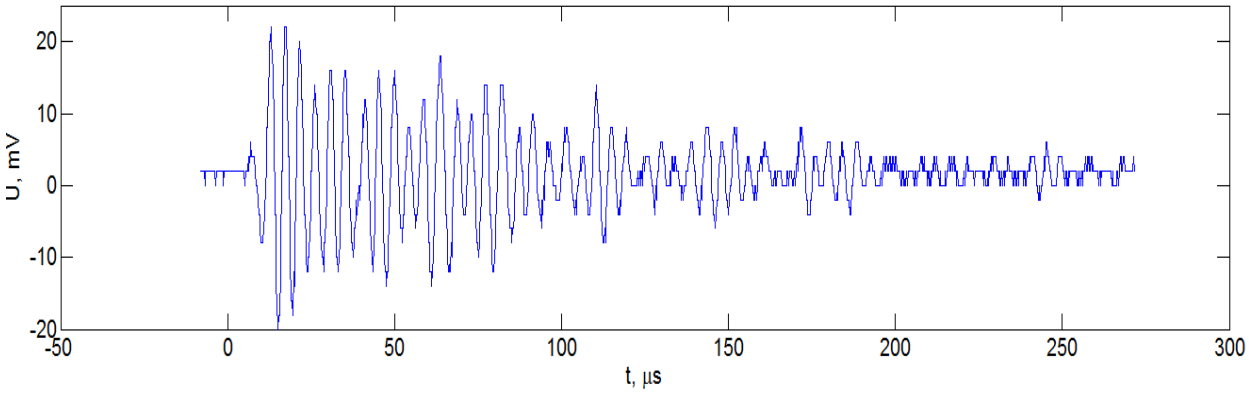

Figure 5.3: Impulse response in time domain.

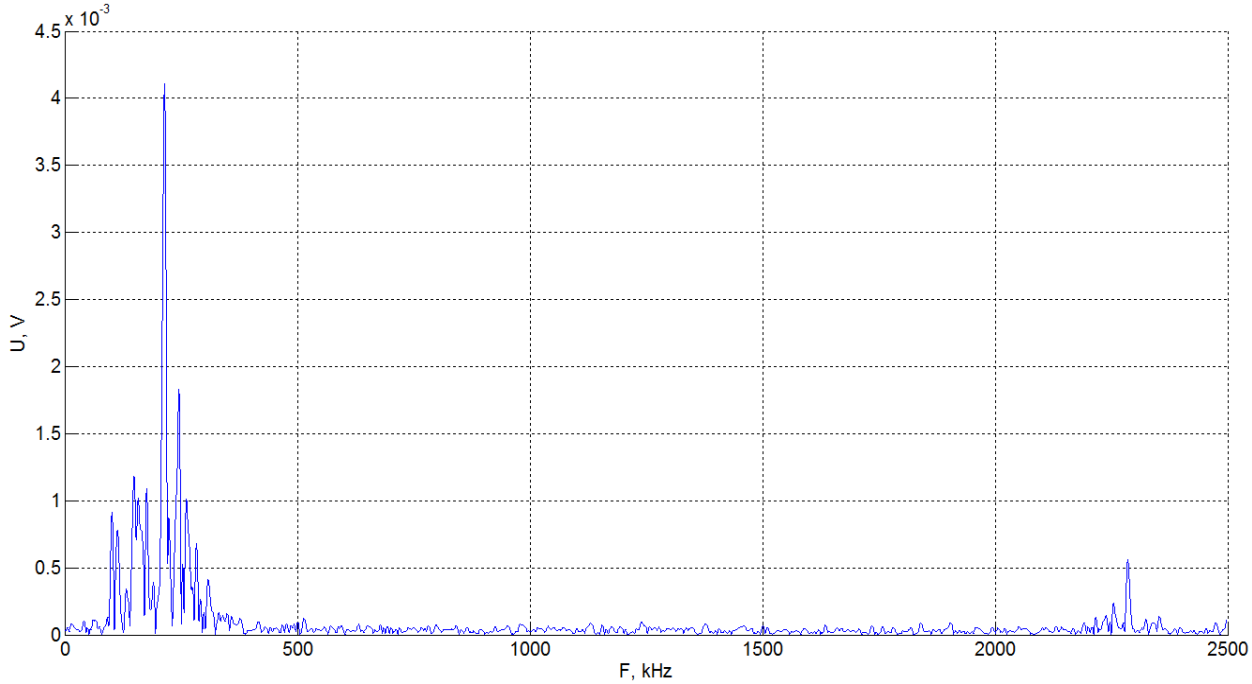

Figure 5.4: Impulse response in frequency domain.

The second experiment the piezoelectric transducer is fed with a pulse generated from the function generator. The pulse has the following characteristics. The pulse voltage is 5 Volts peak to peak with a DC offset of 2.5 Volts. The pulse width is 1 us and the pulse repetition frequency is 1 kHz (Figure 5.5). The impluse response in time and frequency domain can be seen in Figures 5.6 & 5.7.

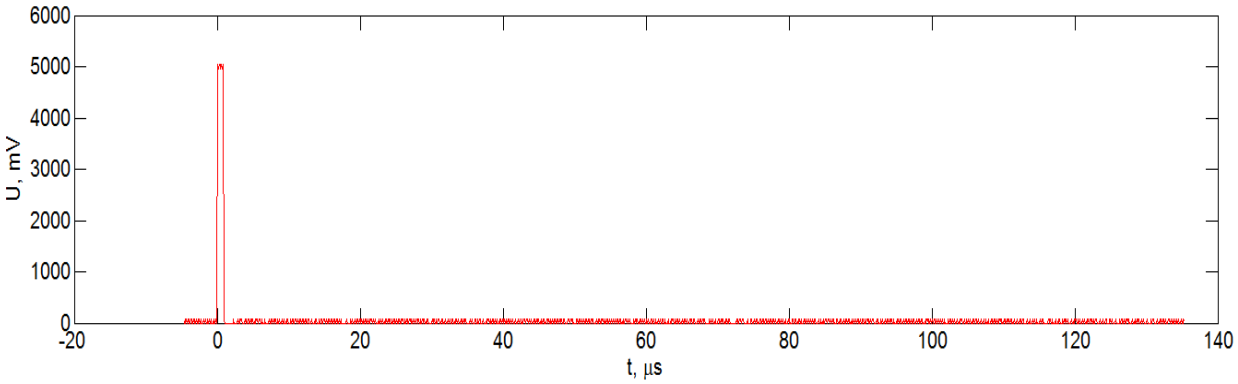

Figure 5.5: The excitation pulse in time domain. Pulse amplitude is 5 Vpp and pulse duration is 1 us.

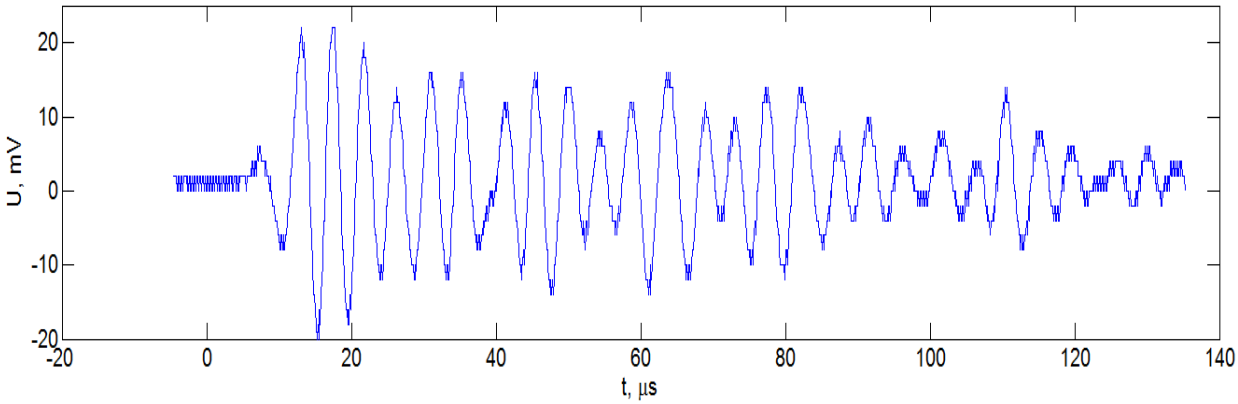

Figure 5.6: Impulse response in time domain.

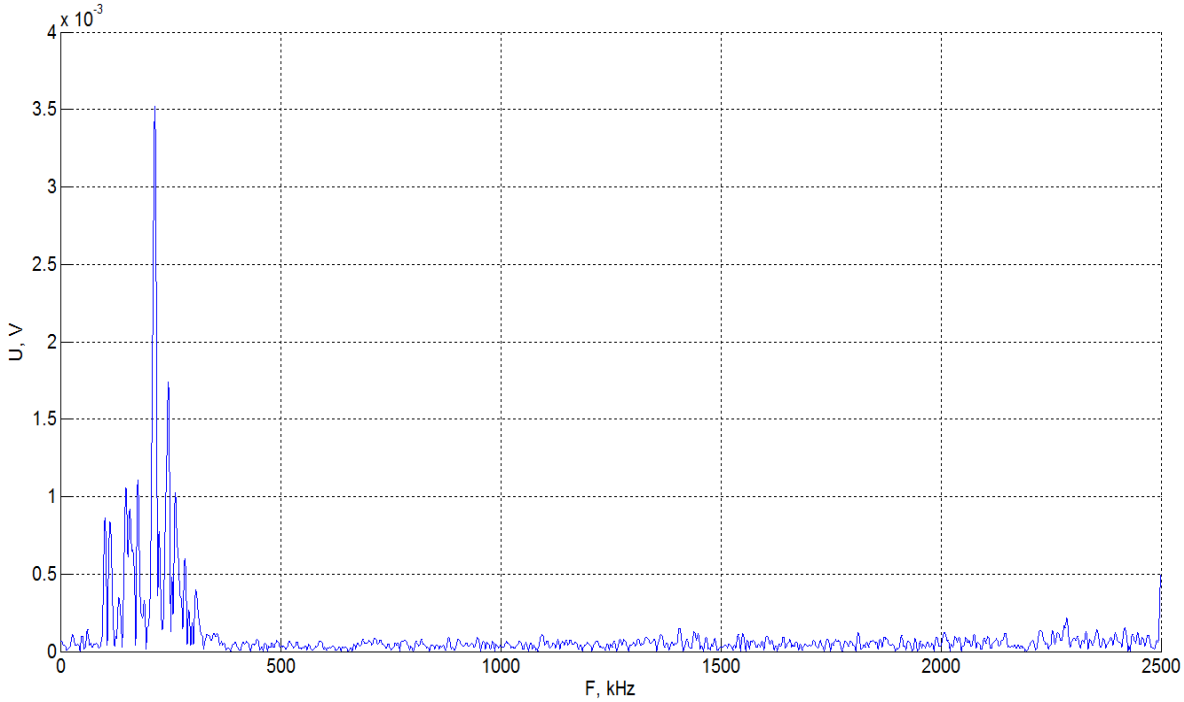

Figure 5.7: Impulse response in frequency domain.

In the final experiment the piezoelectric transducer is fed with a pulse generated from the function generator. The pulse has the following characteristics. The pulse voltage is 5 Volts peak to peak with a DC offset of 2.5 Volts. The pulse width is 100 ns and the pulse repetition frequency is 100 Hz (Figure 5.8). The impluse response in time and frequency domain can be seen in Figures 5.9 & 5.10.

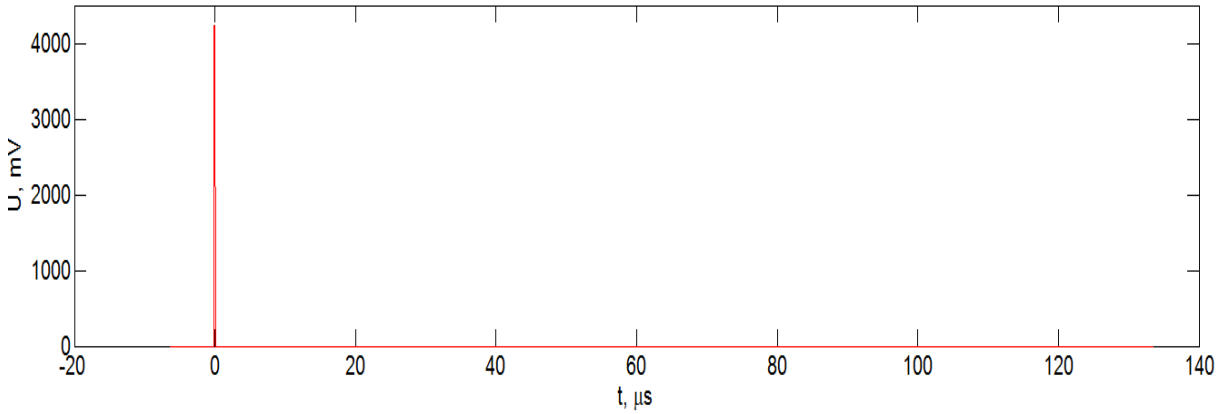

Figure 5.8: The excitation pulse in time domain. Pulse amplitude is 5 Vpp and pulse duration is 100 ns.

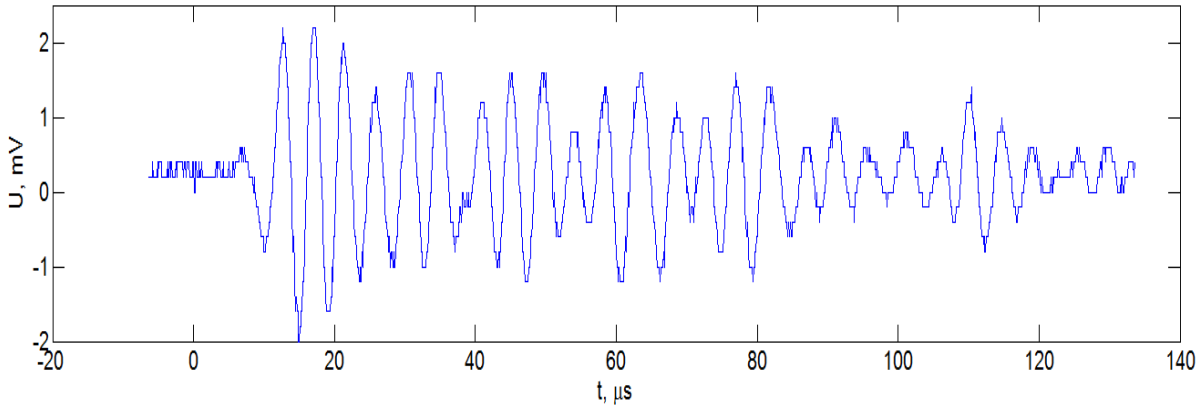

Figure 5.9: Impulse response in time domain.

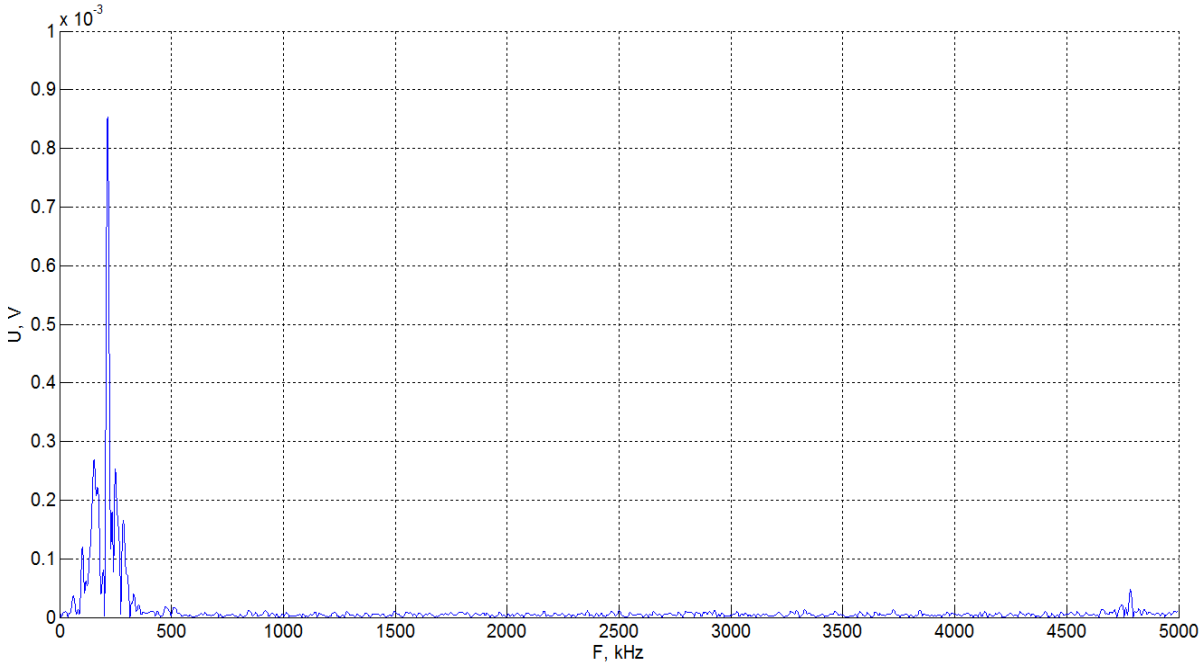

Figure 5.10: Impulse response in frequency domain.

The results from the above experiments are summerized in the followin table (Table 5.1).

Table 5.1: Results summary.

Pulse width	**Repetition frequency**	**Maximum impulse response amplitude (Time domain)**	**Maximum impulse response amplitude (Frequency domain)**	**Peak amplitude frequency**
1 us	100 Hz	42 mV p-p	4.1 mV	214.5 KHz
1 us	1 KHz	42 mV p-p	3.52 mV	214.6 KHz
100 ns	100 Hz	4.2 mV p-p	0.854 mV	214.8 KHz

As it can be concluded from results, the repetition frequency does not affect the wave generation inside the material. What is important and affects the the generated waves is the pulse width that is used to excite the material. More specific, high pulse width (1 us) causes higher impulse response (4.1 mV) , whereas lower pulse width (100 ns) causes lower impulse response (0.854 mV). Interestingly, by lowering ten times the pulse width, it can be seen that the maximum impulse response in time domain is also lowered by a factor of ten. A 1 us pulse width has a maximum amplitude of 42 mV p-p, while a 100 ns pulse width has a maximum amplitude of 4.2 mV p-p. Finally, it can be observed that the frequency where the maximum amplitude occures, depends only on the material properties and for the lens tested is around 214 KHz.

5.2 LASER PULSES ABSORPTION MEASUREMENT

An electro-optically Q-switched nanosecond Nd:YAG laser was used. The laser can provide energy up to 800 mJ per pulse at a wavelength of 1064 nm. The pulse repetition ranging from 10 to 30 Hz and the pulse duration from 3 to 6 ns. For the purposes of this experiment a harmonic generator module was used to generate the second harmonic of the laser pulse. The pulse duration was set at τ = 3.95 ns, the laser radiation wavelength λ = 532 nm and the laser pulse repetition frequency f = 10 Hz. The experiment schematic can be seen in Figure 5.11.

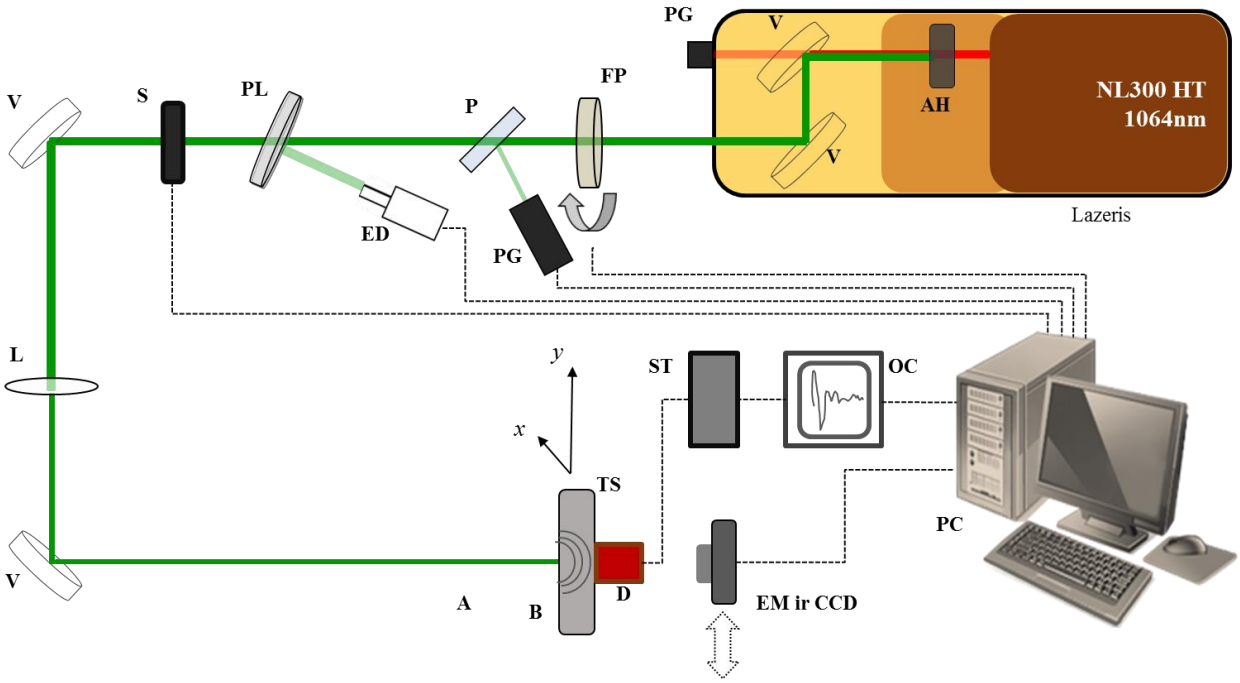

Figure 5.11: Experimental schematic diagram for measuring laser pulses absorption.

The absorption is measured using a piezoelectric transducer. Transducer's signal is then amplified by a low noise amplifier and then is screen on the oscilloscope. Data from oscilloscope are transferred to a computer in order to be captured and using Fast Fourier Transform are transformed from time to frequency domain (Figure 5.12).

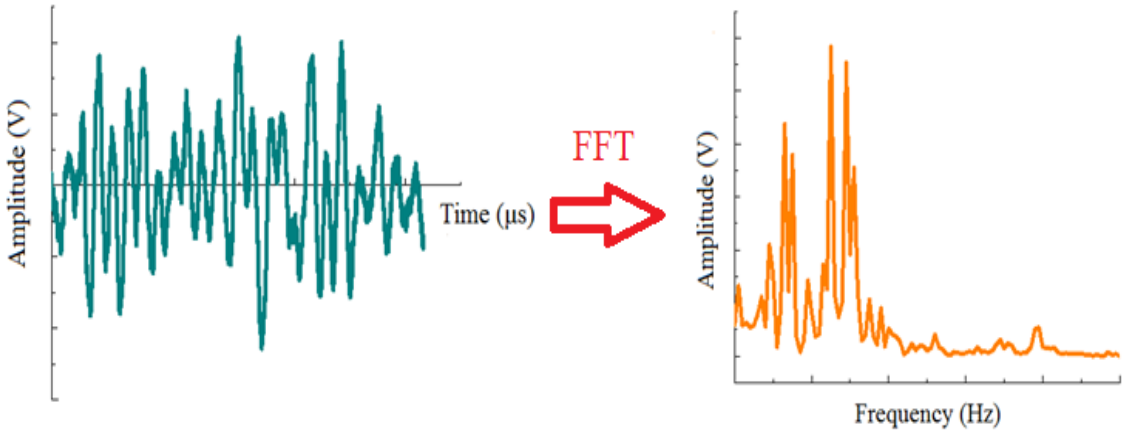

Figure 5.12: Fast Fourier Transform is implemented using Matlab software. Transform data from time domain into frequency domain.

Before beggining the actual expriments, it is useful to examine some feature of the equipment that take part in the experiment, such as the laser itself and the lenses that are used either for focusing or for beam reflection. First we can see an example of the measured laser characteristics of the pulsed laser with energy of 32.4 mJ.

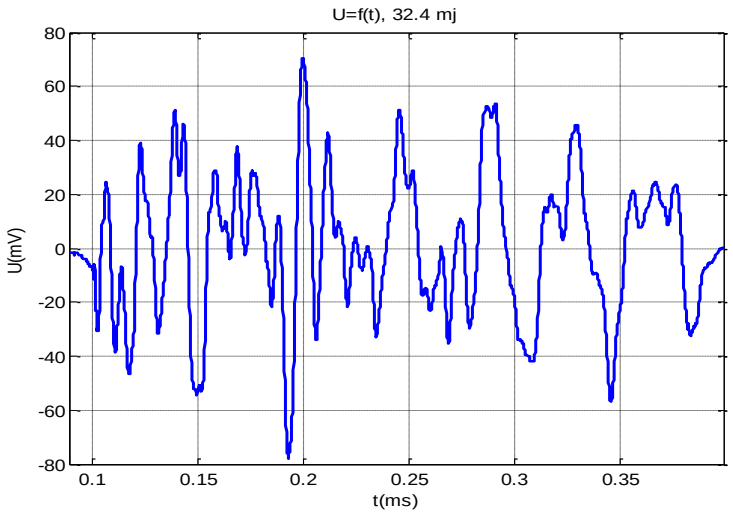

Figure 5.13: Measured characteristics of pulsed laser with energy of 32.4mJ in time domain.

Then, we can calculate the spectra characteristics for laser power configurations as shown in Figure 5.14.

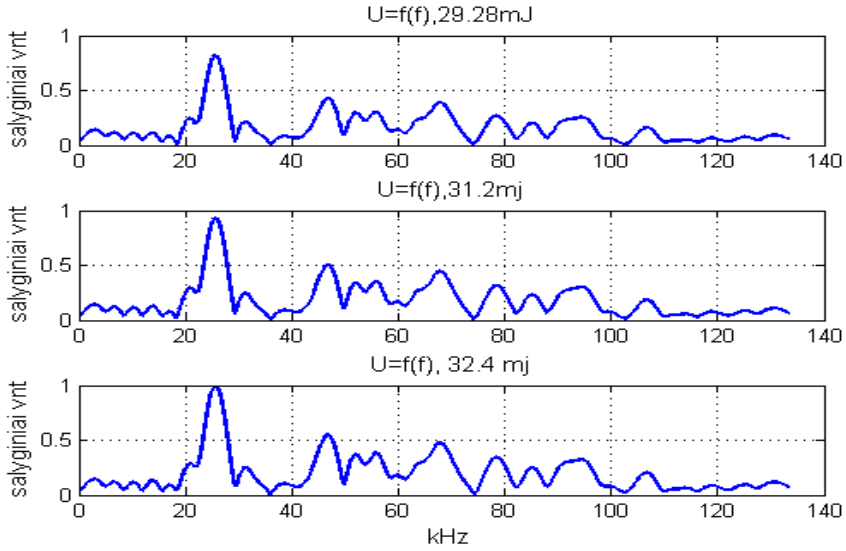

Figure 5.14: Calculated spectra of pulse characteristics for different laser power configuration. Top plot – Laser pulse energy is 29.28 mJ. Middle plot – Laser pulse energy is 31.2 mJ. Bottom plot – Laser pulse energy is 32.4 mJ.

As it can be seen, the laser pulses' frequency characteristics follow the same pattern. The only difference, which is more or less obvious is that higher pulse energy, has higher amplitude.

Next, because uncoated lenses are used with the aim of focusing the pulsed laser beam, I studied the voltage of the uncoated lenses for differemt laser energies. The results can be seen in Figure 5.15. It must be note that the uncoated lenses' voltage rises as the laser pulse energy is increased.

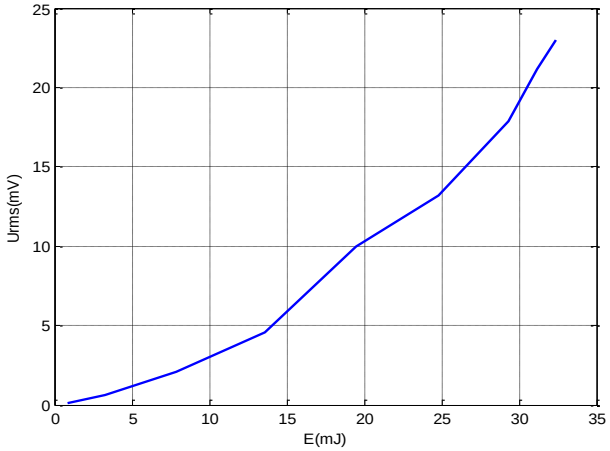

Figure 5.15: The voltage depending on the laser pulse energy for uncoated lens.

Furthermore, lenses with a dielectric coating are used as beam splitters and as reflectors to guide the laser pulsed beam to the material under investigation. In some experiments are also used for pointing the laser pulse to the material under a different incident angle. In this condition, the material not only experiences the main laser pulse, but also a second laser pulse on a different position at 6 degrees angle. Figure 5.16 depicts the voltage of the dielectric coated lens in different angles of incident light. Figure 5.17 shows the pulse spectrum when the incident beam is at six degrees angle. Note that six degrees angle will be used in the experiments where two incident beams will point in the material under investigation.

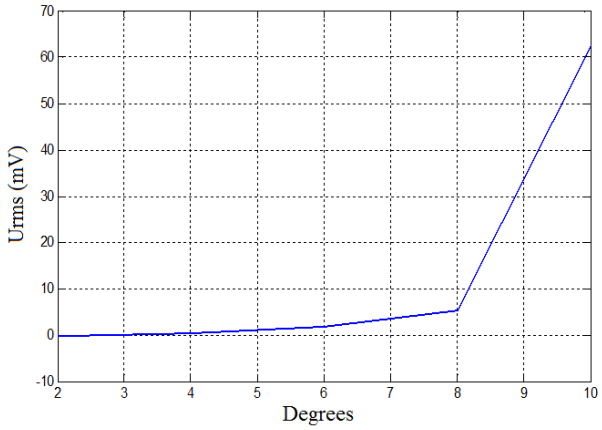

Figure 5.16: Voltage of the lens' surface covered with a dielectric coating in different angle degrees of incident light.

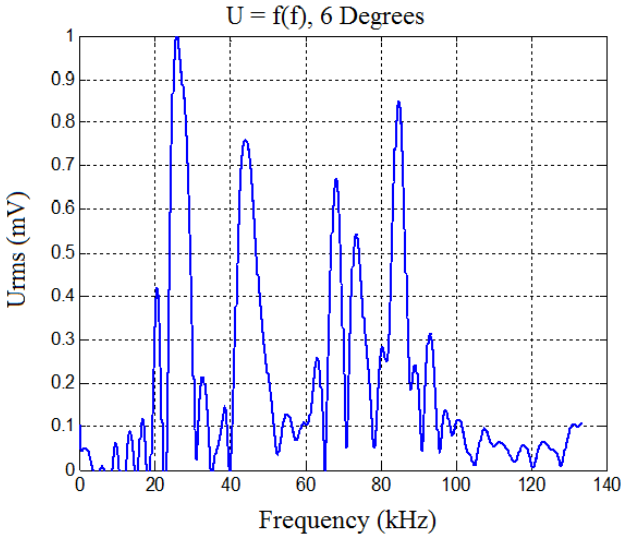

Figure 5.17:Calculated characteristics of the pulse spectrum at six degrees angle from the polarization plane.

5.2.1. Laser Pulses Absorption in BK 7 (Crown Glass) Material

In this section, the absorption of laser pulses is measured in BK 7 material. Three different material widths were examined. More specific, the widths were 4 mm, 12 mm and 3 mm respectively. In the samples that have 4 mm and 12 mm thickness, two incident beams were used. The first one is the direct beam and the second is reflected from a coated mirror in six degrees angle.

In the first experiment, which was conducted in BK 7 (Crown glass) lens material. The laser energy is E = 27.3mJ and the measured absorption is caused by two laser beams, the direct beam and the reflected beam from a mirror at an angle of six degrees. The material dimensions are 25.4 mm x 4 mm. The results can be seen in figures 5.18 & 5.19.

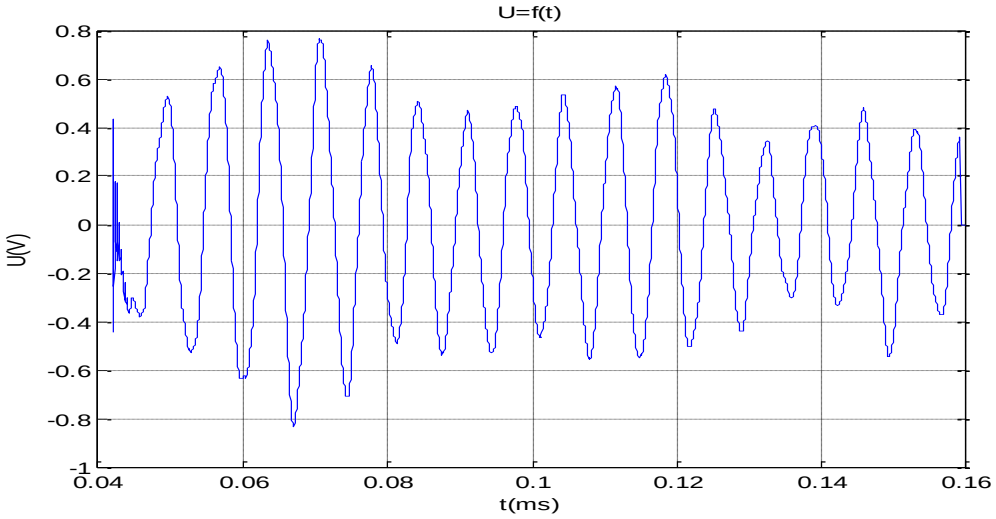

Figure 5.18: Measured signal with the reflection from the mirror in time domain for BK 7 material 4 mm thickness.

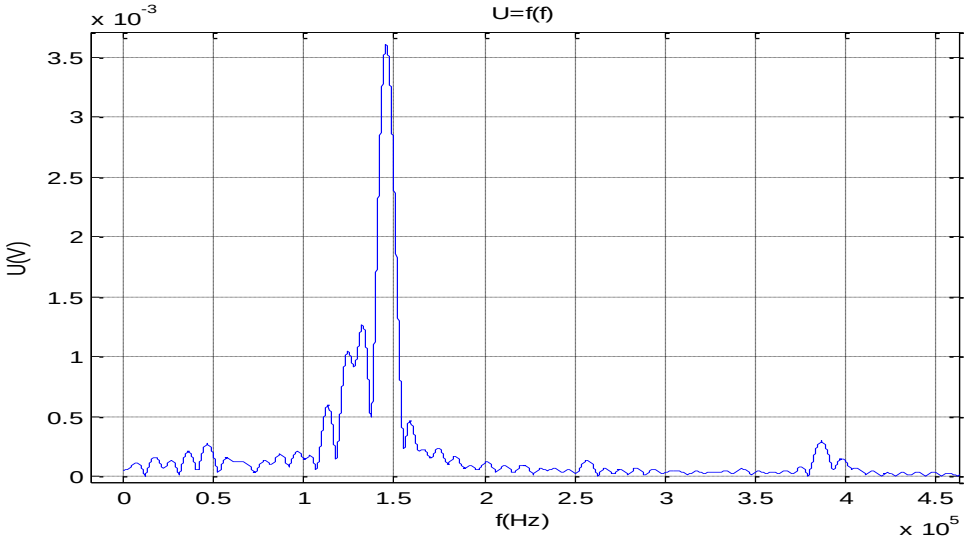

Figure 5.19: Measured signal with the reflection from the mirror in frequency domain for BK 7 material 4 mm thickness.

From the measured signal in time domain, the RMS voltage was calculated and it was found to be 325.3 mV.

In the second experiment, which was conducted in BK 7 (Crown glass) lens material. The laser energy is E = 27.3mJ and the measured absorption is caused by two laser beams, the direct beam and the reflected beam from a mirror at an angle of six degrees. The material dimensions are 25.4 mm x 12 mm. The results can be seen in figures 5.20 & 5.21.

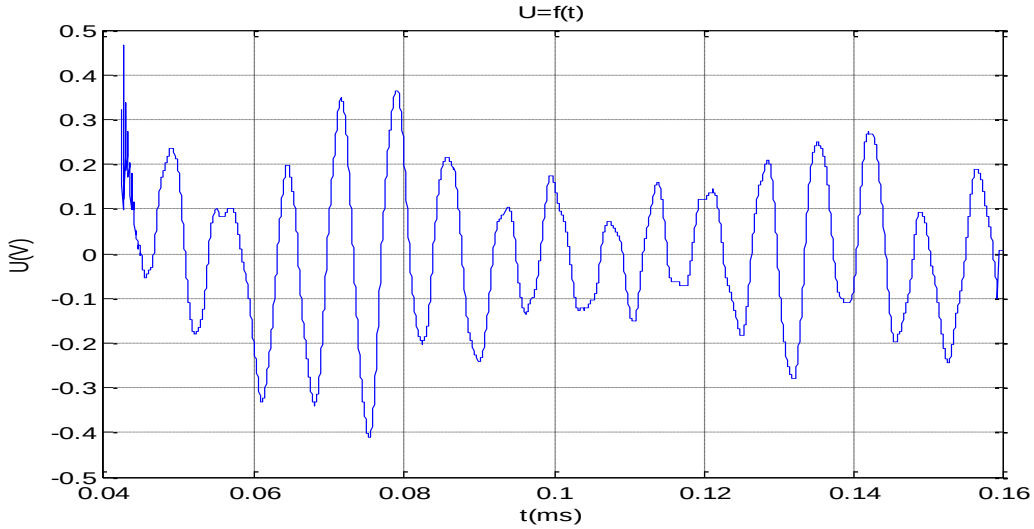

Figure 5.20: Measured signal with the reflection of the mirror in time domain for BK material 12 mm thickness.

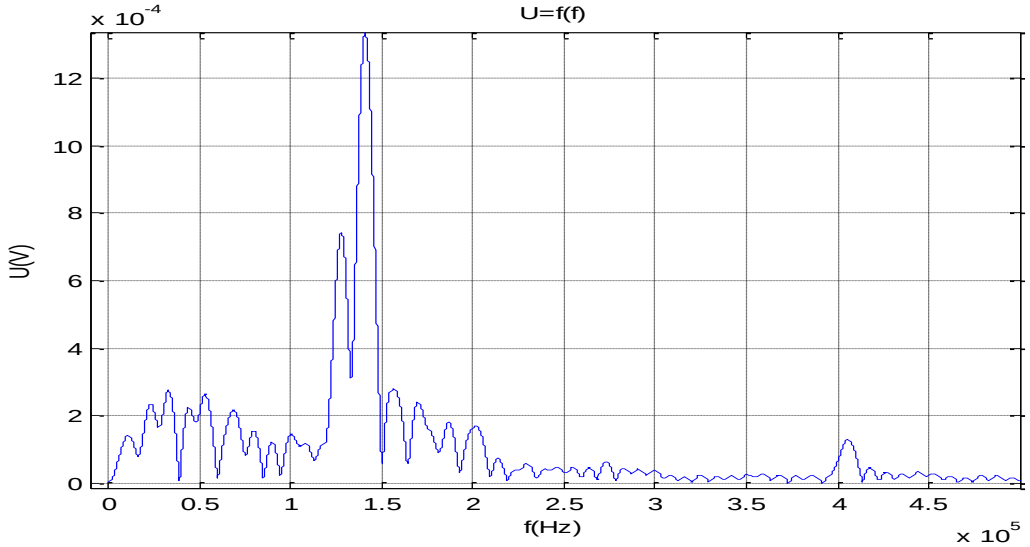

Figure 5.21: Measured signal with the reflection of the mirror in frequency domain for BK material 12 mm thickness.

From the measured signal in time domain, the RMS voltage was calculated and it was found to be 135.5 mV.

In the third experiment, which was conducted in BK 7 (Crown glass) lens material. The laser energy is E = 27.3mJ and the measured absorption is caused by the direct beam without any reflections from the mirror. The laser beam in this experiment passes through a pinhole. The pinhole is used as an aperture and it acts as lens to focus the laser beam. The material dimensions are 25.4 mm x 3 mm. The results can be seen in figures 5.22 & 5.23.

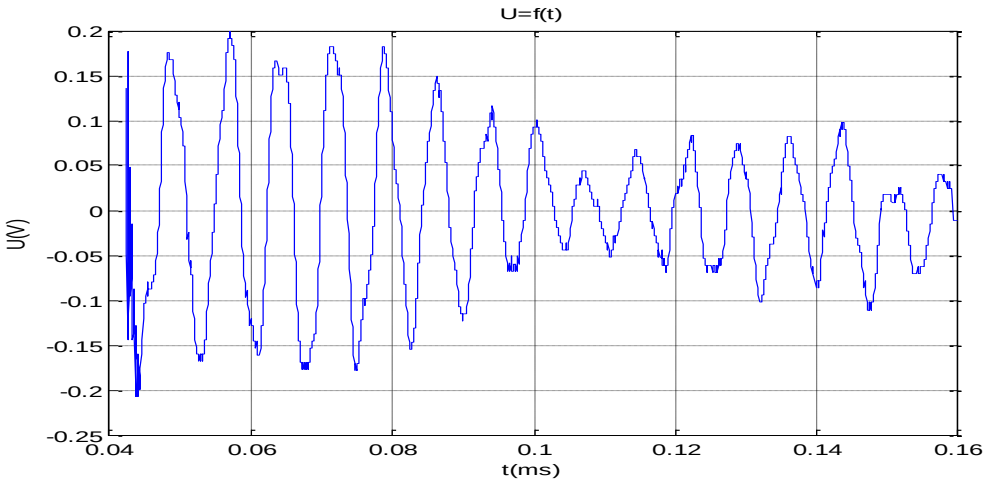

Figure 5.22: Measured signal without reflection of the mirror in time domain for BK material 3 mm thickness.

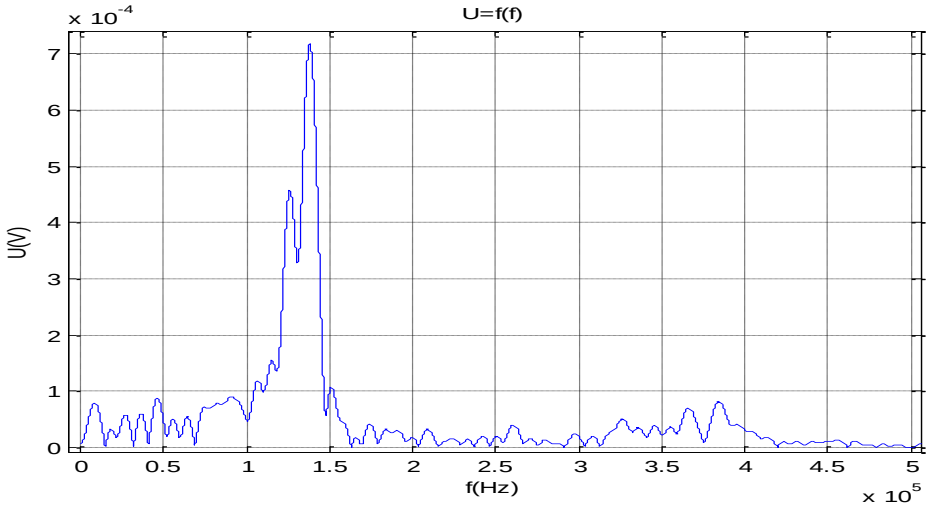

Figure 5.23: Measured signal without reflection of the mirror in frequency domain for BK material 3 mm thickness.

From the measured signal in time domain, the RMS voltage was calculated and it was found to be 73.9 mV.

Table 5.2: Summary results for BK 7 material.

Material BK7 – Laser energy E=27.3mJ (two beams spotting in the material / reflection from a mirror at 6 degrees angle)	
Thickness D(mm)	**Urms (mV)**
4	325.3
12	135.5
Material BK7 (Crown Glass) E=27.3mJ (through pinhole / single point)	
Thickness D(mm)	**Urms (mV)**
3	73.9

*The results summary is discussed at the end of the chapter.

5.2.2. Laser Pulses Absorption in UVFS (Quartz) Material

In this section, the absorption of laser pulses is measured in UVFS material. Two different material widths were examined. More specific, the widths were 1.5 mm and 20 mm respectively. In the sample that has 20 mm thickness, two incident beams were used. The first one is the direct beam and the second is reflected from a coated mirror in six degrees angle.

The first experiment, which was conducted in UVFS Laser Line Mirror (Quartz) lens material, the laser energy is E = 27.3mJ and the measured absorption is caused by the direct beam without any reflections from the mirror. The material dimensions 25.4 mm x 1.5 mm. The results can be seen in figures 5.24 & 5.25.

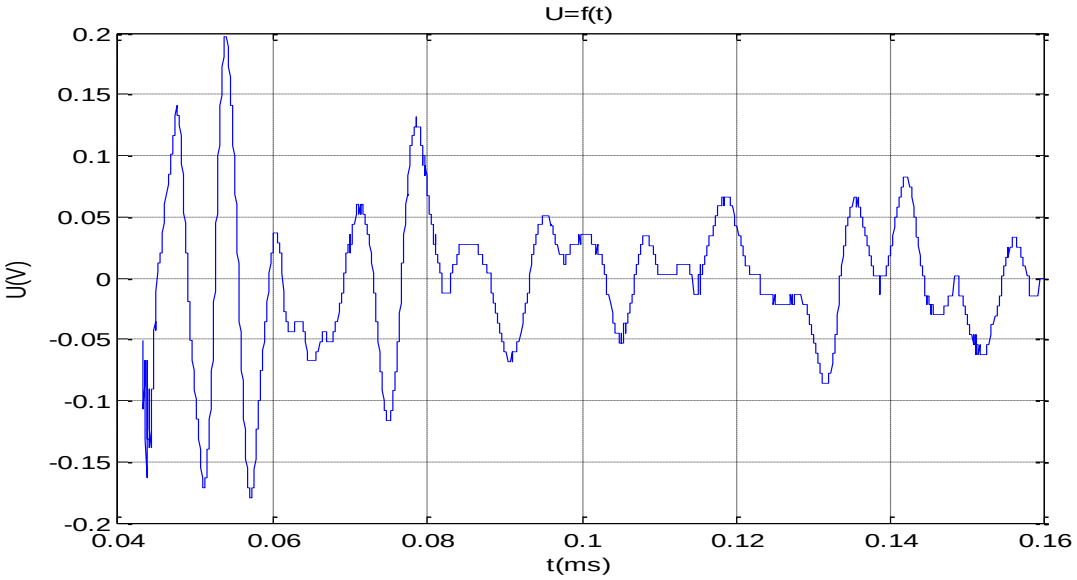

Figure 5.24: Measured signal without reflection of the mirror in time domain for UVFS Laser Line Material (Quartz) material 1.5 mm thickness.

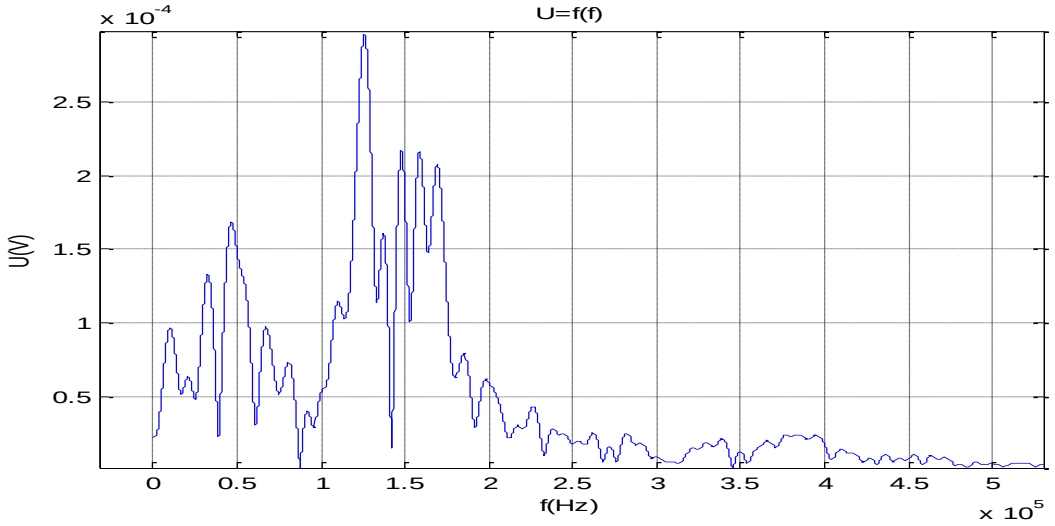

Figure 5.25: Measured signal without reflection of the mirror in frequency domain for UVFS Laser Line Material (Quartz) material 1.5 mm thickness.

From the measured signal in time domain, the RMS voltage was calculated and it was found to be 50 mV.

In the second experiment, which was conducted in UVFS Laser Line Mirror (Quartz) lens material, the laser energy is E = 27.3mJ and the measured absorption is caused by two laser beams, the direct beam and the reflected beam from a mirror at an angle of six degrees. The material dimensions are 25.4 mm x 20 mm. The results can be seen in figures 5.26 & 5.27.

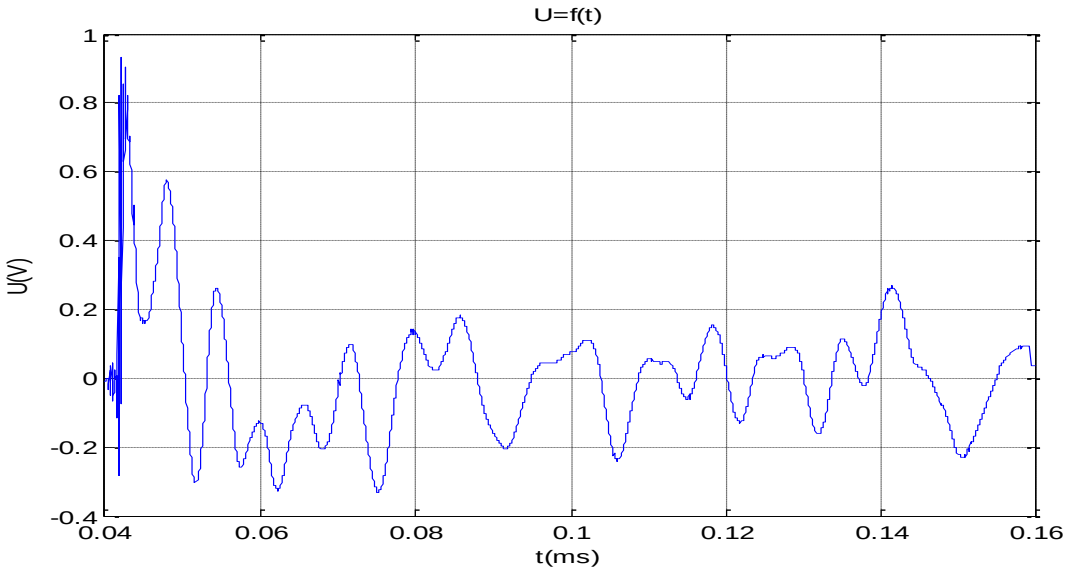

Figure 5.26: Measured signal with reflection of the mirror in time domain for UVFS Laser Line Material (Quartz) material 20 mm thickness.

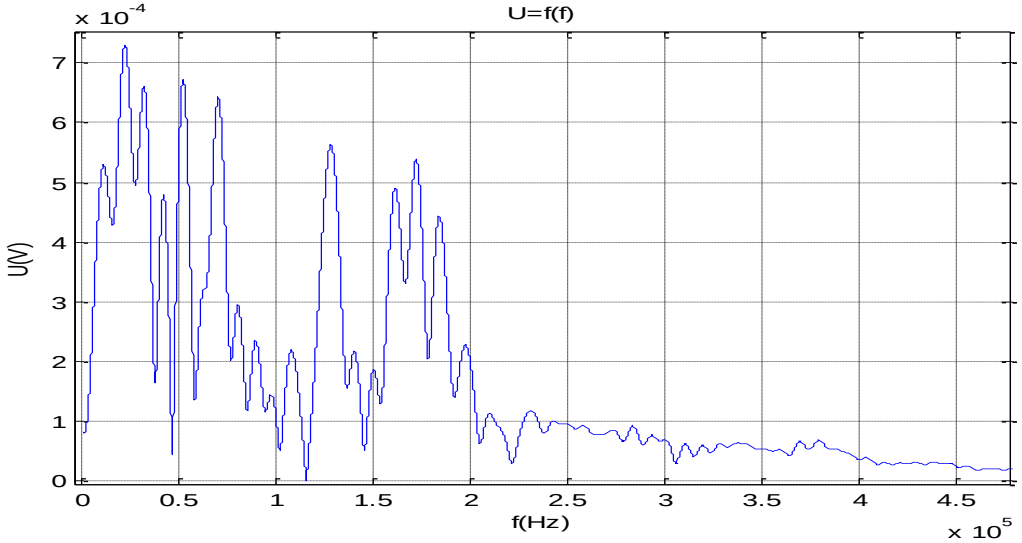

Figure 5.27: Measured signal with reflection of the mirror in frequency domain for UVFS Laser Line Material (Quartz) material 20 mm thickness.

From the measured signal in time domain, the RMS voltage was calculated and it was found to be 151 mV.

Table 5.3: Summary results for UVFS material.

Material UVFS Laser Line Material (Quartz) Laser energy E=27.3mJ	
Thickness D(mm)	**Urms(mV)**
1.5	50 (without reflection)
20	151.6 (with reflection)

*The results summary is discussed at the end of the chapter.

5.2.3. Laser Pulses Absorption in Sapphire Material

In this section, the absorption of laser pulses is measured in Sapphire material. The laser energy is E = 27.3mJ and the measured absorption is caused by two laser beams, the direct beam and the reflected beam from a mirror at an angle of six degrees. The material dimensions are 25.4 mm x 6 mm. The same lens was measured two times in order to compare the measurement repeatability for mounting. The results can be seen in figures 5.28, 5.29, 5.30 & 5.31.

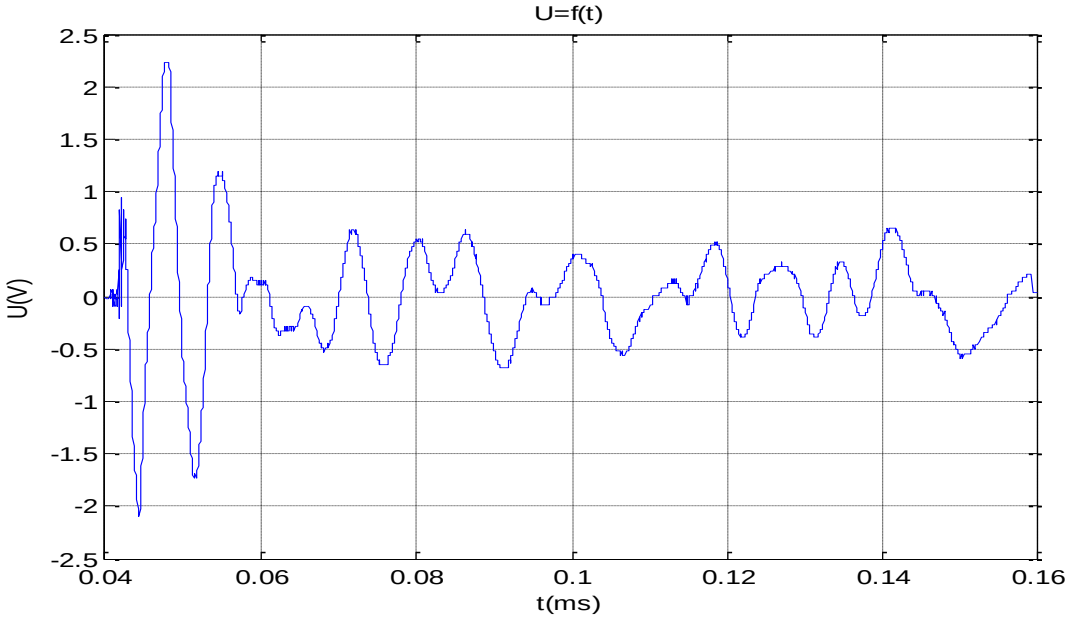

Figure 5.28: First measurement - Measured signal with reflection of the mirror in time domain for Sapphire material 6 mm thickness.

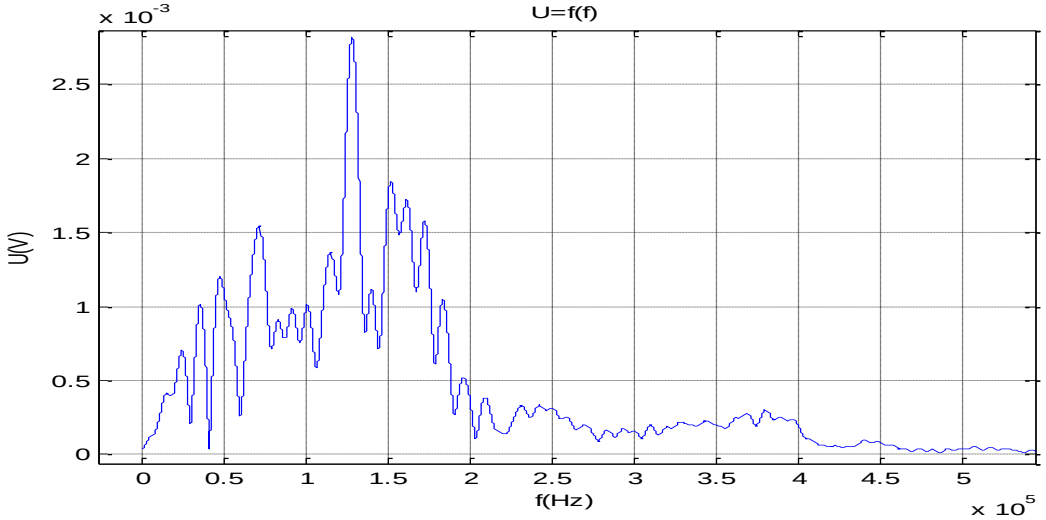

Figure 5.29: First measurement - Measured signal with reflection of the mirror in frequency domain for Sapphire material 6 mm thickness.

In the first measurement, from the measured signal in time domain, the RMS voltage was calculated and it was found to be 451.7 mV.

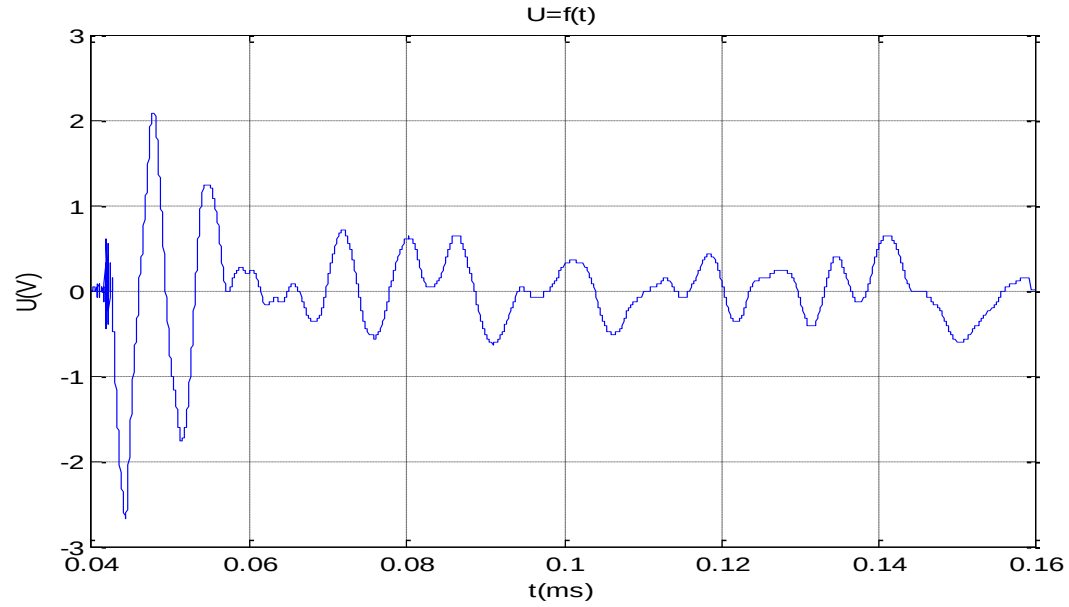

Figure 5.30: Second measurement - Measured signal with reflection of the mirror in time domain for Sapphire material 6 mm thickness.

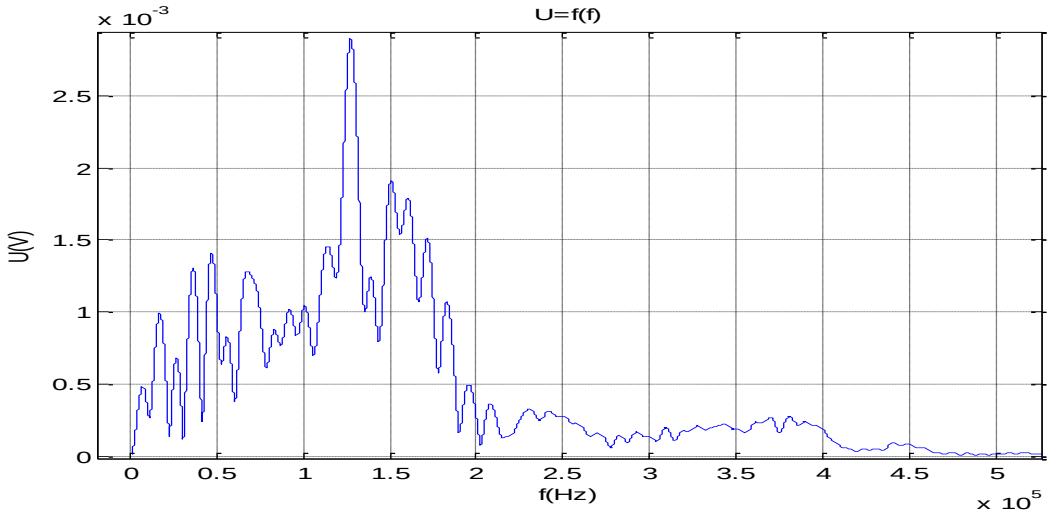

Figure 5.31: Second measurement - Measured signal with reflection of the mirror in frequency domain for Sapphire material 6 mm thickness.

In the first measurement, from the measured signal in time domain, the RMS voltage was calculated and it was found to be 467.6 mV.

Table 5.4: Summary results for Sapphire material.

Sapphire material – Laser energy E=27.3mJ (two beams spotting in the material / reflection from a mrror at 6 degrees angle)	
Thickness (mm)	**Urms (mV)**
6	451.7 (1st measurement)
6	467.6 (2nd measurement)

*The results summary is discussed at the end of the chapter.

5.2.4. Laser Pulses Absorption in Calcium Fluoride Material

In this section, the absorption of laser pulses is measured in calcium fluoride (CaF_2) material. The laser energy is E = 27.3mJ and the measured absorption is caused by the direct beam without any reflections from the mirror. The material dimensions 25.4 mm x 4 mm. The results can be seen in figures 5.32 & 5.33.

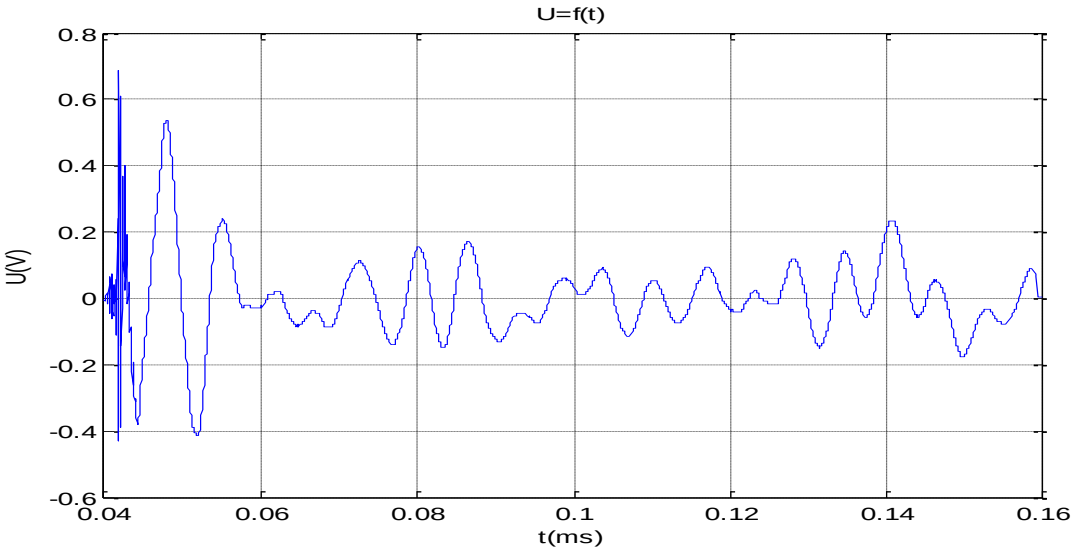

Figure 5.32: Measured signal without reflection of the mirror in time domain for CaF2 material 4 mm thickness.

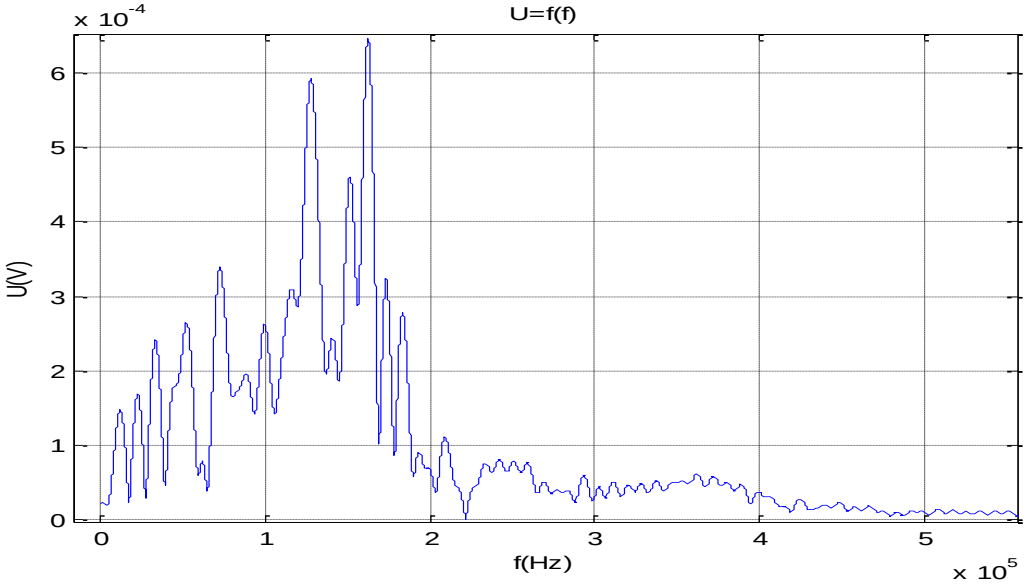

Figure 5.33: Measured signal without reflection of the mirror in frequency domain for CaF2 material 4 mm thickness.

From the measured signal in time domain, the RMS voltage was calculated and it was found to be 107.8 mV.

Table 5.5: Summary results for calcium fluoride material.

Calcium Fluoride material – Laser energy E=27.3mJ	
Thickness (mm)	**Urms (mV)**
4	107.8

*The results summary is discussed at the end of the chapter.

5.2.5. Laser Pulses Absorption in Magnesium Fluoride Material

In this section, the absorption of laser pulses is measured in magnesium fluoride (MgF_2) material. The laser energy is E = 27.3mJ and the measured absorption is caused by the direct beam without any reflections from the mirror. The material dimensions 25.4 mm x 4 mm. The results can be seen in figures 5.34 & 5.35.

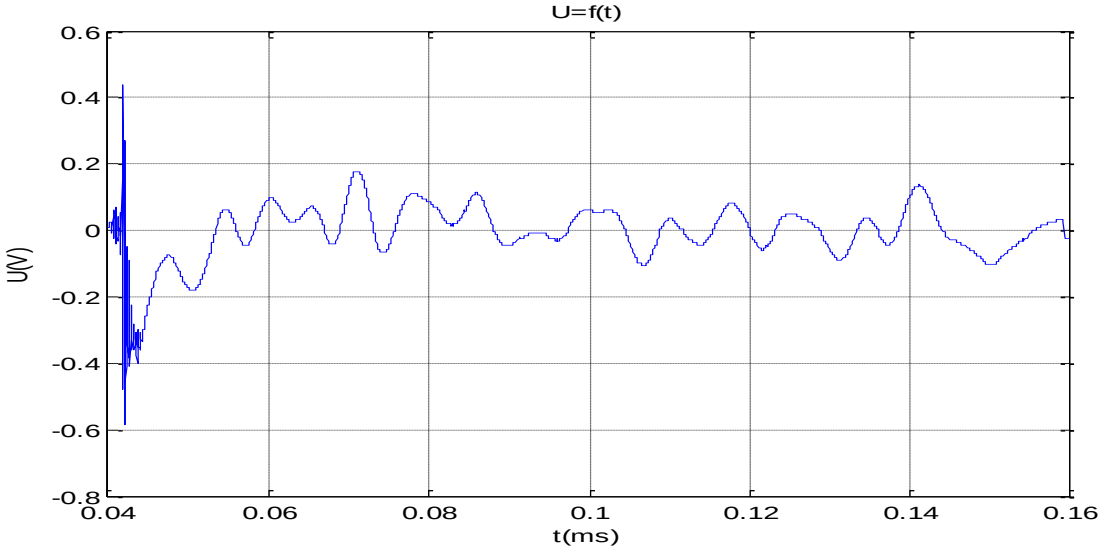

Figure 5.34: Measured signal without reflection of the mirror in time domain for MgF2 material 4 mm thickness.

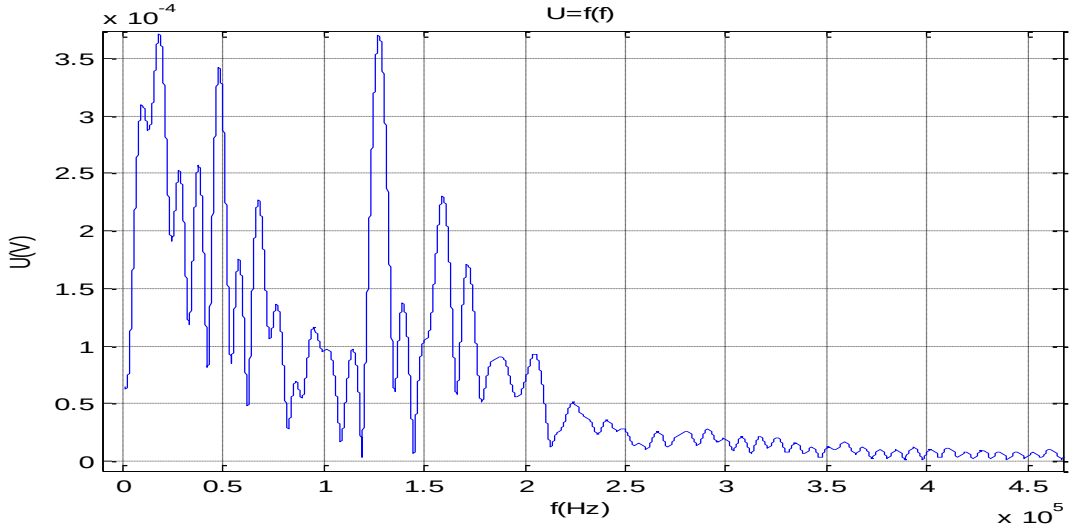

Figure 5.35: Measured signal without reflection of the mirror in frequency domain for MgF2 material 4 mm thickness.

From the measured signal in time domain, the RMS voltage was calculated and it was found to be 72.8 mV.

Table 5.6: Summary results for calcium fluoride material.

Magnesium Fluoride material – Laser energy E=27.3mJ	
Thickness (mm)	**Urms (mV)**
4	72.8

*The results summary is discussed at the end of the chapter.

5.2.6. Laser Pulses Absorption in Infrasil Material

In this section, the absorption of laser pulses is measured in infrasil material. The laser energy is E = 27.3mJ and the measured absorption is caused by the direct beam without any reflections from the mirror. The material dimensions 25.4 mm x 3 mm. The results can be seen in figures 5.36 & 5.37.

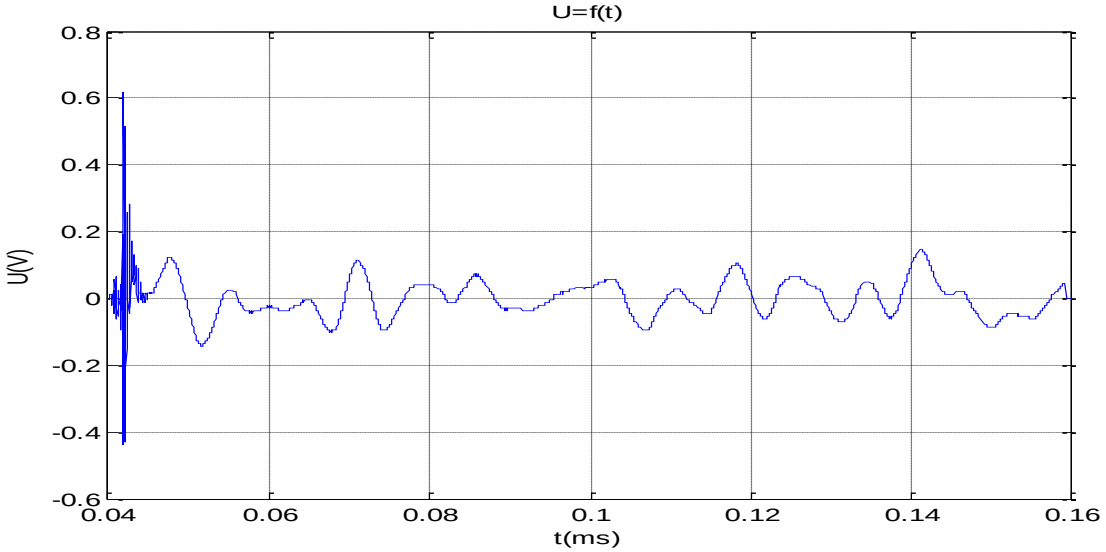

Figure 5.36: Measured signal without reflection of the mirror in time domain for Infrasil material 3 mm thickness.

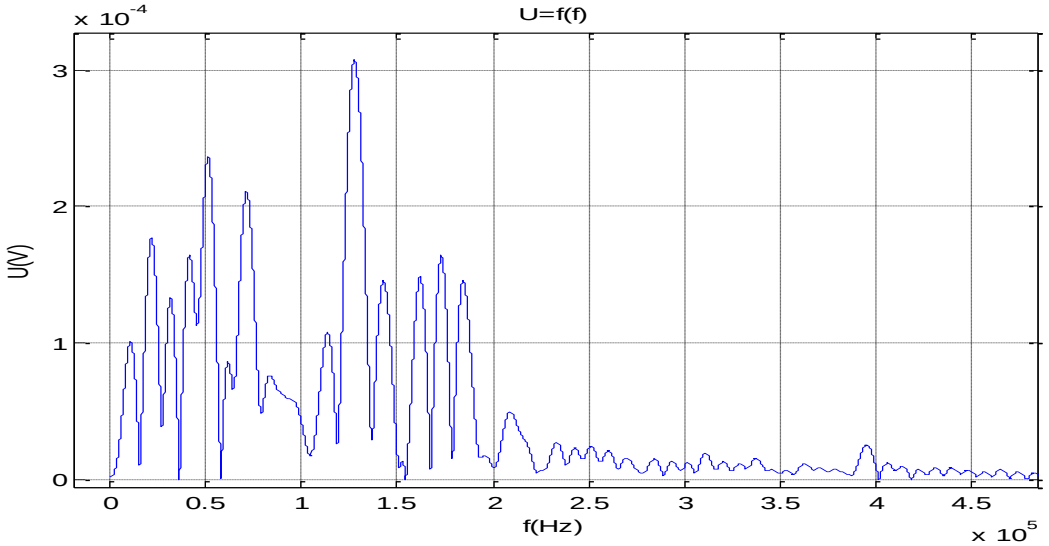

Figure 5.37: Measured signal without reflection of the mirror in frequency domain for Infrasil material 3 mm thickness.

From the measured signal in time domain, the RMS voltage was calculated and it was found to be 52.2 mV.

Table 5.7: Summary results for infrasil material.

Infrasil material Laser Energy E=27.3mJ	
Thickness (mm)	**Urms (mV)**
3	52.2

*The results summary is discussed at the end of the chapter.

5.2.7. Laser Pulses Absorption in Zinc Selenide Material

In this section, the absorption of laser pulses is measured in zinc selenide material. Due to material's high absorption, the laser energy that is used is E = 1.7mJ and the measured absorption is caused by the direct beam without any reflections from the mirror. The material dimensions 25.4 mm x 3 mm. The results can be seen in figures 5.38 & 5.39.

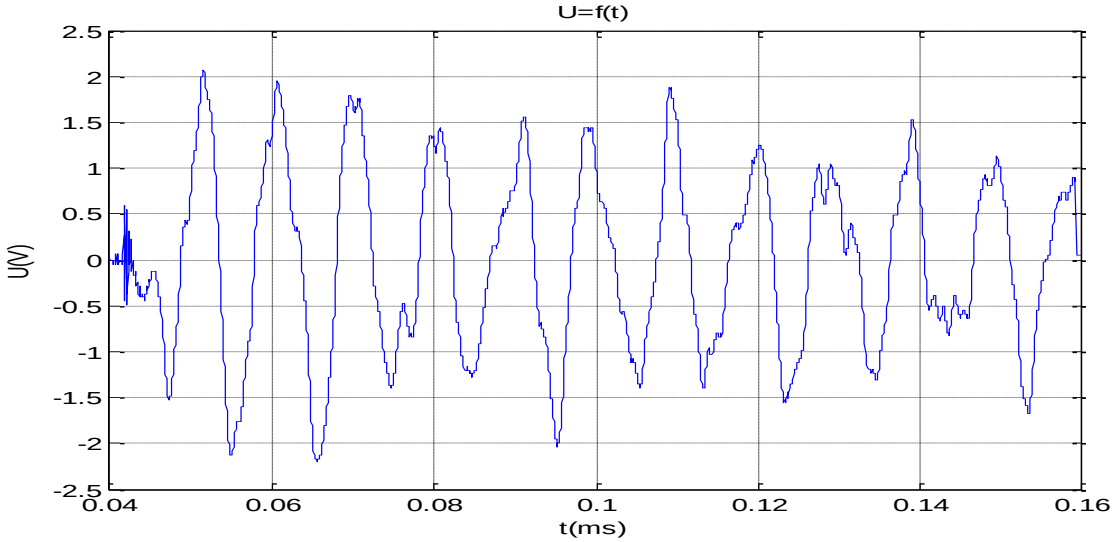

Figure 5.38: Measured signal without reflection of the mirror in time domain for ZnSe high absorbing material 3 mm thickness.

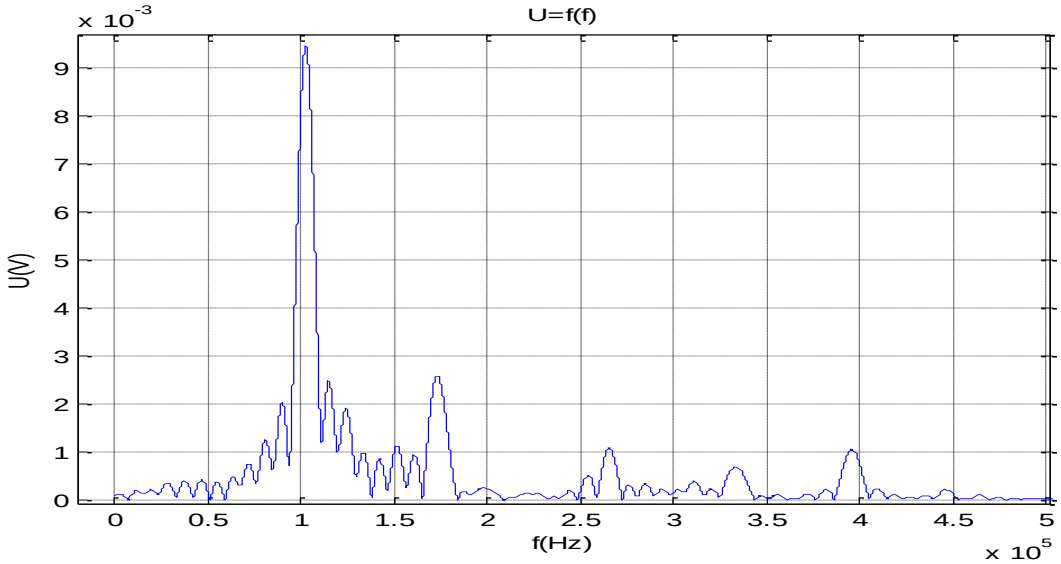

Figure 5.39: Measured signal without reflection of the mirror in frequency domain for ZnSe high absorbing material 3 mm thickness.

From the measured signal in time domain, the RMS voltage was calculated and it was found to be 855.9 mV.

Table 5.8: Summary results for infrasil material.

Zinc Selenide material Laser Energy E = 1.7mJ	
Thickness (mm)	Urms (mV)
3	855.9

*The results summary is discussed at the end of the chapter.

5.3 CONCLUSIONS

The summary of the experimental results can be seen in Table 5.9. With the aim of presenting more clear conclusions, the results will be categorized either by the thickness of the material or if there is a second beam pointed in the material coming from the reflection from the mirror.

Material	Thickness	Laser Energy	Photoacoustic Signal Amplitude	Reflection
BK 7	4 mm	27.3 mJ	325.3 mV	Yes
BK 7	12 mm	27.3 mJ	135.5 mV	Yes
BK 7	3 mm	27.3 mJ	73.9 mV	No
UVFS	1.5 mm	27.3 mJ	50 mV	No
UVFS	20 mm	27.3 mJ	151 mV	Yes
Sapphire (1st measurement)	6 mm	27.3 mJ	451.7 mV	Yes
Sapphire (2nd measurement)	6 mm	27.3 mJ	467.6 mV	Yes
CaF_2	4 mm	27.3 mJ	107.8 mV	No
MgF_2	4 mm	27.3 mJ	72.8 mV	No
Infrasil	3 mm	27.3 mJ	52.2 mV	No
ZnSe	3 mm	1.7 mJ	855.9 mV	No

As far as materials with a thickness of 3 mm are concerned, we can examine BK 7, Infrasil and Zinc Selenide. It can be observed that ZnSe which is a higly absorbing material displays the highest absorption and generates the largest photoacoustic signal, even if the laser energy that was used is only 1.7 mJ. On the other hand, in the rest two materials (BK 7 and Infrasil), Infrasil has the higher absorption.

Comparing the BK 7 material in different thicknesses, we can clearly see the effect of the reflection from the mirror. In the lens with a thickness of 3 mm, the measured signal is produced without reflection and is 73.9 mV. In the lens with the thickness of 4 mm is it expected that without reflection the signal will be weaker. However, in this case we can how the second beam which comes from the reflective mirror affects the photoacoustic signal. It increases it hugely to 325.3 mV. It can also be seen that the use of the reflected beam creates higher amplitude in the lens that has 12 mm thickness than in the 3 mm lens without reflection.

The affect of the reflected beam is also displayed in UVFS material. In this case, in the lens with 20 mm thickness, the photoacoustic signal is much higher than the signal in 1.5 mm lens without the reflection.

In the comparison of calcium fluoride lens and magnesium fluoride lens, where both lenses have the same thickness of 4 mm, it is observed that CaF2 manifests higher absorption. The measurements in both materials were performed without reflection from the mirror.

Finally, the sapphire lens was tested twice in order to prove repeatability for mounting. It is clear that the measurements, even under the same circumstances, will never be exactly similar. In the second measurement the amplitude is almost 16 mV higher. However, the two measurements are close to each other.

CONCLUSIONS AND SUGGESTIONS

In this last chapter, the main achievements that accomplished during this thesis project will be summarized. The conclusions drawn from the present study will be presented in the next section. Finally, suggestions for further work and limitations will be outlined and discussed.

Main achievements

The main achievements can be summarized as follows:

- Develop an absorption measurement tool.
- Propose a methodology approach.
- Set up an experiment for measuring the absorption of laser pulses.
- Analyze the obtained data.
- Analyze the mechanisms of photoacoustic effect.
- Analyze the laser – material interactions.
- Develop computer simulations based on theory.

Conclusions

This thesis project is a research and development work. The main aim was to develop an absorption measurement prototype and formulate the methodology that leads to the final experimental set up. In order to perform the actual measurements, first the theoretical background must be analyzed. For this reason, the photoacoustic technique mechanism and the interactions between lasers and materials must be fully understood. To sum up, Photoacoustic method is based on optical absorption and subsequent detection of pressure fluctuations. It has been shown to be a very useful optical technique for studying optical and thermal properties of materials.

From the simulation that performed using Comsol Multiphysics software and the finite element method was drawn the following conclusions. The amount of transformed energy is determined by the light absorption mechanisms in the material. The laser parameters of importance are the wavelength, the angle with which the beam impinges on the material surface and the polarization of the beam. The factors that affect the heating which is caused by the absorption transfer are the thermal conductivity, heat capacity and material density. It has observed that bigger pulse width leads to bigger penetration width and causes lower temperature rise. On the other side, smaller pulse width leads to smaller penetration depth and causes higher temperature rise. The laser pulses repetition frequency does not affect the wave generation inside the material. What is important and affects the the generated waves is the pulse width that is used to excite the material.

Before proceeding to the measurement of laser pulses absoprtion, the proposed device was tested in simple experiments, using waves from a piezoelectric transducer to cause the vibrations inside the material. These vibrations are the same as the vibrations caused by the termal expansion induced by the absorption that consequently lead to pressure waves. Alongside with the amplifier's testing and evaluation, an algorithm on MATLAB software was implemented with the aim of capturing the data from the oscilloscope and perform Fast Fourier Transform in order to transform the data from time to frequency domain.

From the experiments, it has been concluded that the thicker the material is, the higher the photoacoustic signal generated is. It has also observed that if a second beam coming from a refletive mirror and impringes the material at an angle, then the absorption is higher. This observation is viable only when the insident angle is higher than six degrees. Moreover, the material that shows the highest absorption is zinc selenide, while the material that has the lowest absorption is the UVFS. It is also noticeable that even when performing the same experiment

under the same circumstances, the resulted absorption will never be equal as there are very sensitive pieces of equipment on the experimental set up. The variation is small, but for better and more accurate results, the repeatable performance of the experiment is suggested.

Future work and suggestions

The work carried out in this thesis has revealed many promising areas of further research. This project, however, can be used as guideline in order to understand from the theoretical basics till the methodoly approach and equipment that can be utilized in future works.

A good idea is to further follow the same study and set up with the aim of measuring the absorption of laser pulses on a wider variety of optical materials with the respect that all of them having the same thickness, so as the results can be comparable. It is also interesting to use shorter and longer laser pulses and examine how they affect the generated photoacoustic signal.

Furthermore, using the same set up, it would be adviced to place the piezoelectric transducer in different locations on the material under investigation. This approach can highlight the variation of the photoacoustic signal inside the material.

The photoacoustic technique that was utilized for the measurement of absorption of laser pulses in this thesis, can also be compared with the other techniques. These techniques such as calorimeters, photothermal expansion and mirage effect were briefly mentioned in the first chapter and they can also be used for the measurement of absorption.

It is recommended that another low noise can be proposed that will have a higher bandwidth. For materials that express weaker absorption, more that one low noise amplifiers are needed connected in series, thus the gain will be multiplied, but respect must be taken to the amplifier's noise floor. When using battery-powered amplifiers, the degradation of the batteries must be taken into account before proceeding to further measurements.

It is obvious that all these experiments are highly sensitive and are affected both by the equipment itself as well as from environmental parameters. For better accuracy, the same experiment is it imperative, if possible, to be performed multiple times to provide repeatability for mounting.

Finally, the measurement of absorption of laser pulses can also be performed in opaque materials, as it is not limited only in transparent optical materials that were used in this thesis. The study can also be extended in liquids.

INFORMATION SOURCE LIST

[1] Rosencwaig, A. (1980) Photoacoustics and photoacoustic spectroscopy. Chemical Analysis: a Series of Monographs on Analytical Chemistry and Its Applications, Vol. 57. New York:John Wiley & Sons, ISBN 0471044954.
[2] Tam, A. (1986). "Applications of photoacoustic sensing techniques". Reviews of Modern Physics. 58 (2): 381. Bibcode: 1986RvMP...58..381T. doi:10.1103/RevModPhys.58.381.
[3] Bell, A. G. (1880). "On the production and reproduction of sound by light". American Journal of Science (118): 305. doi:10.2475/ajs.s3-20.118.305.
[4] Bell, A. G. (1881). "LXVIII.Upon the production of sound by radiant energy". Philosophical Magazine Series 5. 11 (71): 510. doi:10.1080/14786448108627053.
[5] Bell, A.G. (1881) "Production of Sound by Radiant Energy", J. Franklin Inst. 111, 147-154.
[6] Tyndall, J. (1880). "Action of an Intermittent Beam of Radiant Heat upon Gaseous Matter". Proceedings of the Royal Society of London. 31 (206–211): 307. doi: 10.1098/ rspl. 1880.0037.
[7] Röntgen, W. C. (1881). "On tones produced by the intermittent irradiation of a gas". Philosophical Magazine Series 5. 11 (68): 308. doi:10.1080/14786448108627021.
[8] Veingerov, M.L. (1938). "New Method of Gas Analysis Based on Tyndall-Roentgen Opto-Acoustic Effect". Dokl. Akad. Nauk. USSR. 19: 687
[9] Rosencwaig, A. (1976). "Theory of the photoacoustic effect with solids". Journal of Applied Physics. 47: 64. doi:10.1063/1.322296.
[10] Gray, R. C.; Bard, A. J. (1978). "Photoacoustic spectroscopy applied to systems involving photoinduced gas evolution or consumption". Analytical Chemistry. 50 (9): 1262. doi :10.1021/ac50031a018.
[11] Bults, G.; Horwitz, B. A.; Malkin, S.; Cahen, D. (1982). "Photoacoustic measurements of photosynthetic activities in whole leaves. Photochemistry and gas exchange". Biochimica et Biophysica Acta (BBA) - Bioenergetics. 679 (3): 452. doi:10.1016/0005-2728(82)90167-0.
[12] Marín, E. (2004). "Thermal wave physics: principles and applications to the characterization of liquids". Revista Ciências Exatas e Naturais. 6 (2): 145.
[13] Tam, A. C. (1985). "Pulsed photothermal radiometry for noncontact spectroscopy, material testing and inspection measurements". Infrared Physics. 25: 305. doi:10.1016/0020-0891(85)90096-X.
[14] Thermal Lens Spectroscopy. photonics.cusat.edu
[15] A. G. Bell, “The spectrophone,” (1981) Bull. Philos. Soc. 4, 42.
[16] V. Ntziachristos, “Going deeper than microscopy: the optical imaging frontier in biology,” (2010) Nat. Methods 7, 603–614.
[17] A. Mandelis, “Diffusion waves and their uses,” Phys. Today 53(8), 29–34 (2000).
[18] A. J. Ångström, “Neue methode, das Wärmeleitungsvermögen der Körper zubestimmen,” Ann. Phys. Chem. 190, 513–530 (1861).
[19] W. H. Preece, “On the conversion of radiant energy into sonorous vibrations,” Proc. R. Soc. London 31, 506–520 (1880).
[20] E. Mercadier, “Sur la radiophonie,” J. Phys. Theor. Appl. 10, 53–68 (1881).
[21] E. Mercadier, “Sur la radiophonie (2e mémoire),” J. Phys. Theor. Appl. 10, 147–154 (1881).
[22] A. Rosencwaig and A. Gersho, “Photoacoustic effect with solids: a theoreticaltreatment,” Science 190, 556–557 (1975).
[23]A. Rosencwaig and A. Gersho, “Theory of the photoacoustic effect with solids,”J. Appl. Phys. 47, 64–69 (1976).

[24] A. Rosencwaig, “Thermal wave microscopy with photoacoustics,” J. Appl. Phys. 51, 2210–2211 (1980).
[25] A. Rosencwaig, “Thermal-wave imaging,” Science 218, 223–228 (1982).
[26] Rayleigh, “The photophone,” Nature 23, 274–275 (1881).
[27] F. A. McDonald and G. C. Wetsel, “Generalized theory of the photoacoustic effect,” J. Appl. Phys. 49, 2313–2322 (1978).
[28] F. A. McDonald, “Photoacoustic effect and the physics of waves,” Am. J. Phys. 48, 41–47 (1980).
[29] A. C. Boccara, D. Fournier, and J. Badoz, “Thermo-optical spectroscopy: detection by the ‘mirage effect’,” Appl. Phys. Lett. 36, 130–132 (1980).
[30] A. Mandelis, “Frequency-domain photopyroelectric spectroscopy of condensed phases (PPES): a new, simple and powerful spectroscopic technique,” Chem. Phys. Lett. 108, 388–392 (1984).
[31] P. E. Nordal and S. O. Kanstad, “Photothermal radiometry,” Phys. Scripta 20, 659–662 (1979).
[32] E. L. Kerr and J. G. Atwood, “The laser illuminated absorptivity spectrophone: a method for measurement of weak absorptivity in gases at laser wavelengths,” Appl. Opt. 7, 915–921 (1968).
[33] F. A. Duck, Physical Properties of Tissue: A Comprehensive Reference Book (Academic, 1990).
[34] H. S. Carslaw and J. C. Jaeger, Heat Conduction in Solids (Clarendon, 1959).
[35] S. L. Jacques, “Role of tissue optics and pulse duration on tissue effects during high-power laser irradiation,” Appl. Opt. 32, 2447–2454 (1993).
[36] A. Karabutov, N. B. Podymova, and V. S. Letokhov, “Time-resolved laser optoacoustic tomography of inhomogeneous media,” Appl. Phys. B 63, 545–563 (1996).
[37] L. V. Wang and H.-I. Wu, Biomedical Optics: Principles and Imaging (Wiley, 2007), Chap. 12, pp. 283–321.
[38] V. E. Gusev and A. A. Karabutov, Laser Optoacoustics (American Institute of Physics, 1993).
[39]J. Curie and P. Curie, “Développement par pression de l’électricité polaire dans les cristaux hémièdres à faces inclines,” Comptes Rendus 91, 294–295(1880).
[40] C. M. Chilowsky and M. P. Langévin, “Procédés et appareils pour la production de signaux sous-marins dirigés et pour la localisation á distance d’obstacles sous-marins,” French patent FR502913 (May 29, 1916).
[41] R. W. Wood and A. L. Loomis, “The physical and biological effects of high frequency sound-waves of great intensity,” Philos. Mag. 4(22), 417–436 (1927).
[42] L. Bergmann, Der Ultraschall und seine Anwendungen in Wissenschaft und Technik (VDI-Verlag, 1937).
[43] K. T. Dussik, “Über die Möglichkeit, hochfrequente mechanische Schwingungen als diagnostisches Hilfsmittel zu verwerten [On the possibility of using ultrasound waves as a diagnostic aid],” Z. gesamte Neurol. Psychiat. 174, 153–168 (1942).
[44] G. D. Ludwig and F. W. Struthers, “Considerations underlying the use of ultrasound to detect gallstones and foreign bodies in tissue,” Technical Report 4 (Naval Medical Research Institute, 1949).
[45] J. J. Wild and J. M. Reid, “Application of echo-ranging techniques to the determination of structure of biological tissues,” Science 115, 226–230 (1952).

[46] D. H. Howry, “Sound-wave portrait in the flesh,” in Life Magazine (Medicine Section) (1954), pp. 71–72.
[47] J. E. Michaels, “Thermal impact—the mechanical response of solids to extreme electromagnetic radiation,” Planet. Space Sci. 7, 427–433 (1961).
[48] R. M. White, “An elastic wave method for the measurement of pulse-power density,” IRE Trans. Instrum. I-11, 294–298 (1962).
[49] R. M. White, “Generation of elastic waves by transient surface heating,” J. Appl. Phys. 34, 3559–3567 (1963).
[50] G. A. Askaryan, A. M. Prokhorov, G. F. Chanturia, and G. P. Shipulo, “Propagation of a laser beam through a liquid,” Zh. Eksp. Teor. Fiz. 44, 2180–2182 (1963).
[51] L. M. Lyamshev, “Lasers in acoustics,” Sov. Phys. Usp. 30, 252–279 (1987).
[52] L. M. Lyamshev, Radiation Acoustics (CRC Press, 2004).
[53] L. M. Lyamshev, “Radiation acoustics,” Sov. Phys. Usp. 35, 276–302 (1987).
[54] E. F. Carome, N. A. Clark, and C. E. Moeller, “Generation of acoustic signals in liquids by ruby laser-induced thermal stress transients,” Appl. Phys. Lett. 4, 95–97 (1964).
[55] L. S. Gournay, “Conversion of electromagnetic to acoustic energy by surface heating,” J. Acoust. Soc. Am. 40, 1322–1330 (1966).
[56] C. L. Hu, “Spherical model of an acoustical wave generated by rapid laser heating in a liquid,” J. Acoust. Soc. Am. 46, 728–736 (1969).
[57] M. W. Sigrist and F. K. Kneubühl, “Laser-generated stress waves in liquids,” J. Acoust. Soc. Am. 64, 1652–1663 (1978).
[58] S. G. Kasoev and L. M. Lyamshev, “Theory of laser-pulse generation of sound in a liquid,” Sov. Phys. Acoust. 23, 510–514 (1977).
[59] E. F. Kozyaev and K. A. Naugol’nikh, “On thermal acousto-optic effect,” Acoust. J. 22, 366–369 (1976).
[60] C. K. N. Patel and A. C. Tam, “Pulsed optoacoustic spectroscopy of condensed matter,” Rev. Mod. Phys. 53, 517–550 (1981).
[61] A. C. Tam, “Applications of photoacoustic sensing techniques,” Rev. Mod. Phys. 58, 381–431 (1986).
[62] V. P. Zharov and V. S. Letokhov, Laser Optoacoustic Spectroscopy, Vol. 37 of Springer Series in Optical Sciences (Springer-Verlag, 1986).
[63] H. M. Ledbetter and J. C. Moulder, “Laser-induced Rayleigh waves in aluminium,”J. Acoust. Soc. Am. 65, 840–842 (1979).
[64] A. N. Bondarenko, Yu. B. Drobot, and S. V. Kruglov, “Optical excitation and registration of nanosecond pulses in non-destructive testing,” Defectoskopiya 6, 85–88 (1976) [in Russian].
[65] R. J. Von Gutfeld and R. L. Melcher, “MHz acoustic waves from pulsed thermoelastic expansions and their application to flaw detection,” Mater. Eval. 35, 97–99 (1977).
[66] C. B. Scruby, “Some applications of laser ultrasound,” Ultrasonics 27, 195–209 (1989).
[67] C. B. Scruby and L. E. Drain, Laser Ultrasonics Techniques and Applications (CRC Press, 1990).
[68] S. J. Davies, C. Edwards, G. S. Taylor, and S. B. Palmer, “Laser-generated ultrasound: its properties, mechanisms and multifarious applications,” J. Phys. D 26, 329–348 (1993).
[69] C. B. Scruby and H. N. G. Wadley, “A calibrated capacitance transducer for the detection of acoustic emission,” J. Phys. D 11, 1487–1494 (1978).
[70] A. M. Aindow, J. A. Cooper, R. J. Dewhurst, and S. B. Palmer, “A spherical capacitance transducer for ultrasonic displacement measurements in NDE,” J. Phys. E 20, 204–209 (1987).

[71] R. J. Dewhurst, C. Edwards, and S. B. Palmer, "Noncontact detection of surfacebreaking cracks using a laser acoustic source and an electromagnetic acoustic receiver," Appl. Phys. Lett. 49, 374–376 (1986).
[72] D. A. Hutchins and D. E.Wilkins, "Elastic waveforms using laser generation and electromagnetic acoustic transducer detection," J. Appl. Phys. 58, 2469–2477 (1985).
[73] J. P. Monchalin, "Optical detection of ultrasound at a distance using a confocal Fabry-Perot interferometer," Appl. Phys. Lett. 47, 14–16 (1985).
[74] J. P. Monchalin, "Optical detection of ultrasound," IEEE Trans. Ultrasonic Ferroelectric Frequency. Control 33, 485–499 (1986).
[75] J. D. Aussel and J. P. Monchalin, "Precision laser-ultrasonic velocity measurement and elastic constant determination," Ultrasonics 27, 165–177 (1989).
[76] A. C. Tam, "Pulsed-laser generation of ultrashort acoustic pulses: application for thin-film ultrasonic measurements," Appl. Phys. Lett. 45, 510–512 (1984).
[77] H. K. Wickramasinghe, R. C. Bray, V. Jipson, C. F. Quate, and J. R. Salcedo, "Photoacoustics on a microscopic scale," Appl. Phys. Lett. 33, 923–925 (1978).
[78] C. Haisch and R.Niessner, "Light and sound – photoacoustic spectroscopy"
[79] David Bergstrom, "The Absorption of Laser Light by Rough Metal Surfaces", Doctoral Thesis, Department of Applied Physics and Mechanical Engineering, Lulea, Sweden (2008)
[80] P. Campbell, J. Opt. Soc. Am. B 10(12) (1993)
[81] V. Semak, N. Dahotre, in Lasers in Surface Engineering, Surface Engineering Series, vol. 1,ed. By N. Dahotre (ASM International, Materials Park, OH, USA, 1998), pp. 35–67
[82] M. Sheehy, B. Tull, C. Friend, E. Mazur, Mat. Sci. Eng. B 137, 289 (2006)
[83] N. Dahotre, Lasers in Surface Engineering, Surface Engineering Series, vol. 1 (ASM International, Materials Park, OH, USA, 1998)
[84] D. Bäuerle, Laser Processing and Chemistry (Springer, Berlin, 2000)
[85] W.M. Steen, Laser Material Processing, 3rd edn. (Springer, London, 2003)
[86] J.C. Ion, Laser Processing of Engineering Materials: Principles, Procedure and Industrial Applications (Elsevier Butterworth-Heinemann, Oxford, 2005)
[87] S.Y. Zhang, Y.H. Ren, G. Lupke, Appl. Opt. 42(4), 715 (2003)
[88] L.A. Romero, F.M. Dickey, J. Opt. Soc. Am. A: 13(4), 751 (1996)
[89] C.Momma, S. Nolte, G. Kamlage, F. von Alvensleben, A. Tunnermann, Appl. Phys. AMater. Sci. Process. 67(5), 517 (1998)
[90] N. Sanner, N. Huot, E. Audouard, C. Larat, J.P. Huignard, B. Loiseaux, Opt. Lett. 30(12),1479 (2005)
[91] K. Nemoto, T. Nayuki, T. Fujii, N. Goto, Y. Kanai, Appl. Opt. 36(30), 7689 (1997)
92] E. McLeod, A.B. Hopkins, C.B. Arnold, Opt. Lett. 31(21), 3155 (2006)
[93] S. Heinemann, Opt. Commun. 119(5–6), 613 (1995)
[94] F.M. Dickey, S.C. Holswade (eds.), Laser Beam Shaping: Theory and Techniques (Marcel Dekker, New York, 2000)
95] E. Hecht, Optics, 4th edn. (Addison Wesley, San Francisco, 2002)
[96] J. Heller, J.W. Bartha, C.C. Poon, A.C. Tam, Appl. Phys. Lett. 75(1), 43 (1999)
[97] J.C.Weeber, J.R. Krenn, A. Dereux, B. Lamprecht, Y. Lacroute, J.P. Goudonnet, Phys. Rev. B 64(4) (2001)
[98] R.E. Slusher, B.J. Eggleton, Nonlinear Photonic Crystals, 1st edn. (Springer, Berlin, 2004)
[99] N. Ghofraniha, C. Conti, G. Ruocco, S. Trillo, Phys. Rev. Lett. 99(4) (2007)
[100] W. Staudt, S. Borneis, K.D. Pippert, Phys. Status Solidi A Appl. Res. 166(2), 743 (1998)
[101] N. Mori, T. Ando, Phys. Rev. B 40(9), 6175 (1989)

[102] B.N. Chichkov, C. Momma, S. Nolte, F. vonAlvensleben, A. Tunnermann, Appl. Phys. A Mater. Sci. Process. 63(2), 109 (1996)
[103] M. von Allmen, A. Blatter, Laser-Beam Interactions with Materials: Physical Principles and Applications. Springer Series in Materials Science (Springer, Berlin, 1995)
[104] 30. Y. Hirayama, M. Obara, Appl. Surf. Sci. 197, 741 (2002)
[105] 31. L.V. Zhigilei, P.B.S. Kodali, B.J. Garrison, J. Phys. Chem. B 101(11), 2028 (1997)
[106] Comsol Multiphysics, "Modeling Laser-Material Interactions with the Beer-Lambert Law"
[107] Manoj Kumar Sharma, "Optimization of Laser Induced Forward Transfer by Finite Element Modeling, Royal Institute of Technology-KTH, Stockholm, SWEDEN (2013)
[108] Comsol Myltiphysics, "Beam Splitter Modelling"
[109] Low Noise Amplifiers (Wikipedia)
[110] Motchenbacher, C. D.; Connelly, J. A., Low-noise electronic systems design. Wiley Interscience (1993)
[111] Whitham D. Reeve. "Noise Tutorial", Anchorage, Alaska USA, (1994)
[112] Keysight Technologies Signal Analysis Measurement Fundamentals, Optimize Noise Floor, Resolution Bandwidth, and More, Application Note
[113] Agilent Spectrum Analyzer Measurements and Noise, Application Note 1303.
[114] M. Leidinger, S. Fieberg, N.Waasem, F. Kuhnemann, K. Buse, I. Breuning. „Comparative study on three highly sensitive absorption techniques characterizing lithium niobate over its entire transparent spectral range", University of Freiburg, Germany (2015)
[115] http://photonics.cusat.edu/Research_Photoacoustics.html
[116] Shimshon Levy, „Spectrum analyzer and spectrum analysis" (2012)